The Endothelium and the Bone Marrow Microenvironment

Surya Shree Kotha

A dissertation

submitted in partial fulfillment of the

requirements for the degree of

Doctor of Philosophy

University of Washington

2018

Reading Committee:

Ying Zheng, Chair

Beverly Torok-Storb

Nathan Sniadecki

Program Authorized to Offer Degree:

Bioengineering

University of Washington

Abstract

The Endothelium and the Bone Marrow Microenvironment

Surya Shree Kotha

Chair of the Supervisory Committee:
Ying Zheng, Ph.D., Assistant Professor
Department of Bioengineering

The bone marrow vasculature provides an interface between the circulation and hematopoietic tissue, allowing for hundreds of billions of blood cells to enter the circulation in an adult human every day. Much is unknown, however, about the characteristics of marrow vasculature and interactions of hematopoietic progenitor cells or their progeny with the endothelium. This is largely due to the cellular and architectural complexity *in vivo* and lack of appropriate *in vitro* hematopoietic vascular models. The following dissertation reports on the development of *in vitro* 3D human marrow microvascular platforms to study endothelial cells in the context of the marrow microenvironment. We describe the isolation and characterization of marrow-specific endothelial cells to determine their structural properties and their functional contributions to the marrow microenvironment. We demonstrate the co-culture of human marrow cells and endothelial cells to recapitulate an *in vitro* marrow microenvironment. To gain insight on thrombopoiesis, differentiating megakaryocytes were cultured in the microvessel platform observed over time. To examine the role of the microenvironment on the vasculature, we assessed the ability of marrow stromal fibroblasts to modify endothelial phenotype and demonstrated a role for fibroblasts and

monocytes in directing hematopoietic cell trafficking. The effect of leukemic cells on vasculature was assessed in the microvessel platform to examine disease-induced vascular remodeling. Overall, these studies demonstrate the utility of a marrow-specific microvessel platform to examine hematopoietic cell interactions with vasculature. By guiding the interplay of heterogeneous cell populations, we have demonstrated the capacity to define distinct microenvironment spaces. Further development of this 3D marrow platform will further our understanding of the endothelial role in stem cell trafficking, residence, and differentiation in health and disease.

TABLE OF CONTENTS

LIST OF FIGURES

ACKNOWLEDGEMENTS

I have been fortunate to learn and work alongside many generous and exceptional scientists during my time in graduate school. First and foremost, would like to thank my advisor, Dr. Ying Zheng, for her unparalleled support, advice, and encouragement. I am grateful for Ying's positivity and enthusiasm for science during my years of training. Her faith in me has instilled confidence in my abilities as a researcher and readiness to tackle challenges as they arise. I would also like to thank Dr. Beverly Torok-Storb for her incomparable dedication and guidance. I am so grateful for Bev's commitment to supporting my training and challenging me to become a better scientist. Both Ying and Bev are strong role models, and I will always be thankful for their influence on my life. I would also like to thank Dr. Nathan Sniadecki and Dr. Buddy Ratner for their insightful feedback and guidance in shaping the work presented here.

It has been a pleasure to work alongside the members of the Zheng lab, past and present. Their camaraderie, generosity, and genuine friendship have made time in the lab truly enjoyable and filled with humor. The Torok-Storb lab members have also provided immense support (and many vials of blood) towards this work. I also wish to thank the staff at the Garvey Imaging Core and Fred Hutchinson Electron Microscopy Core for their patience and many hours of training and assistance.

Finally, I would like to thank my family and friends. I am lucky to be surrounded by so many genuine and lovely people. I am grateful for all the long conversations, scientific and life advice, coffee runs, and lots of tasty food adventures, which have remedied any bad days and amplified the good days. To my parents, Minnu and Mohan, and my sister, Bhavani – your unconditional love and patience mean more to me than words can express.

CHAPTER 1

Introduction

1.1 BACKGROUND

Hematopoietic cells make up 90% of the cells in the body [1]. The bone marrow is the source of all these cells, where hematopoietic stem cells (HSCs) differentiate into the myeloid and lymphoid lineages to make up the red, white, and platelet fractions of blood. To maintain the number of cells in circulation, the marrow produces and mobilizes many billions of cells a day into the vasculature [2]. HSC maintenance, self-renewal, and differentiation is tightly controlled by not only spatiotemporal separation, but also the formation of distinct niche spaces within the marrow. The presence of bone marrow niches was first proposed by Schofield in 1978, who theorized that “specific cell-cell contact” created an environment to support HSC self-renewal [3]. Since then, interest in this topic has broadened alongside growing therapeutic usage of HSCs [4–7].

Though defining the hematopoietic stem cell niche and its relation to marrow vasculature have been contentious, improved definitions of hematopoietic cell types and imaging capabilities have resulted in a better visualization of these spaces [8,9]. Many studies have shown that the niche consists of a heterogeneous cell population (including osteoblasts, perivascular cells, and non-stem hematopoietic cells), matrix, and vasculature [10–12]. An understanding of the cell populations and architecture of these niche spaces, particularly in a human context, is necessary for further insight into the vascular marrow space and hematopoiesis. Furthermore, understanding the composition and functionality of the stem cell niche is critical to improving and expanding our knowledge of how the healthy microenvironment forms and how it is disrupted by disease.

This chapter reviews the components of the marrow hematopoietic niche, including the cell types and interactions involved in stem cell maintenance and differentiation followed by a brief summary of disruptions and therapeutic interventions to this microenvironment in disease.

1.2 HEMATOPOIETIC STEM AND PROGENITOR CELLS

HSCs are broadly defined by their ability to give rise to blood cells. HSCs in human marrow represent 0.01% of the nucleated marrow population, though they give rise to billions of blood cells per day [1,13–16]. There are two types of HSCs in the marrow, as determined by their differential ability to repopulate the entire hematopoietic system [13,14,17]. The most broad division of HSC populations include “long-term HSCs” (LT-HSCs), the most primitive and quiescent stem cells, and “short term HSCs” (ST-HSCs) which are more differentiated progenitor cells [13,14,18].

In humans, the most primitive HSCs are characterized by CD34+CD38-CD45RA-Thy1+ expression and have the potential to repopulate the entire hematopoietic compartment from a single cell [19]. As HSCs mature to multipotent progenitors they lose Thy1 expression, gain CD38 expression, and are characterized by reduced repopulating capacity and increased cell cycling [19,20]. Advanced imaging techniques in mice have shown that HSCs are typically located close to the sinusoidal vasculature of the marrow [7]. In the course of aging, more primitive HSCs appear further from the vasculature and closer to the endosteum [21].

1.3 THE HEMATOPOIETIC NICHE

In healthy bone marrow, HSC maintenance and differentiation are controlled by heterogeneous microenvironments termed niches, which can be located proximal to the bone (endosteal niche) or marrow vasculature (vascular niche) **(Figure 1.1)**. Though the vascular and endosteal niches are distinctly described in the literature, they are not fully separated from each other *in vivo* [22]. Rather, each of these spaces contains complementary signals for HSC maintenance and activation.

The endosteal niche is located at the border between the bone and marrow, and is described as a primarily osteoblast-defined space for LT-HSCs [21–24]. Studies on the endosteal niche in mice have noted that this space is relatively hypoxic, which has been shown to maintain the HSCs in a quiescent state [18]. The direct association of HSCs and osteoblasts allows direct and paracrine signaling to maintain the number and phenotype of HSCs in the niche [25–27]. Cytokines identified in this crosstalk include IL-6, GM-CSF, G-CSF, IL-1, TGFβ, and LIF, which have been associated with modulating HSC function [4,13,24].

The vascular niche consists of bone marrow endothelial cells (BMECs), pericytes, and HSCs. Pericytes and HSCs reside on the abluminal surface of the BMECs within the marrow, creating a microenvironment that involves crosstalk between all three cell types [7,18,28–32]. Pericytes, identified by their expression of Nestin+ or LeptinR+ in mice, support the sinusoidal vasculature to create a supportive HSC niche. In human marrow, stromal reticular cells characterized by CD146+ (MCAM) play an analogous role in supporting sinusoidal vasculature and promoting hematopoiesis within the marrow

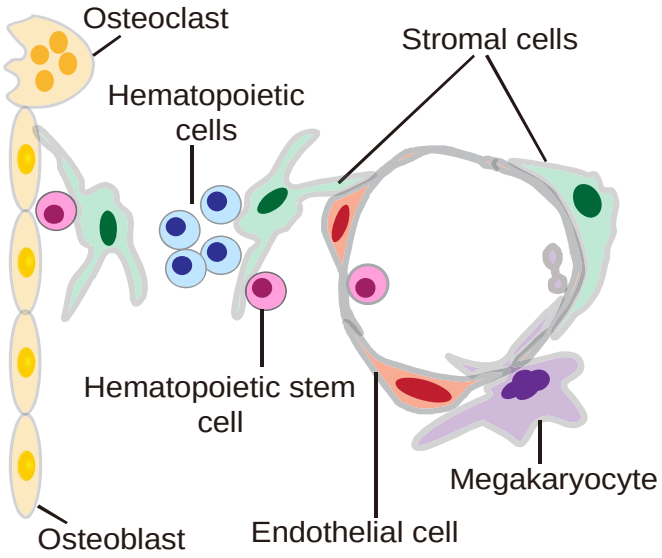

Figure 1.1. Model of the hematopoietic niche. The complex microenvironment supporting hematopoiesis within the marrow consists of multiple cell types, including endothelial cells, stromal cells, osteoblasts, and osteoclasts.

[33–35]. Pericytes secrete stem cell factor (SCF) and angiopoietin-1 (Ang-1), which are important for HSC quiescence through anti-apoptotic signaling [7,36–38]. These pericyte populations are also responsible for anchoring the HSCs in this space primarily through CXCL12 (SDF-1) interactions with CXCR4, which is expressed on HSCs and other hematopoietic cells [4,31,39]. The full complement of cytokines, adhesion molecules, and cell types that comprise the HSC niche, particularly outside of the murine context, are yet to be understood.

1.4 BONE MARROW VASCULATURE

The bone marrow vasculature acts as a checkpoint for migrating hematopoietic cells, and exerts control over cell trafficking through its complex signaling with the hematopoietic niche [15,40]. The marrow vasculature branches out from central arteries to smaller, thin-walled arterioles which terminate in sinusoids evenly distributed throughout the marrow [41]. First described in the 1960s and 1970s, the marrow sinusoidal vasculature is characterized by increased fenestrae, pores, and gaps in the endothelium [42–44]. These structural features contribute to the functional role of the marrow vasculature in supporting and modulating hematopoiesis. Observations of marrow endothelium notes its role in the passage of mature and maturing blood cells, such as erythrocytes, monocytes, and other cells **(Figure 1.2)** [42,44]. Megakaryocytes (MKs), for example, create pores through MMP secretion at the basement membrane from which they are able to shed platelets into the circulation [45,46]. However, whether similar processes occur in the case of erythrocytes or other myeloid cell types is not fully defined [47–50].

For resident hematopoietic cells, the low flow rate and leaky walls of the sinusoidal endothelium result in increased reactive oxygen species (ROS) levels near the vessel wall. For HSCs, increased ROS contributes to an activated rather than quiescent state, promoting differentiation towards mature blood cells [51,52]. Characterizing the role of the endothelial cell itself shows that when isolated from marrow aspirates and expanded *in vitro*, hBMECs directly support HSC maintenance and promote differentiation towards the MK and myeloid

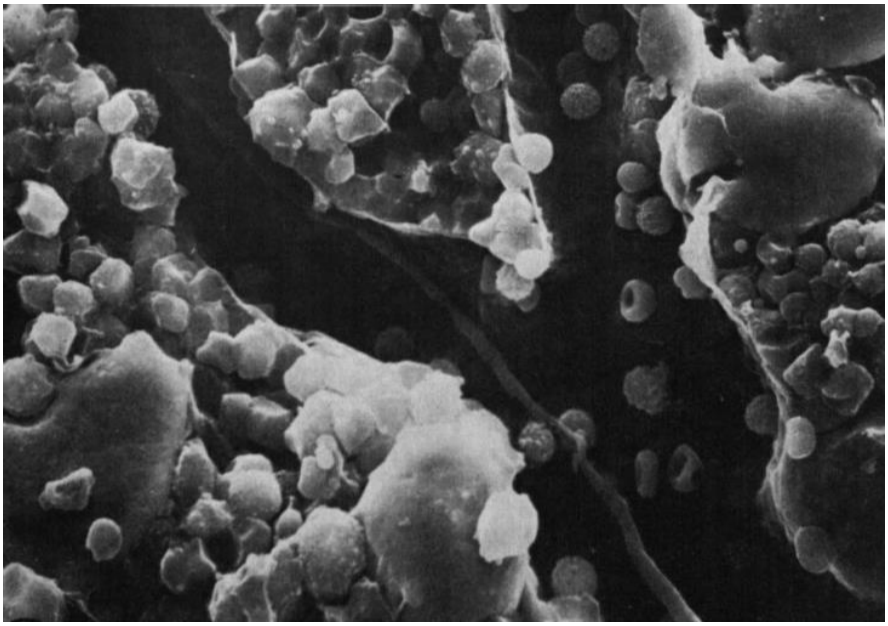

Figure 1.2. Scanning electron microscopic view of rat bone marrow. Luminal view of a sinusoid containing a proplatelet process (red arrow). Original magnification X900. Image from [53].

lineages [53,54].

In this and similar studies, marrow endothelial cells were isolated based on binding to Ulex europaeus agglutinin I (UEA1) and expanded *in vitro* [53,55]. Further characterization of this population shows expression of VCAM1, ICAM1, and E-Selectin compared to a more widely used human umbilical vein endothelial cell (HUVEC) population [56,57]. Murine marrow has been shown to display the same phenotype [58]. In addition, whole mounts of mouse marrow show intervascular heterogeneity, separating the marrow sinusoid from the arterioles, venules, and large vessels through expression of CD31, VE-Cadherin, and other endothelial markers [59,60]. The source of microvascular heterogeneity has been attributed to not only intrinsic cell phenotype but also microenvironmental influences [58]. While several studies have focused on the influence of endothelial cells on hematopoiesis, there has not been a reciprocal focus on the effect of the marrow microenvironments on endothelial phenotype [25,53,61]. An analysis of these complex niche contributions to endothelial phenotype would better inform the relationships between cellular components of the vascular niche.

1.5 THROMBOPOIESIS

HSC differentiation to specific lineages is compartmentalized within the marrow, as demonstrated through the process of megakaryocyte (MK) maturation. Differentiation of HSCs to MKs is directed by thrombopoietin (TPO) in the endosteal niche, which lies at the osteoblast layer near the bone. Collagen I secreted by osteoblasts anchors MKs via α2β1 integrin to the niche [62]. Collagen I allows for MK differentiation but prevents proplatelet release [62,63]. TPO drives the maturation of MKs through DNA replication without cytokinesis and the formation of a membrane reservoir for proplatelets [62,64–66].

Chemokines CXCL12 (SDF-1) and the soluble form of FGF-4 promote the migration of CXCR4+ MKs towards the sinusoidal microvasculature and away from the endosteal niche [67–71]. These factors, along with fibrinogen, enhance the spatiotemporal cues for MK migration, maturation, granule formation, and platelet release [62,72–

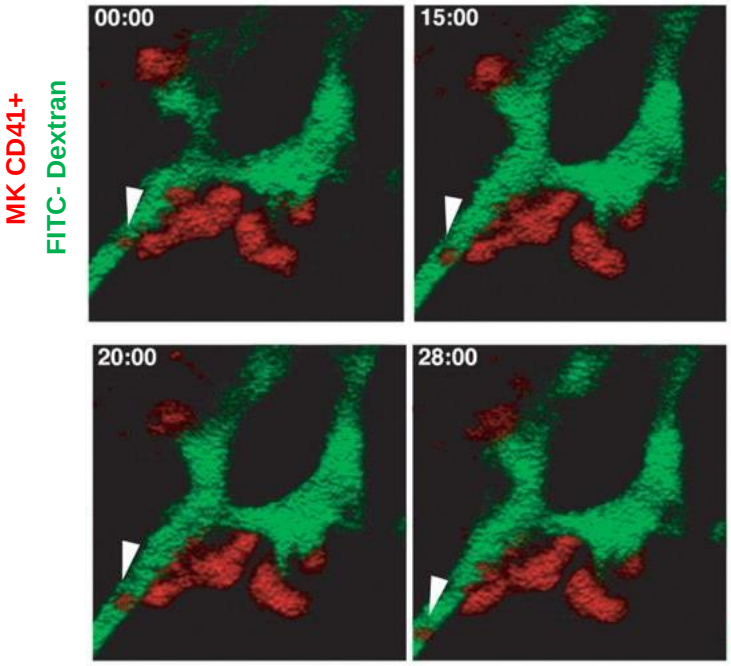

Figure 1.3. Platelet release from megakaryocytes into the circulation. Multiphoton imaging shows intravascular shedding of a MK fragment (arrowhead) in mouse marrow. Numbers at top left in each panel correspond to minutes and seconds. Scale bar = 50 μm. Image from [85].

74]. MKs develop an extended intercellular membrane network called the demarcation membrane system, from which platelets are formed [75]. Once at the vessel wall, MKs extend and release proplatelets fragments into the circulation (**Figure 1.3**) [74,76,77]. The signaling between MKs and vasculature that allows trans-endothelial projections and the final release of platelets into the circulation is complex, though recent studies have begun to visualize and characterize this process both *in vitro* and *in vivo* [45,46,74,77–79]. Of particular interest are the mechanisms behind endothelial pore formation, which, as evidence shows, is mediated by MMP secretion by MKs [45,46]. Platelet release has also been shown to rely on shear stress experience by proplatelets extensions in the circulation, highlighting the necessity of perfused vasculature in any *in vitro* platforms aimed understanding this process [76,80].

1.6 LEUKEMIA AND THE VASCULAR NICHE

Myeloid diseases disrupt the complex cell-cell signaling and architecture that control normal hematopoiesis. Acute myeloid leukemia is defined by the abnormal differentiation of hematopoietic cells within the myeloid lineages (granulocytes, monocytes, erythrocytes, megakaryocytes) coupled with unchecked proliferation. The accumulation of these abnormal cells within the marrow and peripheral blood overwhelm normal hematopoietic differentiation, and hijack the marrow microenvironment [81–84]. The leukemic niche is marked by malignant manipulation of CXCL12-mediated adhesion, appropriation of endosteal and vascular anti-apoptotic signaling, and expansion of hypoxic regions [81,84,85]. Colmone et al have demonstrated that leukemic cells take over the endosteal niche, then expand to the vascular niches. There, the leukemic cells secrete SCF and change CXCL12 expression by pericytes to disrupt normal HSC maintenance signals [81]. Subsequently, CXCL12 expression is downregulated and normal HSCs are no longer found in leukemia-corrupted vascular niches [81]. Expansion of the normal hypoxic and acidic regions in the bone marrow is also observed with the progression of leukemia [86]. Leukemic cells appear to adapt to proliferation in a hypoxic environment and induce HIF-1α production [83,86,87]. HIF-1α is known to control CXCR4 and VEGF, further modifying the normal marrow to create a leukemic niche. Normal hematopoietic differentiation fails in an overcrowded and hypoxic space created by leukemic cells.

Leukemic cells further modify the marrow space through remodeling the marrow vasculature [83,88]. Angiogenic induction in the tumor context is achieved when the malignant cells overwhelm negative regulators of angiogenesis [89]. In leukemic marrow, HIF-1α has been shown to control the upregulation of VEGF expression in both the leukemic cells and endothelial cells [90]. Clinically, increased angiogenesis correlates with worse prognosis, but not all AML patients display this phenotype [91,92]. More insight is required to understand vascular remodeling in leukemic marrow.

1.7 HEMATOPOIETIC STEM CELL TRANSPLANT

Hematopoietic cell transplant is one of the success stories of cancer therapy. Hematopoietic cell transplant is a potentially curative procedure for malignancies such as leukemias, lymphomas, certain anemias, or myelodysplastic syndromes. In these conditions, differentiation of hematopoietic cells is

disrupted, leading to improper blood cell production, cytopenias, or marrow failure. Patients first undergo chemotherapy and/or radiation to destroy the malfunctioning hematopoietic and immune cells present in the body. Then, healthy HSCs are infused intravenously into the recipient in order to reconstitute hematopoietic lineages with healthy, donor cells.

HSCs are obtained from cord blood, aspirated marrow, or collection of G-CSF-mediated HSC enriched peripheral blood [93–95]. In these applications, it is not practical for HSCs to be purified using a full complement of lineage markers. Instead, the total nucleated cell fraction is infused intravenously to the recipient. When HSCs are infused intravenously for a bone marrow transplant, HSCs recognize the marrow vascular environment, preferentially adhere, and transmigrate into the marrow space. This ability of transplanted to HSCs to home to and engraft within the marrow underscores the microenvironment-specific cues sensed from the circulation. The mechanisms behind HSC mobilization and homing, particularly in the context of marrow transplantation, have been the subject of intense study.

The process of HSC homing in bone marrow transplantation has been detailed using *in vitro* assays and murine *in vivo* experiments. Similar to leukocyte trans-endothelial migration, HSC homing occurs in three phases: rolling, adhesion, and transmigration through the vascular wall [6]. The initial rolling and tethering interactions occur primarily between CD44, P-Selectin glycoprotein ligand-1 (PSGL-1), LFA-1 (αLβ2 integrin) and VLA-4 (α4β1 integrin) expressed on the homing HSCs. These ligands attach to E-Selectin, P-Selectin, ICAM-1 and VCAM-1 on the endothelial cells [6,96–98]. Stromal cues support these interactions, as pericyte-derived CXCL12 triggers an increase in VLA-4 expression on CD34+ HSCs, which increases the chance of HSC-EC tethering via VCAM-1 [39,99,100]. CXCL12 gradients, along with other factors such as hyaluronic acid and osteopontin (expressed on osteoblasts) promote engraftment and adhesion within the marrow [6,101]. Increased understanding of these individual adhesive interactions along with the plethora of microenvironmental cues is important to better understand HSC homing and engraftment in marrow niche spaces.

1.8 ENGINEERING THE MICROVASCULAR SPACE

In vivo studies, particularly in mice, have enabled extensive and highly significant knowledge of the marrow microenvironment, including repopulation, homing, mobilization, and the influence of stromal cell populations [7,22,27,30,31,34,102,103]. Much of what is known today about human hematopoiesis has arisen from the study of long term bone marrow cultures *in vitro* [10,11]. This culture method has enabled detailed study of the maintenance and differentiation of hematopoietic progenitors alongside macrophages, stromal fibroblasts, and adipocytes, as cultures can be sustained *in vitro* for up to 1 year without the addition of serum [10,11].

More complex 3D culture platforms have improved access to media, incorporated perfusion, or allowed for multicellular compositions [78,104–106]. For example, Braccini et al fabricated a porous ceramic scaffold seeded with human marrow cells and perfused with media, supporting HSC expansion [107]. Di

Buduo et al fabricated a silk microtube embedded in silk sponge that incorporates flow to study the effect of shear stress on platelet generation from megakaryocytes [78]. While these approaches can mimic specific aspects of the bone marrow space, they do not incorporate key aspects of the niche such as functional vasculature, natural extracellular matrix, and multicellular composition. Overall, limitations to both *in vivo* and current *in vitro* culture systems remain. *In vitro* long-term cultures are able to utilize a human only cell system but lack the complexity present *in vivo*; *in vivo* systems, on the other hand, can be overly complex, limiting cell-level examination of specific interactions in a stepwise manner.

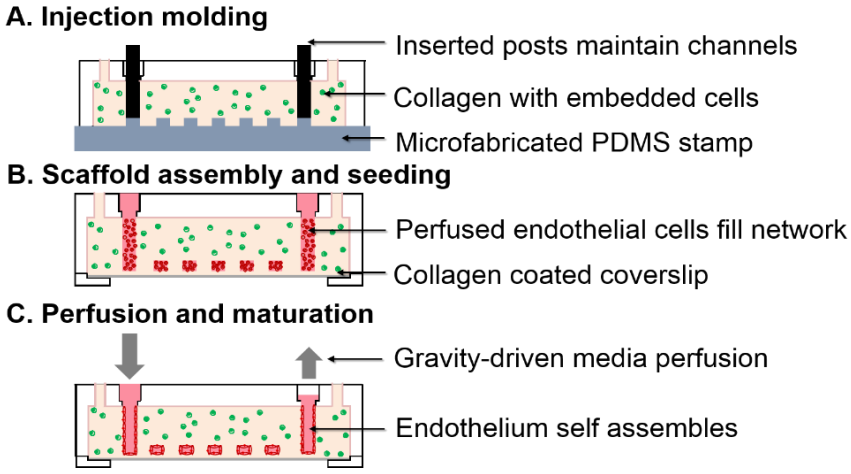

Figure 1.4. Microvessel Fabrication. (A) The vessel network is formed by injection molding of collagen with or without embedded cells onto a patterned stamp. (B) The network is sealed with a thin collagen layer followed by endothelial cell perfusion. (C) Endothelial cells self-assemble into an intact lumen. Media from the inlet is perfused through the network.

Attempts to model the marrow vascular microenvironment *in vitro* require the recapitulation of the 3D cellular architecture present *in vivo*, including the vasculature. Specifically, platforms must consider interconnectivity, luminal geometry, and appropriate perfusion to develop more biologically relevant vessels *in vitro*. There is a burgeoning need to engineer *in vitro* platforms that can incorporate appropriate cell types, architecture, and are capable of long term culture. Our lab has developed an engineered microvessel platform in type I collagen that can be modified to mimic organ-specific microenvironments containing functional vasculature [108–110]. Microvessels are fabricated through injection molding and soft lithographic patterning of collagen 1 to generate embedded networks (**Figure 1.4**). generated microvessels have endothelialized lumens, defined network structure, fully perfusable, and can incorporate organ-specific cells embedded in the surrounding matrix. Endothelial cells in this system are generally quiescent and form stable CD31 and VE-Cadherin junctions. These microvessels have been previous demonstrated to display important physiologic behaviors, such as the ability to initiate clot formation and angiogenic sprouting with the appropriate stimuli [108]. The incorporation of human marrow-specific cell types within this system enables the development of an *in vitro* vascular niche platform.

1.9 DISSERTATION OVERVIEW AND SIGNIFICANCE

The research presented in this dissertation pursues new strategies in modeling multi-cellular interactions of the human marrow cells with endothelium *in vitro*. Chapters 2 through 5 describe the rationale, scientific methods, and results of the four following aims:

Aim 1: Isolation and characterization of a 3D marrow endothelial niche

Aim 2: Development of an *in vitro* thrombopoietic niche

Aim 3: Hematopoietic cell trafficking in a fibroblast-directed niche

Aim 4: *In vitro* modeling of leukemia-induced angiogenic sprouting

The work contained in the following chapters has implications for the field of marrow engineering. The results of aim 1 provide insight into the characteristics of primary isolated human marrow cells applied to *in vitro* vessel cultures. Further, the co-culture of complex marrow populations with endothelial cell types demonstrates the potential use of engineered vessels to examine hematopoietic-vascular interactions. The results of aim 2 detail the terminal differentiation of megakaryocytes in the context of vasculature. The details of this interaction provide insight into the modulation of endothelial cells during platelet release. This demonstrates the potential use of an engineered system to study hematopoietic differentiation in many contexts. The results of aim 3 demonstrate the role of marrow stromal fibroblasts and hematopoietic cells in generating microenvironmental cues for stem cell migration. This co-culture model can enable detailed studies on the functional role of marrow cellular populations within the niche. The results of aim 4 demonstrate, to our knowledge, the first model of leukemia-induced vascular remodeling *in vitro*. This work represents significant progress in the advancement of *in vitro* strategies to model marrow vasculature and microenvironment for the study of hematopoietic cell mobilization, homing, differentiation, and disease with human cells.

Chapter 2

Isolation and characterization of a 3D marrow endothelial niche

2.1 ABSTRACT

Vasculature is a key component of hematopoietic processes within the bone marrow, acting as the checkpoint for cells entering and exiting circulation. The specific structural and function features of vasculature, particularly in the human context, that define the marrow endothelium are not fully understood. Here, we describe the isolation and characterization of human bone marrow endothelial cells (hBMECs). We describe the phenotypic distinctions between hBMECs and a standard endothelial cell type, human umbilical vein endothelial cells (HUVECs), including the expression of hematopoietically active cytokines and extracellular matrix. Detailed immunofluorescence and electron microscopy reveal key structural features such as large gaps, fenestrae, and caveloae in hBMECs, characteristic of sinusoidal endothelium. Analysis of monocyte interactions shows similarities of HUVECs and hBMECs in unstimulated conditions, but divergent response to inflammatory conditions. Further, we demonstrate the use of a 3D microvessel platform, incorporating fully human marrow populations, to reveal cell-cell interactions and the recapitulation of an *in vitro* endothelial niche.

2.2 INTRODUCTION

The endothelium controls blood cell trafficking, filtration, homeostasis, inflammation, and vasomotor tone, yielding diverse structure and function for each tissue in the body. This spatiotemporal heterogeneity has been appreciated in vascular biology for decades, yet much remains unknown about the intrinsic and extrinsic signals that support diverse endothelial phenotypes [111–115]. Early studies on the structural differences between tissue-specific endothelia revealed variation in shape, size, thickness, and transport structures present in these cells [111,116]. To reflect the major structural differences, three categories of endothelia have been defined: continuous non-fenestrated (brain, skin, heart, lung), continuous fenestrated (renal tubules, gastric and intestinal mucosa, endocrine and exocrine glands), and discontinuous or sinusoidal endothelium (liver, bone marrow) [111,117]. Each of these categories represent the tissue requirements for transport and permeability. In fenestrated and discontinuous endothelial beds, transport is facilitated by fenestrae, or transcellular pores with a diaphragm across the opening, caveolae, and vesiculo-vascular organelles, which are collections of vesicles and vacuoles [43,111,118,119]. Discontinuous endothelia also contain large gaps in the cell body.

The vasculature of the bone marrow acts as the gatekeeper to billions of hematopoietic cells released into the circulation daily [15,40]. As such, marrow endothelial cells must support hematopoiesis and the transmigration of mature blood cells [53]. Though studies have demonstrated isolation and culture of human bone marrow endothelial cells (hBMECs), the use of these cells has not been widely adopted in

modern vascular biology and bioengineering efforts [57,100,120]. Recent insight in the molecular phenotype of various mouse endothelial cells as related to both intrinsic and environmental influences points to a need for similar efforts in human marrow endothelial cells [58,115].

Ongoing efforts to understand marrow vascular function and microenvironment have relied on both simplified 2D and complex 3D platforms, particularly when using human cells. However, the current state-of-the-art for marrow vascular microenvironmental studies use human umbilical vein endothelial cells (HUVECs) [78,104,121]. These cells are from large vessels, and their native environment supports a vastly different function than the marrow environment. The marrow sinusoidal vasculature, contrastingly, is relatively smaller in diameter (50-100 μm) and are the major component to the marrow vascular niche, home to hematopoietic stem and progenitor cell populations [cite sinusoid size] [7,36,117]. Studies on both human and mouse marrow endothelial cells highlight the contribution of endothelial cells to support hematopoiesis and differentiation [53,60,122]. The use of hBMECs in 3D cultures and advanced *in vitro* models can allow us to gain insight into the function of the human vascular niche.

The isolation of human marrow endothelial cells highlights the unique structural and functional properties of marrow-specific endothelial cells compared to a standard HUVEC cell. These differences will promote the use of hBMECs in human specific *in vitro* marrow platforms to more completely model the marrow space. Here, we have demonstrated our ability to isolate, maintain, and use these cells along with the full marrow cell fraction to create an *in vitro* human marrow platform.

2.3 EXPERIMENTAL METHODS

Marrow cell isolation

Marrow cells were obtained from discarded filters used to strain bone marrow following marrow aspiration from healthy donors in compliance with Institutional Review Board protocol, approved by the University of Washington and Fred Hutchinson Cancer Research Institute. The screen and filters containing hematopoietic cells as well as marrow fibroblasts, stromal cells, bone spicules, and fat cells were reverse perfused with 30-60 mL of phosphate buffered saline (PBS) with 0.2 mM EDTA and was passed through a 40 μm filter to separate out large cells, bone chunks, and fat globules from the single cells. The collected cell clumps larger than 40 μm were digested with trypsin (0.05%) with EDTA. Trypsin (0.05%) with EDTA was also perfused to dissociate remaining cells from the filter and tubing. The resulting cell suspension was collected in a 50 ml conical tube and spun at 400 g.

For endothelial cell isolation, the isolated marrow cells were plated in gelatin coated T75 flasks with Endothelial Cell Basal Medium (Sigma) supplemented with heparin (50 μg/mL, Sigma), endothelial cell growth supplement (100 μg/mL, Sigma), 10% fetal bovine serum, 1% antibiotic-antimycotic (Life Technologies), and VEGFA (40ng/mL, R&D Systems). Cells were expanded in a low oxygen incubator (5% O2) for 7-10 days with periodic removal of non-adherent cells. Cells were dissociated using Trypsin-EDTA

(0.05%), stained with VE-Cad (CD144)-APC and CD45-Pacific Blue (BD), and flow sorted to purify the endothelial population. The resulting VECAD+CD45- population was plated in gelatin-coated T25 flasks in normoxic conditions and allowed to reach confluence in endothelial growth media for 7-10 days.

Mononuclear cells from the filtrate were isolated through centrifugation with Ficoll-Paque (specific gravity 1.077) at 450 g for 30 minutes at room temperature. For marrow mononuclear cell (hBMMC) studies, this fraction was resuspended and stored at 4C overnight in PBS with 10% fetal bovine serum (FBS) or frozen in CryoStor CS10 prior to use.

RNA Sequencing

Purified hBMECs were isolated and RNA was harvested from a well of a six-well plate using an RNeasy mini kit (Qiagen) with on-column DNase digestion to remove genomic DNA. RNA concentration was quantified using 2µL of total RNA with a Nanodrop 1000 Spectrophotometer. RNA Seq was performed using Illumina something. Processing the resulting data included the removal of reads that didn't pass Illumina's base call quality threshold and alignment to hg38 using TopHat v2.1.0. Counts generated for each gene using htseq-count v0.6.1p1 (using the "intersection-strict" overlapping mode). Genes that did not have at least 1 count/million in at least both samples were removed. Data was normalized and significance testing was performed using the GLM method in edgeR v3.18.1. A gene was considered significantly differentially expressed if |logFC| >= 0.585 & FDR 5%. Functional enrichment of top 200 significantly upregulated genes was performed via ToppFun. The top GO terms in Molecular Function and Cellular Components were represented via heatmaps generated with MultiExpression Viewer, with means clustering by gene. The top 200 most significantly upregulated genes were visualized via Ingenuity Pathway Analysis and displayed in pathway format.

Vessel Fabrication

3D microfluidic networks were fabricated as described previously [108–110]. Briefly, soft lithography created a PDMS mold patterning a 100µm-diameter network, and injection molding over the PDMS mold created a 100 µm collagen I gel microvessel which was sealed with a collagen-coated coverslip (Figure 1A) [108–110]. For vessels with embedded marrow cells, hBMMCs were embedded within the collagen at 8-10million cells per mL. The channels were then perfused with either hBMECs (matched donor, passage 1) or HUVECs (passage 5-6), which adhered to the collagen and self-assembled into a functional microvessel with an open lumen. Endothelial cell culture media added to the inlet reservoir flowed through the network driven by gravity, undergoing approximately an 8-fold reduction in flow (~0.1 dyn/cm at minimum). Vessels were cultured for 2 days prior to analysis.

Immunofluorescence Microscopy

hBMECs were plated on gelatin coverslips and cultured for 3 days prior to fixation in 4% formaldehyde. After washing with PBS, cells were permeabilized with PBS and 0.05% Triton-X 100 for 10

minutes, then primary antibodies for von Willebrand Factor, VE-Cadherin, PV-1 or Caveolin-1 were added in 2% bovine serum albumin overnight at 4C. Secondary antibodies Alexa Fluor-488, -568, or -647 or Phalloidin-568 were added for one hour after washing with PBS along with Hoechst.

For vessel studies, staining was accomplished through perfusion of immunofluorescence reagents through the microvessel network as described previously [108]. Coverslips and microvessels were imaged on a Nikon A1R confocal microscope with a 10X, 20X or 40x oil immersion objective. Z-projections generated using Image J.

Electron Microscopy

Cells on gelatin-coated glass coverslips were fixed in half-strength Karnovsky's solution (2% paraformaldehyde/2.5% glutaraldehyde in 0.2 M cacodylate buffer) overnight. Microvessels were fixed *in situ* by perfusing half strength Karnovsky's solution overnight, then fully immersed in the same solution for 2-3 days after disassembly to expose the luminal surface. Samples were then washed with 0.1M Cacodylate Buffer wash 3X for 10min. Coverslips were treated with post-fix was in 2% aqueous Osmium tetraoxide in 0.2 M Cacodylate Buffer (1:1) for 2 hours at 4C. All samples were washed in 0.1 M Cacodylate Buffer wash 3X for 10 min each prior to dehydration in graded ethanol solutions (50%, 70%, 85% and 100% ethanol).

For scanning electron microscopy, coverslips were immersed in hexamethyldisilazane (HDMS) and dehydrated overnight in a fume hood. Microvessels were dehydrated using critical point drying. All samples were sputter coated with Gold/Palladium and imaged using a JSM-6610LV Series Scanning Electron Microscope with accelerating voltage of 5 kV, spot size 25.

For transmission electron microscopy, samples were immersed in propylene oxide (PO), before 1:1 PO/Epon 812 (Ted Pella Inc) immersion overnight. Fresh Epon 812 was then exchanged for 2 hours after which the blocks were cured for 48 hours at 60°C. Ultrathin sections (70 nm) were cut from blocks using a diamond (Diatome US) blade on a Leica EMUC6 ultra-microtome and placed onto grids. Grids were stained with uranyl acetate for 2 hours and lead citrate for 5 minutes. Sections were imaged using a JEOL JEM-1400 Transmission Electron Microscope (JEOL Ltd.) using 100 kV acceleration voltage. Images were acquired with a Gatan Ultrascan 1000XP camera (Gatan, Inc.)

Monocyte Adhesion

For 2D monocyte adhesion studies, hBMEC cells (passage 1) and HUVECs (passage 5) were seeded into 96 well plates and allowed to reach confluence for 2 days. Peripheral monocytes were obtained from fresh blood samples under protocols approved by the Institutional Review Board at the Fred Hutchinson Cancer Research Institute. Mononuclear cells were isolated from fresh blood through Ficoll-Paque centrifugation (specific gravity 1.077) at 450 g for 30 minutes at room temperature. Monocytes were purified from this fraction through incubation with CD14 microbeads (Miltenyi Biotec) for 40 minutes at 4°C,

washed with PBS/1% FBS, and purified using magnetic cell sorting (Miltenyi Biotec). The monocytes were then incubated with CD14-PE, CD11b, and CD45-PE (BD Biosciences) for 20 minutes at 4C, washed twice, and stained with Anti-R Phycoerythrin (Texas Red) for 1 hour. After washing with PBS/2% FBS, labeled monocytes were resuspended to 2 million cells per mL in PBS/5% FBS.

Cytokines IL-1β (2ng/mL) or TNFα (10ng/mL) were added to cell culture media for 2 hours and 1 hour respectively prior to monocyte solution. Endothelial cell wells were washed once with warm media, and then 100uL of monocyte cell solution was added to the wells (200,000 total cells per well) and incubated for 30 minutes at 37C. Wells were washed with PBS/5% FBS 5X and immediately fixed in 4% formaldehyde. After 3 PBS washes (10 minutes each), cells were permeabilized with PBS and 0.05% Triton-X100 for 20 minutes. Cells were stained with Hoechst and Phalloidin-647 in PBS for 40 minutes. Wells were imaged using a Nikon TiE Inverted Widefield Fluorescence Microscope with 10X or 20X objectives. Conditions were run in triplicate. Quantification of the number of monocytes was compared to the number of EC nuclei (total nuclei minus number of monocytes) was performed for 6 fields of view per well. Statistical differences were calculated using a Welch's t-test. Error bars represent standard error measurement.

Monocyte Perfusion

For monocyte adhesion studies in vessels, monocytes were perfused through vessels after 2 days of culture. Monocytes were added to the inlet of the vessel (100,000 cells in 100 µL PBS/5% FBS) and allowed to perfuse for 30 minutes. Any remaining cell solution was then removed and vessels were washed with media twice for 30 minutes each. 24 hours after perfusion with cells, vessels were fixed in 3.7% formaldehyde (20 minutes) and washed with PBS three times (20 minutes each). Vessels were stained with Hoechst and phalloidin-647 as described for 2D assay and imaged with a Nikon A1R confocal microscope with a 10x objective. Z-projections generated using Image J.

Quantification of monocyte adhesion and migration with relation to the vessel wall was analyzed using 3-10 confocal images of each vessel (n=3). Image stacks of the vessel (120 µm depth) were z-projected to a single plane and coordinates of vessel borders were manually selected. Coordinates of PE-labeled monocytes were located via particle analysis on thresholded images. Distances from cells to the vessel were calculated assuming that the cells migrated from the closest vessel wall. Cells that were located within the vessel boundaries were counted as adherent to the vessel wall. Distance from the nearest vessel was normalized to the vessel radius. Cell adhesion and migration data of perfused hematopoietic cells was calculated as a percent of estimated total perfused cells (based on the concentration and volume of cell suspension added to the reservoir and the gravity driven flow rate). A sensitivity analysis of high, middle, and low estimates (75,000; 50,000; and 25,000 cells) was performed, showing no effect of the total number perfused cells on significant differences between groups. Data is presented based on a low estimated number of perfused cells. Significant differences between groups were determined using 2 sample, 2 tailed student’s t-test. Error bars represent standard error measurement.

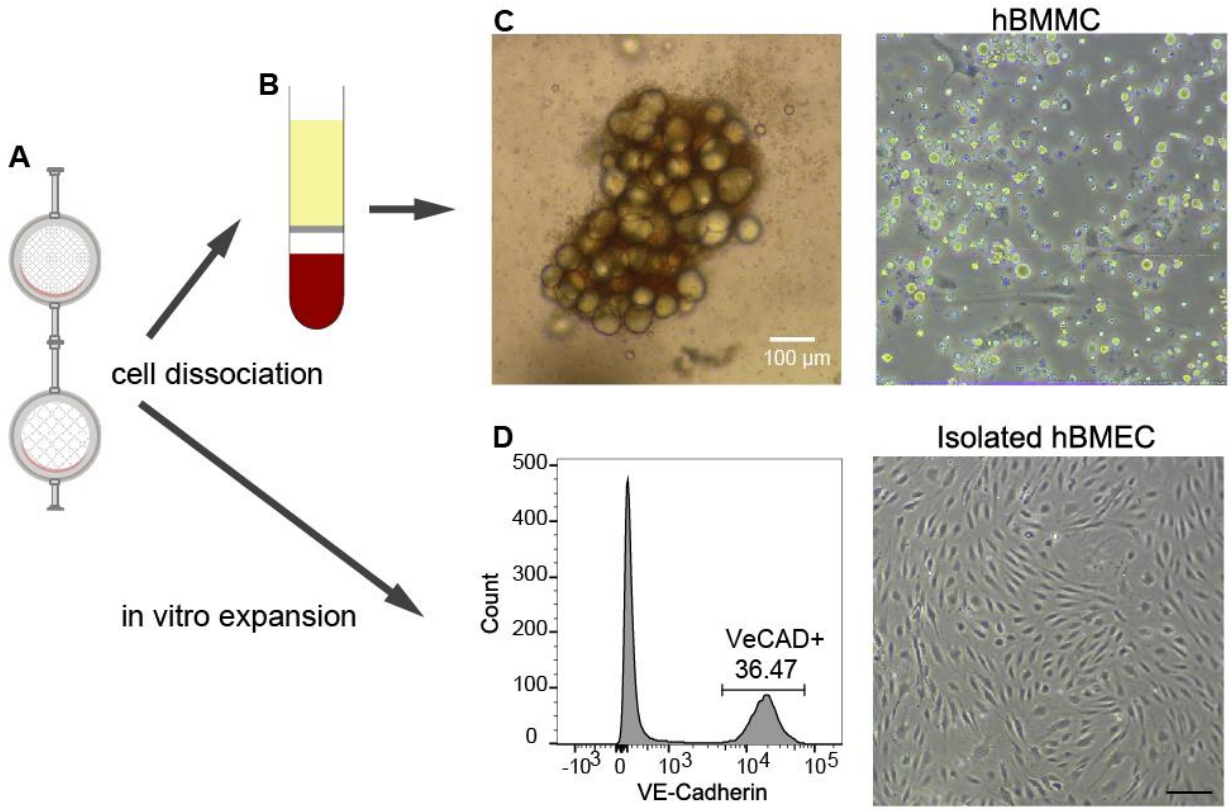

Figure 2.1. Marrow cell isolation and endothelial cell purification. (A). Filters from healthy marrow donors containing hematopoietic, stromal, adipogenic, and endothelial cell populations are reverse perfused to remove cells. (B) Ficoll-paque separation yielded a mixed mononuclear and stromal fraction. (C) Larger cell clumps were digested. Plated cells are heterogeneous. (D) After *in vitro* expansion, CD45-VECAD+ endothelial cell populations were purified and expanded. Scale bar = 50 um.

2.4 RESULTS

RNASeq reveals marrow-specific endothelial phenotype

Marrow cells were sourced from screens used to filter marrow donations from healthy donors. The reverse perfusion of these screens with PBS and trypsin allowed for mechanical and enzymatic dissociation and isolation of complete marrow populations. These cells (Figure 2.1 C) were either frozen as a complete population or the adherent cell population was expanded. After 7-10 days of culture, the CD45-VECAD+ endothelial population was purified using fluorescence activated cell sorting (Figure 2.1 D). The resulting cell population displayed cobblestone morphology in culture, typical of endothelial cells.

RNASeq was performed to examine global differences between hBMECs and a standard endothelial cell type, HUVECs. Functional enrichment of the top 200 genes with significantly increased expression in the hBMECs included genes for extracellular matrix components, including collagens (types 22, 1, 3, 5, 6, 7, 15) and laminin A1, and versican. Matrix metalloproteinases MMP1 and procollagen aminopropeptidases (ADAMTS14, ADAMTS2, ADAMTS5) also have increased expression in the hBMEC populations suggesting an increased role for matrix remodeling by marrow endothelial cells (**Figure 2.2 B*)***.

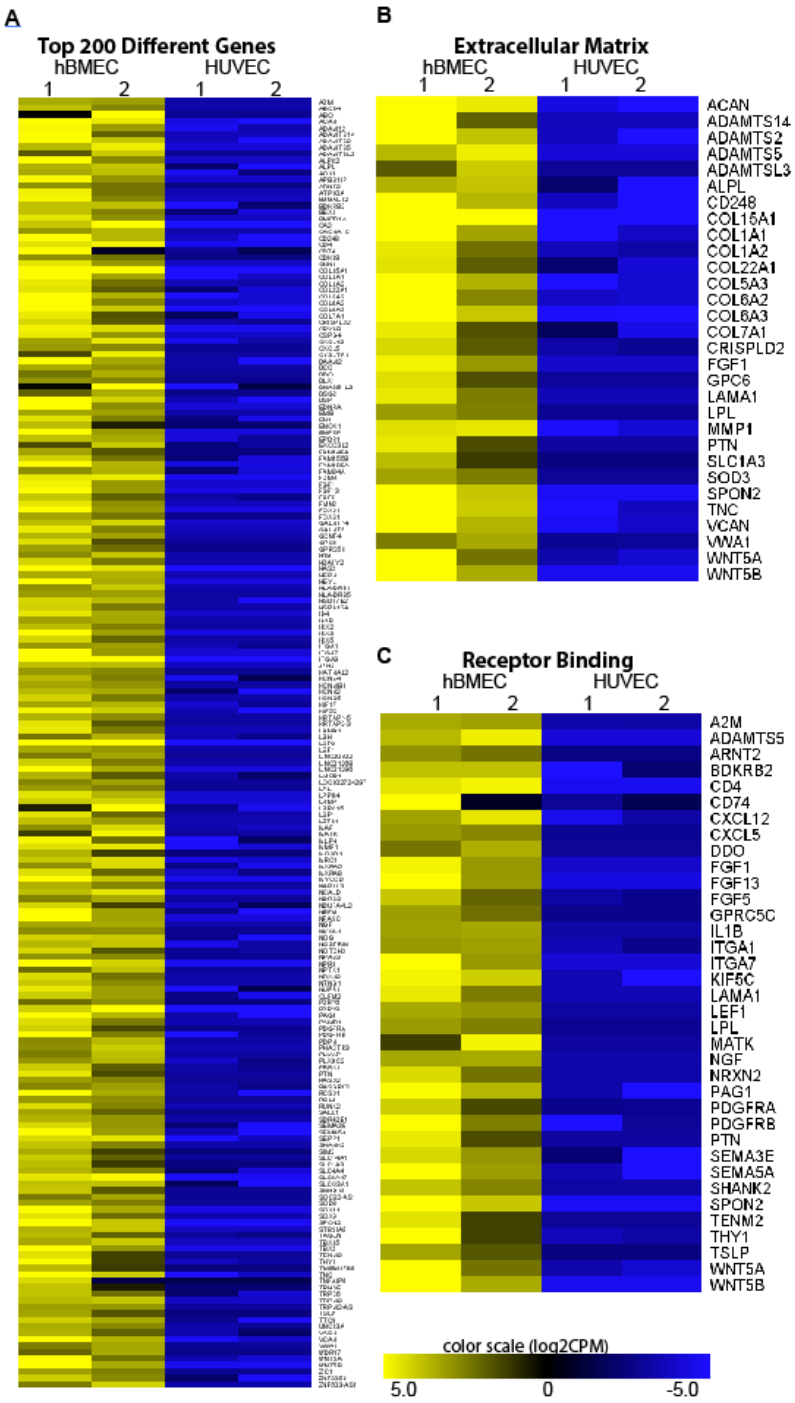

Figure 2.2. Expression profile of hBMECs compared to HUVECs. (A) The top 200 most significantly upregulated genes in hBMECs are displayed in a heatmap. Yellow indicates higher than average expression and blue indicated lower than average expression. (B) Functional enrichment shows upregulated extracellular matrix associated genes and (C) receptor binding genes in hBMECs.

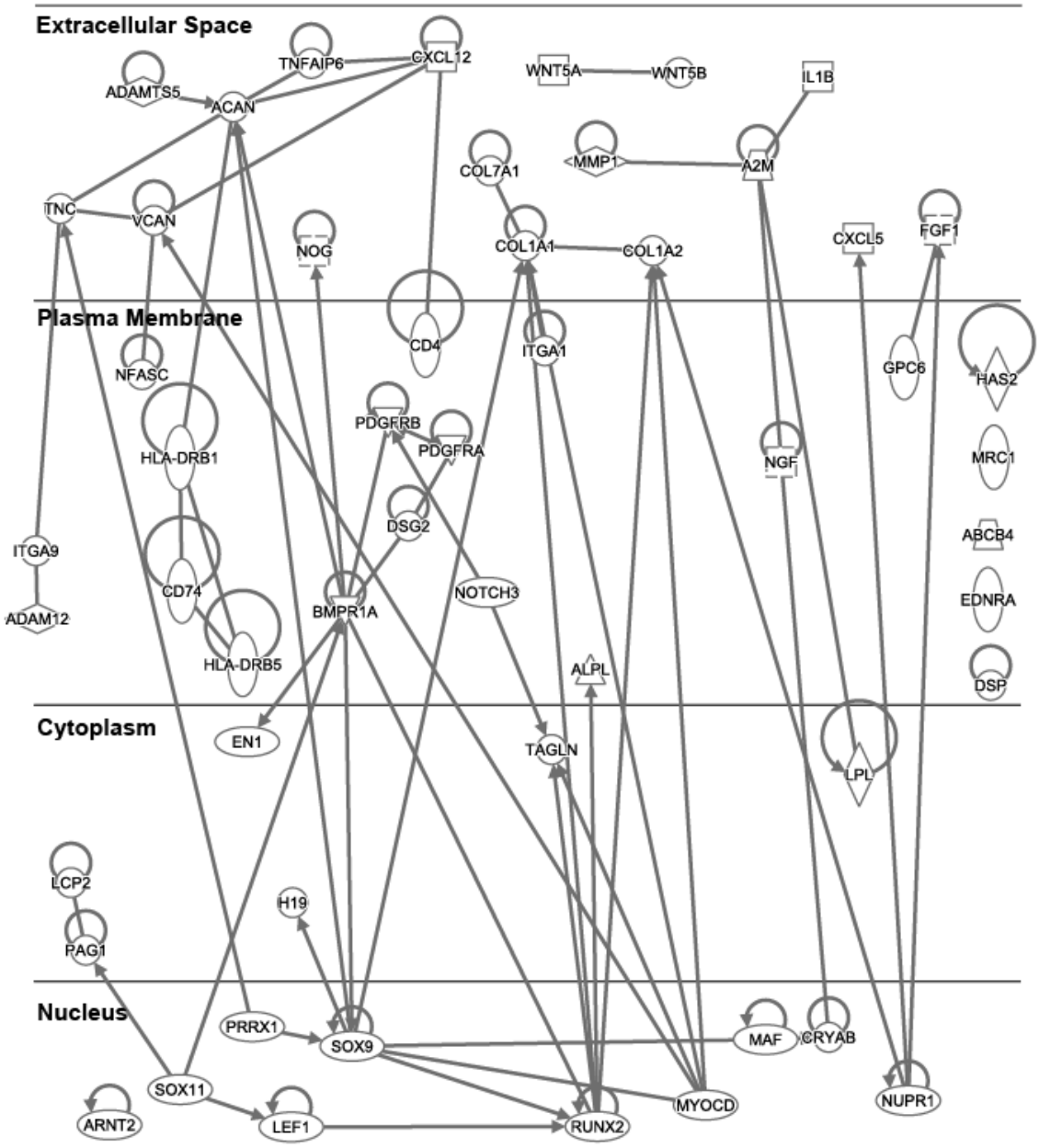

Figure 2.3. Pathway representation of upregulated genes in hBMECs. The top 200 significantly upregulated genes are represented in pathway format, separating genes operating in the extracellular space, plasma membrane, cytoplasm, and nucleus. Arrows between genes indicate activation interactions.

Increased expression of hematopoietically active secreted proteins are also present in hBMECs, such as CXCL12, CXCL5, IL-1β, WNT5A, and WNT5B (**Figure 2.2 C**). Interestingly, genes involved in neuronal guidance such as SEMA3E, SEMA5A, NRXN2 and TENM2 are also present, reflecting the close relationship of marrow vasculature with the nervous system [123]. Expression of cell surface proteins such as PLVAP (PV-1), a protein involved in the formation of diaphragms in permeable endothelium is also

increased in hBMECs. These molecules have been implicated in inflammation chemoattraction, and the maintenance of hematopoietic cells *in vivo* [36,124–130]. Activation of these factors visualized in a pathway map illustrates the multifaceted implications on cell signaling based on the gene expression profile and secreted cytokines such as IL-1b, CXCL12, and CXCL5 (**Figure 2.3**).

Structural characterization of hBMECs

Characterization of hBMECs using immunofluorescence staining and electron microscopy revealed expression of standard endothelial markers, such as Weibel Palade bodies and VE-cadherin (**Figure 2.4 A**). Bone marrow sinusoidal endothelial cells are characterized by the presence of gaps, which are large circular pores, and fenestrations with and without diaphragms [111]. PV-1, a protein associated with diaphragms and caveolae in endothelial cells, is detected throughout the hBMEC body supporting the RNAseq data. The co-localization of caveolin-1 and PV-1 indicates the presence of stomatal diaphragms on the endothelium (**Figure 2.4 B**) [131]. PV-1 is also detected independent from caveolin-1, suggesting the presence of fenestral diaphragms. In contrast, PV-1 was detected at very low levels in HUVECs, supporting the RNAseq data which also indicates very low expression of PV-1 in HUVECs (**Appendix A, Supplementary Figure 1**) [109]. These features are also apparent in electron microscopy images. We observe both strong junctional association and the presence of gaps through the cell body via scanning electron microscopy and transmission electron microscopy (**Figure 2.4 C**). Fenestrae and caveolae, both with and without diaphragms are also observed via transmission electron microscopy (**Figure 2.4 D,E**).

Monocyte adhesion to hBMECs and HUVECs responds to inflammatory cytokine stimulation

In vitro assessment of monocyte adhesion can indicate the adhesiveness and inflammatory status of endothelial cells. Immunofluorescence imaging shows the adhesion of monocytes to hBMECs, associated holes in the cell cytoskeleton, and the transmigration of nuclei through the monolayer (**Figure 2.5 A**) [132]. These phenomena are also observed in scanning electron microscopy (**Figure 2.5 B**). Quantification of monocyte adhesion showed no differences in monocyte adhesion between unstimulated hBMEC or HUVEC monolayers (**Figure 2.5 C**). Upon stimulation with either TNFα or IL-1β, more monocytes adhere to both cell types compared to the baseline. In IL-1β treated conditions, monocyte adhesion increased by 0.71 +/- 0.11 and 4.73 +/- 0.29 fold in hBMEC and HUVEC conditions, respectively (**Figure 2.5 D**). In TNFα treated conditions, a 1.11+/- 0.27 and 3.43+/- 0.44 fold increase in monocyte adhesion was observed on hBMEC and HUVEC monolayers, respectively. In both IL-1β and TNFα treated conditions, the relative increase in adhesion compared to unstimulated controls is observed to be much higher in HUVECs than hBMECs.

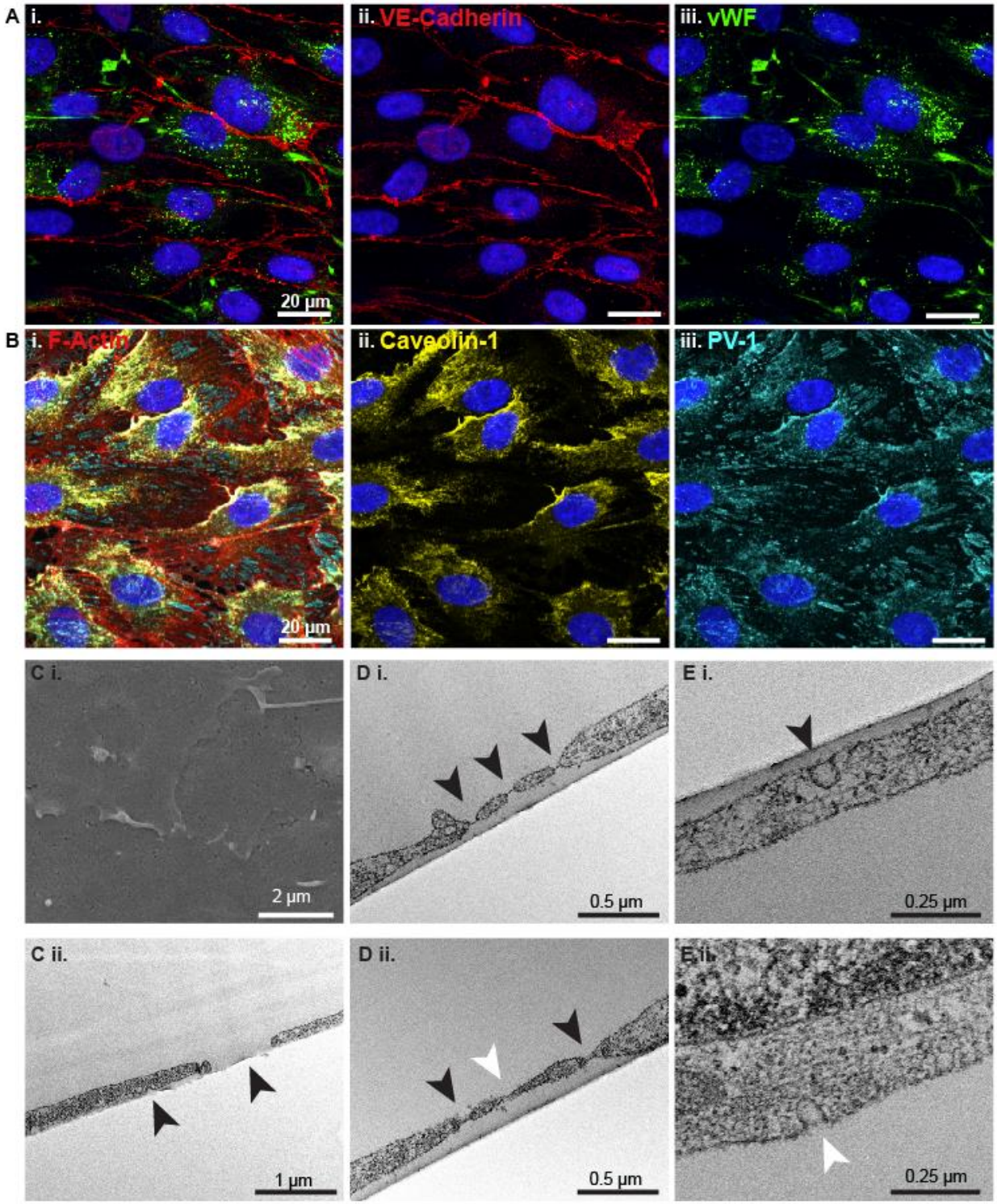

Figure 2.4. Immunofluorescence confocal and electron microscopic characterization of hBMECs. (A) Immunofluorescence staining of VE-Cadherin (ii) and von Willebrand Factor (iii). (B) Immunofluorescence staining of F-actin, caveolin-1 (ii), and PV-1 staining (iii). (C) (i) Scanning electron microscopy of hBMEC monolayers shows endothelial junctions. (ii) large gaps within the cell body are seen via transmission electron microscopy. (D) Fenestrae (i) with diaphragms (black arrowheads) and (ii) no diaphragms (white arrowhead) are indicated. (E) Caveolae with diaphragms (i, black arrowhead) and without diaphragms (ii, white arrowhead) are observed via transmission electron microscopy.

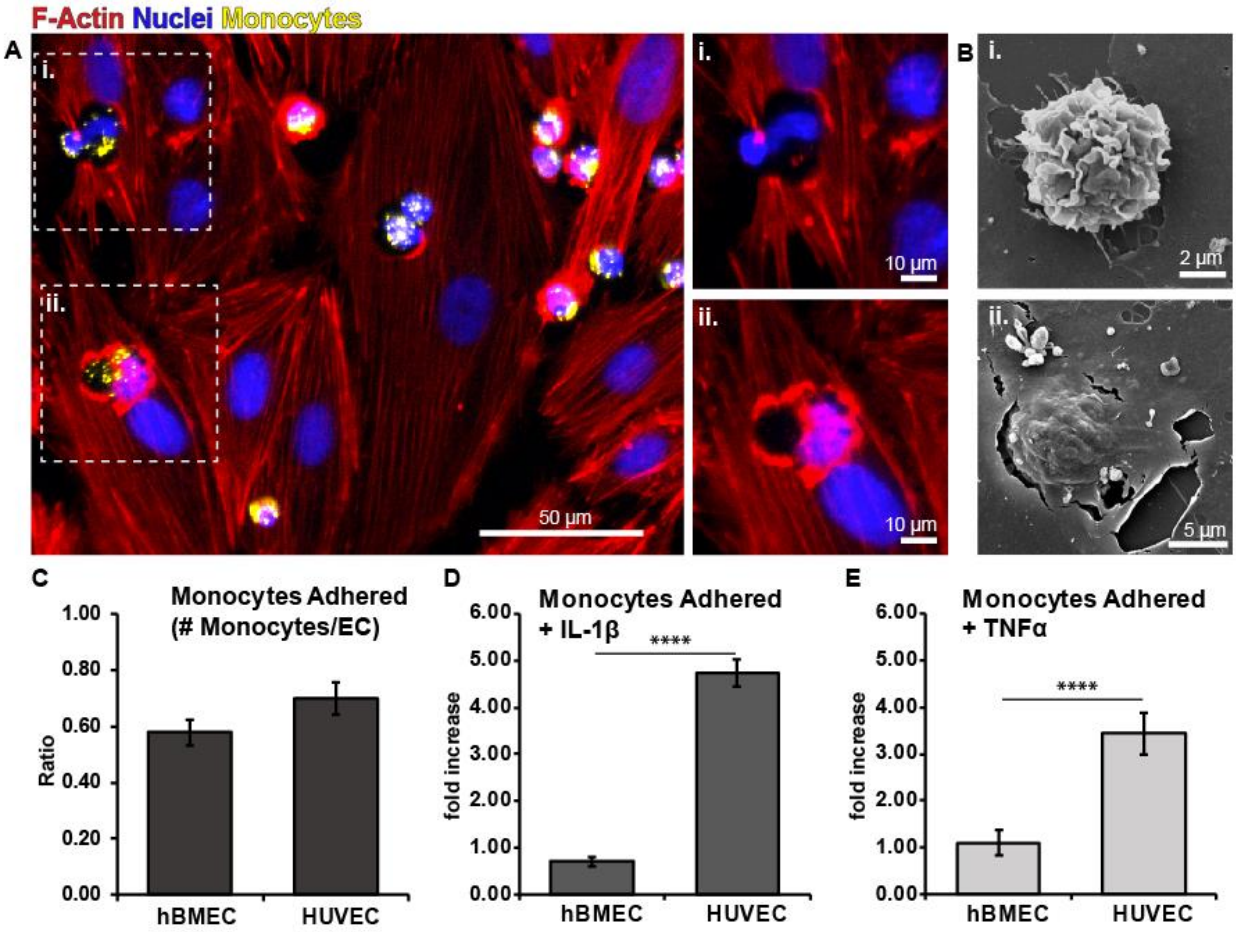

Figure 2.5. Monocyte adhesion on hBMECs and HUVECs. (A) Immunofluorescence imaging of F-actin shows and monocyte adhesion to endothelial cells. Zoomed views of monocytes in regions (i) and (ii) shows modification of endothelial actin during transmigration under the endothelial monolayer. (B) Scanning electron microscopy shows monocytes interacting with hBMEC monolayers. (C) quantification of monocyte adhesion to unstimulated hBMEC and HUVEC monolayers shows no differences in the ration of monocytes adhered per EC. (D-E) hBMEC and HUVEC monolayers stimulated with IL-1β (2ng/mL) or (E) TNFα (10ng/mL) show increases in monocyte adhesion. Fold increases to adhesion in stimulated HUVECs are significantly greater.

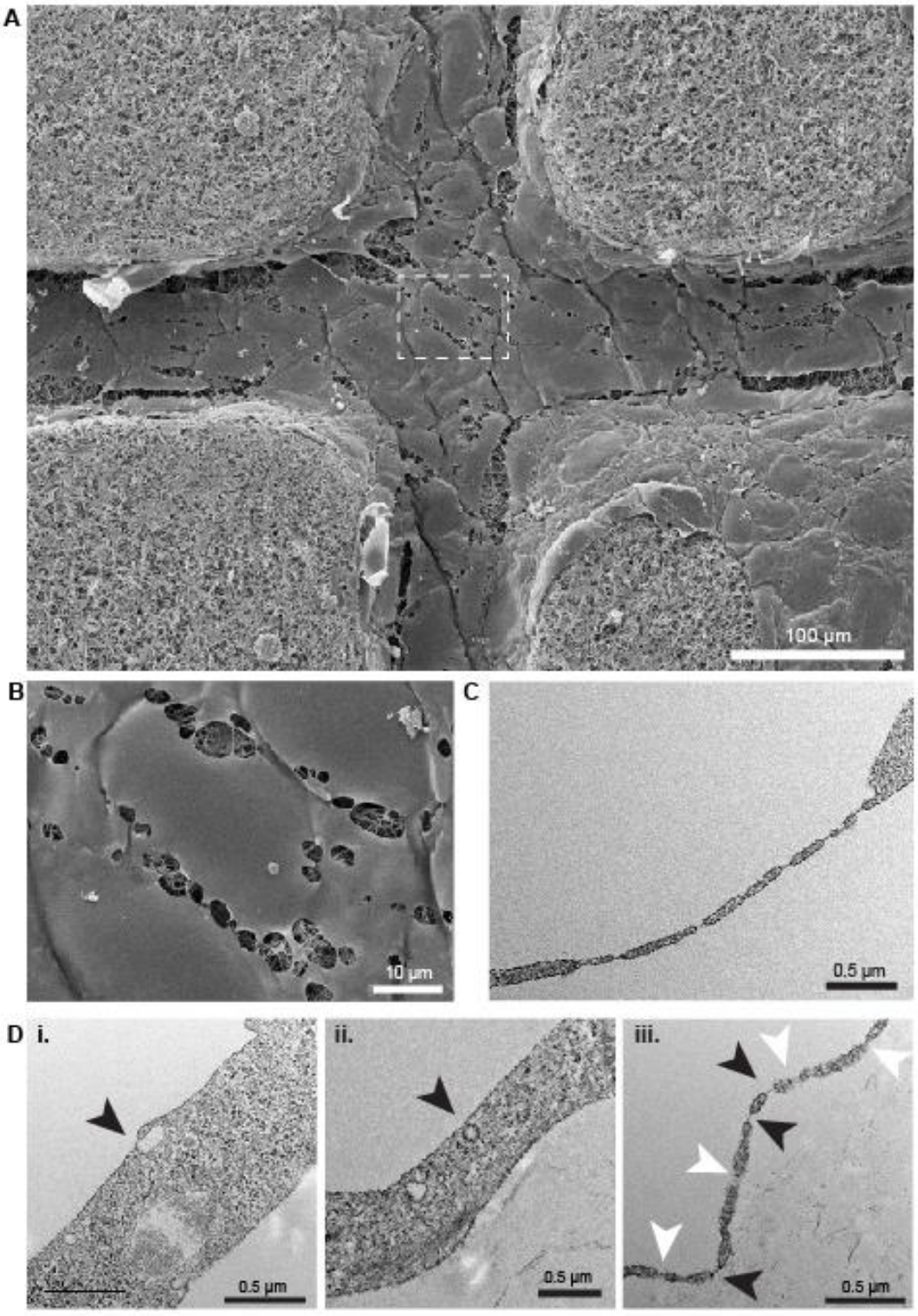

Figure 2.6. hBMECs in 3D microvessels. (A) Scanning electron microscopy of hBMECs in a 3D microvessel shows many endothelial pores. (B) zoomed view of boxed region in (A). (C) Transmission electron microscopy shows fenestral diaphragms. (D) Caveloae (i, arrowhead) with and (ii, arrowhead) without diaphragms are observed. (iii) Fenestrae with diaphragms (black arrowheads) and without diaphragms (white arrowheads) are observed.

Structural and functional features of hBMECs are maintained in 3D cultures

To recapitulate a more biologically relevant geometry, endothelial cells were seeded into a collagen-based 3D microvessel network as described previously [108–110]. Briefly, soft lithography and injection molding allows the fabrication of perfusable embedded channels in type I collagen. Perfused hBMECs self-assembled into an intact lumen. Electron microscopy revealed extensive endothelial gap formation, both at endothelial junctions and through the cell body (**Figure 2.6 A,B**). Gaps averaged 8.6 +/- 5.0 µm in diameter. Transmission electron microscopy revealed the presence of fenestral diaphragms and caveolae maintained in 3D perfused culture (**Figure 2.6 C,D, arrowheads**).

Monocyte - endothelial interactions have been shown to change adhesion dynamics under flow compared to static cultures [133–135]. Freshly isolated, labeled monocytes were perfused through 3D microvessels to assess monocyte adhesion and transmigration events (**Figure 2.7 A**). The estimated percent of perfused monocytes that adhered to the endothelium or transmigrated into the surrounding matrix was calculated. Similar to 2D conditions, monocytes do not adhere significantly differently to hBMECs or HUVECs, as determined by a 2 sample, 2 tailed student's t-test (**Figure 2.7 B**). The percent of perfused monocytes that transmigrated into the collagen matrix also show no difference between hBMEC and HUVEC vessels (**Figure 2.7 C**).

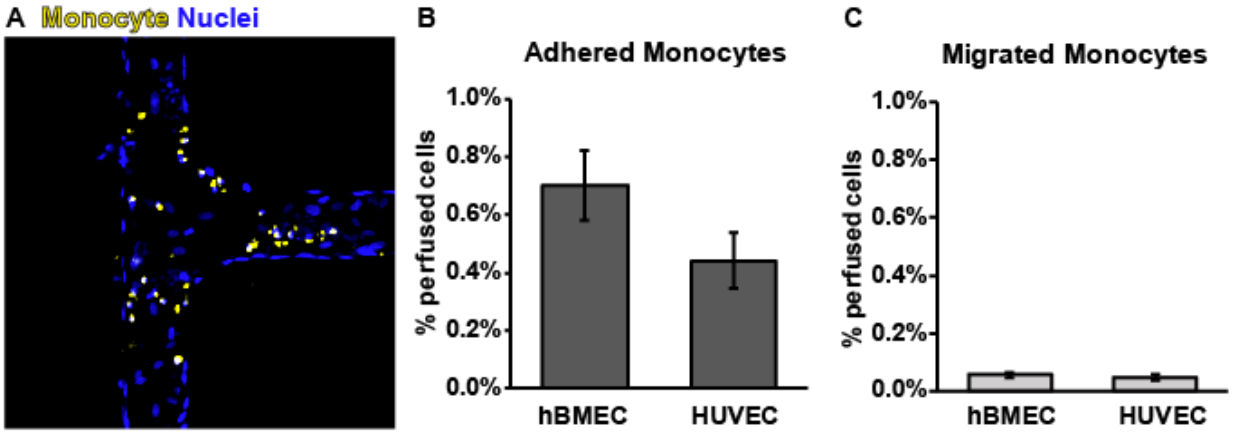

Figure 2.7. Monocyte perfusion through 3D microvessels. (A) Immunofluorescence imaging of monocytes adhered to hBMECs in a 3D microvessel. (B-C) Quantification of the adhesion (B) and transmigration (C) of monocytes in hBMEC and HUVEC vessels shows no significant differences.

Recapitulating 3D vascular marrow microenvironment

Further efforts to develop a platform to explore the behavior of marrow endothelial cells requires the surrounding microenvironment, complete with the many hematopoietic cell types present in the marrow vascular environment. To model this space, the complete mononuclear cell fraction of cells isolated from marrow screens was embedded within the collagen matrix space of the microvessel platform. Either hBMECs from a matched donor or HUVECs were seeded within the luminal space and allowed to form

intact vessels. After co-culture, both the hBMEC and HUVEC-seeded vessels contained large pores in the endothelium as seen by immunofluorescence microcopy of junctional CD31 (**Figure 2.8 A,B**). Unlike hBMECs, HUVECs did not display these pores when cultured alone (**Appendix A, Supplementary Figure 2**). Scanning electron microscopy on the lumen of these vessels confirmed the presence of these pores and also showed that matrix-seeded cells interact with the endothelium. In both vessel types, we observed cells with fibroblast morphology on the abluminal side of the endothelium, macrophage-like cells transmigrating through the vessel wall, and proplatelet-like clusters or strings (**Figure 2.8 C,D**).

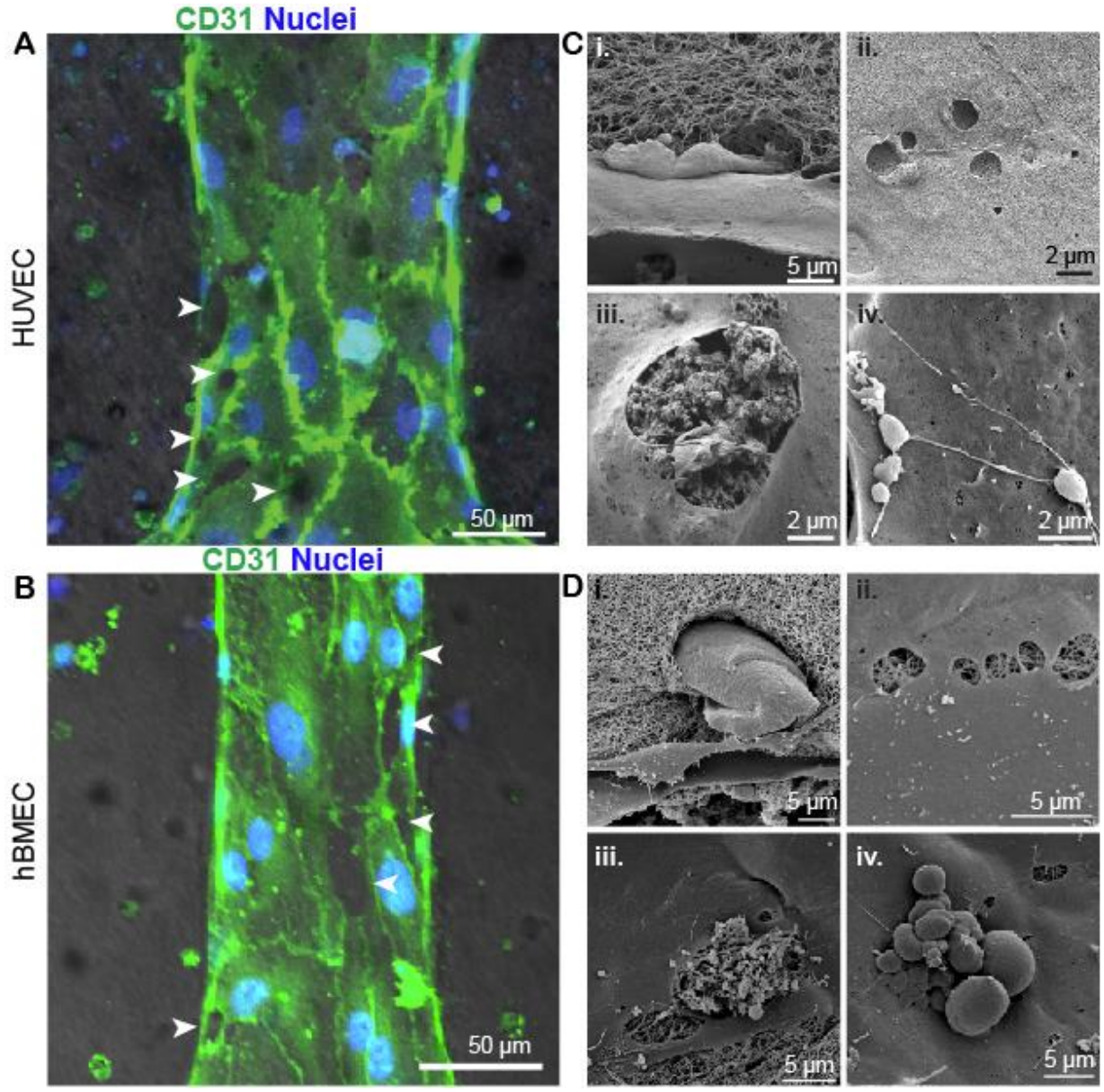

Figure 2.8. Marrow cell co-cultures in 3D microvessels. (A,B) Immunofluorescence imaging of endothelial CD31 in hBMEC (A) and (B) HUVEC microvessels co-cultured with marrow mononuclear cell populations. Arrowheads indicate large pores in the vessel wall. (C-D) Scanning electron microscopy shows various cell interactions of matrix-seeded marrow cell populations with the endothelium including (i) fibroblasts associated with the abluminal endothelium, (ii) endothelial pores, (iii) macrophage-like cells transmigrating into the lumen and (iv) pro-platelet-like structures on the lumen.

2.5 DISCUSSION

Endothelial heterogeneity reflects the tissue specific structure and function of vasculature within different organs. Characterization of the vasculature in various organs has shown three broad types of endothelium: continuous non-fenestrated, continuous fenestrated, or discontinuous [111], which reflect the degree of filtration, transport, and transmigration occurring in the specific vascular bed. For example, in the brain, heart, and lung, endothelial transport is more limited than in the liver and marrow, yielding continuous rather than sinusoidal vasculature in those organs. The structure and function of marrow vasculature, particularly in the human context is not fully understood. While studies have shown the isolation and culture of marrow endothelial cells, there has been insufficient use of modern techniques to examine the phenotypic differences from more widely used endothelial populations [55,58,120]. Fewer studies employ 3D tissue engineering platforms to recapitulate biologically relevant geometries, matrix, and tissue-specific cellular populations to explore marrow endothelial function. Through the isolation of cells from healthy donors, we have examined marrow endothelial gene expression, structure, and function *in vitro*.

RNA sequencing analysis reveals significant phenotypic differences between hBMECs and HUVECs. Specifically, hBMECs express more matrix-related proteins, including collagens, laminin, and MMPs, suggesting that hBMECs contribute to and remodel their immediate extracellular microenvironment. Hematopoietically active cytokines, such as IL-1β, CXCL12, WNT5A, and surface proteins such as PV-1 are increased in hBMEC as well. These cytokines play significant roles in the hematopoietic microenvironment within the marrow [39,60,128,129]. Specifically, CXCL12 is widely regarded as a primary chemoattractant modulating the residence and migration of hematopoietic cells, including hematopoietic stem cells, within the marrow microenvironment. The secretion of CXCL12 by hBMECs supports the role of endothelial cells in hematopoiesis and the marrow niche [117,136]. The expression pattern of hBMECs reflects the tissue of origin as a hematopoietically active environment expected in the marrow space.

Characterization of hBMECs using immunofluorescence and electron microscopy show expression of standard endothelial markers such as VECAD+ and vWF. Immunofluorescence imaging also revealed robust expression of PV-1 co-localized with and independent of caveolin-1. PV-1 is associated with the presence of diaphragms on endothelial cells on both caveolae and fenestrae [131]. Electron microscopy shows saw-toothed junctions, and further supports the presence of diaphragms and caveolae, both with and without diaphragms. When seeded in 3D perfusion cultures, hBMECs maintain these structures as seen via electron microscopy. Fenestrae and PV-1-rich diaphragms in endothelial cells has been shown to play a functional role in modulating permeability and cell trafficking [137,138]. Specifically, the presence of PV-1 on fenestral diaphragms has been reported to contribute to the egress of monocytes from the fetal liver, however, further studies are needed to determine whether a similar function is observed in the bone marrow [138]. Caveolae, present in many endothelial cell types and characterized by the caveolin-1 protein, are known to inhibit endothelial nitric oxide synthase activity [139,140]. Transport of macromolecules, signaling proteins, and cells through the endothelium is critical to the regulation of hematopoietic stem cell

maintenance and differentiation along with the release of mature blood cells into the circulation.

Monocyte adhesion, a functional indicator for inflammatory adhesion, was not significantly different between unstimulated hBMECs and HUVECs in both the 2D and 3D conditions. However, in 2D, stimulation with TNFα or IL-1β significantly increased adhesion over baseline on both cell types, with adhesion to stimulated HUVECs significantly more than adhesion to stimulated hBMECs. This relatively muted response to IL-1β may arise from the fact that IL-1β is upregulated in hBMECs as seen through RNASeq), suggesting that hBMECs are not a primary location for adhesion. The lack of significant differences in monocyte adhesion or migration between unstimulated hBMEC and HUVEC microvessels suggest that despite their phenotypic differences, the two cell types support monocyte trafficking similarly.

The addition of marrow-specific cells, including stromal fibroblast, hematopoietic, and adipogenic populations to the matrix support a more complex organ-specific microenvironment. After co-culture, we observed structural changes in HUVECs, such as the opening of large pores and discontinuities in the vessel wall. These pores were present in hBMECs cultured alone and co-cultured with marrow cells. In both HUVEC and hBMEC vessels, cells were observed to interact with the abluminal side of the vessel, transmigrate into the lumen, and adhere within the lumen.

These observations support the fabrication of an *in vitro* marrow space, enabling further studies on human marrow cells and the vascular microenvironment. Currently, the state-of-the-art for *in vitro* marrow studies centers on using HUVECs to model any vascular component [78,104,121]. However, the importance of organ-specific cells has been underscored for decades [58,112,113,141]. Though the isolation and hematopoietic supporting characteristics of hBMECs have been demonstrated previously [55,58,117,120], their use in modern bioengineered platforms has been limited. Currently, the reasons behind their limited use are apparent from our study as well. The cells isolated here and in previous studies are sourced from healthy donors during marrow transplant procedures. This yields inconsistent tissue sourcing, donor-specific variation, and small populations of endothelial cells per isolation. Limitations to passaging and fibroblast overgrowth present challenges to long term cultures of hBMECs. Optimized culture parameters of hBMECs are still under investigation. In the marrow, additional extracellular matrix components collagen IV, fibronectin, and laminin are present around sinusoids and play a role in hematopoietic cell interaction with the vasculature [142,143]. The inclusion of additional matrix components, particularly in 3D, could provide a more amenable microenvironment for hBMECs *in vitro*.

While there are some restrictions to the use of hBMECs at this stage, including limited cell number and expansion potential, the current work provides clues to the specific differences between hBMECs and other endothelial populations. We specify a robust isolation procedure for human marrow endothelial cells and describe their phenotype and structure in 2D and 3D culture platforms. We also show that HUVECs and hBMECs interact similarly to perfused monocytes and complex marrow cell populations when cultured in 3D microvessels. Further applications of hBMECs co-cultured with marrow cell populations can elucidate key interactions between cells in the vascular niche.

Chapter 3.

Development of an *In Vitro* Thrombopoietic Niche

This chapter has been submitted for publication in *PLOS ONE*:

Surya S Kotha,* Sijie Sun,* et al. “Microvasculature-Directed Thrombopoiesis in a 3D *in vitro* Marrow Microenvironment.” *PLOS ONE.* [Under Review] *equal contribution

3.1 ABSTRACT

Vasculature is an interface between the circulation and the hematopoietic tissue providing the means for hundreds of billions of blood cells to enter the circulation every day in a regulated fashion. The precise mechanisms that control the interactions of hematopoietic cells with the vessel wall are largely undefined. Here, we report on the development of an *in vitro* 3D human marrow vascular microenvironment (VME) to study hematopoietic trafficking and the release of blood cells, specifically platelets. We show that mature megakaryocytes differentiated in culture from CD34+ cells can be embedded in a collagen matrix containing engineered microvessels to create a thrombopoietic VME. These megakaryocytes continue to mature, penetrate the vessel wall, and release platelets into the vessel lumen. This process can be blocked with the addition of antibodies specific for CXCR4, indicating that CXCR4 is required for megakaryocyte migration, though whether it is sufficient is unclear. The 3D marrow VME system shows considerable potential for mechanistic studies defining the role of marrow vasculature in thrombopoiesis. Through a stepwise addition or removal of individual marrow components, this model provides potential to define key pathways responsible for the release of platelets and other blood cells.

3.2 INTRODUCTION

The adult human bone marrow releases nearly 500 billion cells into the blood each day [15,40]. Intravital imaging techniques have made it possible to visualize these complex processes in animal models, and have led to the identification of several pathways that mediate transmigration of cells from the marrow to the blood. However, the detailed interactions between the marrow vasculature and differentiated blood cells, particularly at the terminal stages of maturation and blood cell release remain elusive for human cells. There is a growing appreciation that differences in scale between man and small animals are most likely not addressed by reiterating simple three dimensional cellular relationships to compensate for increased volume. Discrepancies in kinetics and outcomes in marrow regeneration between small animals and

humans underscore this point [144–147]. Therefore, *in vitro* models are needed to model these phenomena and better understand human blood cell production and release. To address this, we have developed an engineered *in vitro* platform to approximate the vascular microenvironment (VME) and examine megakaryopoiesis.

The marrow is known for its complex architecture and diverse cell types. The vasculature, adipose tissue, fibroblasts, osteoblasts, osteoclasts, and hematopoietic cells have spatial relations that are critical for ordered blood cell production [29]. Recent studies, primarily from animal models, indicate that components of the VME can play more than one role in hematopoietic regulation [2,7,36,38,148,149]. For example, the endothelium contributes signals for lineage commitment, differentiation, and mobilization of progenitors [2,60,122]. *In vitro* work shows that human endothelial cells specifically support the development and differentiation of myeloid and megakaryocytic progenitors [53]. In small animals, hematopoietic stem cells (HSCs) localize in the perivascular space and, as they differentiate into megakaryocytes, they are in the perfect position to release platelets into the circulation [62,64,76,150,151]. In large animals, the difference in scale could mean that megakaryocytes may not be restricted to perivascular spaces alone. The release of platelets into the blood vessels requires that the megakaryocytes or some part thereof to come in contact with the vessel. The model presented here suggests that megakaryocytes migrate to achieve this end.

In vitro studies in liquid culture have proven useful for identifying cytokines and chemokines that contribute to hematopoietic regulation, cell proliferation, maturation, and motility [11,67]. Recent studies suggest the importance of physical factors that cannot be recapitulated in liquid culture, but can be approximated in 3D cultures, such as extracellular matrix, patent vasculature, and flow to facilitate processes such as platelet shedding [78,104,152,153]. Systematically addressing these components should allow for an optimized vascular platform.

Here, we developed an *in vitro* microvessel system to investigate and identify thrombopoietic processes within a 3D marrow VME. We show that megakaryocytes, differentiated from hematopoietic progenitor cells *in vitro,* seeded into the matrix of the VME migrate to make contact with the vessel. Once in contact, they induce endothelial pore formation and release platelets into the lumen of the vessel. This closely approximates megakaryocyte behavior *in vivo*. Our study demonstrates the possibility of using such a 3D *in vitro* system to assemble the marrow microenvironment and examine complex hematopoietic processes.

3.3 EXPERIMENTAL METHODS

Generation of megakaryocytes from human umbilical cord blood and peripheral blood

Human umbilical cord blood was purchased from BloodWorksNW blood bank. Human G-CSF mobilized peripheral blood CD34+ cells were purchased from the NIDDK-supported cell processing core at

the Fred Hutchinson Cancer Research Center (CCEH; U54 DK106829). Cord blood was processed in the same method as a previous publication [154]. Hetastarch 6% wt/vol (Hospira) was added to cord blood to a final concentration of 1.2%, and cells were processed by gravity sedimentation for 60 min. The leukocyte-enriched component was separated, centrifuged for 10 min at 300g and the supernatant was removed. The cell pellet was treated with ACK lysing buffer (Invitrogen) and washed with PBS. The cells were labeled with anti-CD34 antibody conjugated to magnetic microbeads (Miltenyi Biotec). The CD34+ fraction of cells was positively selected with an autoMACS separator, yielding over 90% CD34+ cell purity, as confirmed by flow cytometry (FACSCaliber).

Human cord blood or peripheral blood CD34+ cells were differentiated to megakaryocytes as described previously [154]. CD34+ cells were plated in 6-well plates at a density of $5x10^4$ cells/ml and cultured in serum-free X-VIVO 10 medium supplemented with a cytokine combination consisting of IL3 (10 ng/mL), IL6 (10 ng/mL), SCF (10 ng/mL) (R&D Systems), and TPO (50 ng/mL, Peprotech) [154]. The suspension cultures were incubated at 37^oC in a 5% CO_2 humidified chamber. Media was changed after 7 days of culture. After 10 days, cells were collected and stained with PE conjugated CD41a antibody. CD41a+ megakaryocytes were sorted at >90% purity with a BD Biosciences FACSAria III sorter.

Washed platelets preparation

Fresh blood was drawn from healthy donors into 6mL ACD tubes (Solution B, BD Vacutainer) with written consent under protocols approved by the Institutional Review Board of the University of Washington. Washed platelets were isolated in a manner described previously [155]. Briefly, freshly drawn blood collected in 6mL ACD tubes was centrifuged at 120 x g for 15 minutes at RT medium acceleration and without brake. The platelet rich plasma (PRP) was transferred to a FACS tube using a transfer pipet. The PRP was centrifuged at 500 x g for 10 minutes at RT on slow brake and medium acceleration. The plasma was carefully removed leaving a pellet of platelets at the bottom of the tube. CGS buffer (13 mM Sodium Citrate, 120 mM Sodium Chloride,30mM Glucose, pH 6.5) was used to suspend the pellet gently and more CGS was added for a total volume of 10mL. Human recombinant PGI_2 (Sigma-Aldrich) was added to the solution at 500ng/ml and the tube was inverted once to gently mix. A final centrifugation was performed at 400 x g for 10 minutes at RT with medium acceleration and slow brake. After the supernatant was removed, the platelets were resuspended in Tyrode's Buffer at half the volume of the original PRP volume.

Culture of human umbilical vein endothelial cells (HUVECs) and bone marrow stromal cells

HUVECs (Lonza) were cultured in endothelial cell growth media (EGM, Lonza) at 37^oC in a 5% CO2 humidified chamber. HUVECs at passage 5 or 6 were used in experiments. Bone marrow stromal cell line HS5 cells were received from Dr. Beverly Torok-Storb, Fred Hutchinson Cancer Research Center, as a gift. HS5 cells were cultured in RPMI-1640 supplemented with 10% fetal bovine serum, sodium pyruvate (1 mM), L-glutamine (0.4 mg/mL), penicillin (100 U/mL), and streptomycin sulfate (100 µg/mL, Invitrogen).

Fabrication and culture of 3D engineered microvessels and marrow VME

A microfluidic network was built via soft lithography using collagen gel (6-7.5mg/ml), as described previously [108,110]. For permeability, migration, and maturation experiments, sorted megakaryocytes were added to the collagen at 10^6 cells/mL, whereas for particle collection studies, unsorted megakaryocytes were added at 8-10 $\times 10^6$ cells/mL. Cells were thoroughly mixed into collagen yielding a uniform distribution in devices.

To seed the devices, HUVECs were trypsinized and resuspended at a concentration of 5 x 10^6 cells/mL [108,110]. After removal of media from the inlet and outlet of the devices, 10uL of HUVEC suspension was added into the inlet of microvessel and allowed to attach at 37°C for 15 min. After attachment, media was added to the inlet reservoir for perfusion culture. In megakaryocyte vessels, endothelial networks were perfused with EGM supplemented with 100ng/ml TPO. Media from MK differentiation culture was mixed 1:1 with EGM and supplemented with 100ng/ml TPO for conditioned media studies. The media for all vessels was replenished every 12 hours. In gravity driven conditions, the flow rate peaked initially at approximately 10 µL/min and decreased with time until the inlet balanced with the outlet. This range of flow rates leads to a peak wall shear stress in the inlet or outlet vessels of approximately 10 dynes/cm^2 and an average of ~ 0.1 dynes/cm^2 throughout the culture time.

For particle collection studies, megakaryocyte vessels were cultured under syringe pump-driven flow starting 2 days after fabrication (Model 11 Plus, Harvard Apparatus). Syringes were connected to tubing (1/32”ID, 3/32”OD Silicon Tubing, McMaster) fit securely into the inlet with a tube-to-tube 90° elbow connector. The flow rate was set at 3 µL/min so that the averaged wall shear stress in the inlet and outlet vessels remains 3 dynes/cm^2. Perfusate was collected via outlet tubing connected to a FACS tube containing 500 µL ACD buffer (Solution B, BD Vacutainer) and 400 µL PBS (Lonza). Every 24 hours, perfusate with released particles and/or cells was collected and media was refilled.

Functional testing and FACS

Collected particles, whole blood, and washed platelets were analyzed using flow cytometry. Half of each sample was activated with 3U/mL thrombin for 5 minutes. All samples were fixed in 3.7% formaldehyde, washed in FACS buffer (2% fetal bovine serum in PBS), and stained for CD41a, IgG (BD Biosciences), DAPI, and 7AAD (Beckman Coulter) for 30 minutes at RT. The cells were washed and analyzed on FACS CANTO2. The number of particles collected from each vessel was calculated using AccuCount Ultra Rainbow Fluorescent Particles (Spherotech). Analysis was performed on FLOWJO. Fixed quiescent and activated particles were permeabilized with Triton X-100, stained with β-tubulin (1:100, Abcam) overnight, washed, and incubated with Alexa Fluor 488 for 1 hour. Particles were washed, resuspended into a 1% agarose solution, mounted on coverslips, and imaged with a Zeiss LSM 880 confocal microscope.

Immunofluorescence staining and confocal imaging

In situ fixation and immunofluorescence staining was carried out as described previously [108]. After 3 to 7 days of culture, co-cultured microvessels were fixed *in situ* by perfusion of 3.7% formaldehyde for 20 minutes, followed by three 15 minute washes with PBS. The devices were then perfused with blocking solution containing 2% bovine serum albumin (BSA) and 0.1% Triton X-100 (Invitrogen, Carlsbad, CA) before immunostaining. Primary antibodies rabbit antihuman CD31 (Abcam) or VE-cadherin (Abcam) were diluted in the blocking solution and perfused through the vessel overnight at 4°C. The devices were washed three times with PBS for 15 minutes each. The secondary antibody goat anti-rabbit Alexa Fluor 647 or Alexa Fluor 488 (Invitrogen) and nuclear counterstain Hoechst 33342 were then perfused through the vessel for one hour, and washed three times for 20 minutes each. Immunofluorescence z-stack images (step size 1-3μm) of microvessels were taken with a Nikon A1R confocal microscope with a 10x or 20x objective. Z-projections and cross sections were generated using Image J. Zoomed views of MKs on the vessel wall and 3D reconstructions of confocal images were generated using contour surface creation in Imaris.

Manual quantification of megakaryocyte migration and ploidy was performed in ImageJ. Migration was quantified using 5 image stacks (120 μm depth) each from 5 different vessels, with distance from the vessel wall normalized to the radius of each vessel. The number of lobes per megakaryocyte was quantified through manual lobe counting of Hoechst-stained MK nuclei from z-projected image stacks of 6 vessels. Data are presented as mean +/- SEM. Significant differences were determined with an unpaired Student's t-test, with significance considered at $p < 0.05$. The number of nucleus lobes in peripheral blood-derived megakaryocytes (**Figure 3.1**) and cord blood-derived megakaryocytes (**Appendix B, Supplementary Figure 1**) were reported separately.

Scanning electron microscopy imaging

The co-cultured devices were fixed *in situ* by perfusing 25% glutaraldehyde overnight before disassembly, where the vessel was opened to expose the luminal surface. The collagen was dehydrated in serial ethanol washes (50%, 70%, 85% and 100% ethanol) and critical point drying (Tousimis, SamDri-780). The vessels and matrices were then sputter coated with gold-palladium and analyzed by a FEI Sirion scanning electron microscope with an accelerating voltage of 5 kV, spot size 3.

Transmission electron microscopy imaging

Microvessels were fixed in half-strength Karnovsky's solution (2% paraformaldehyde/2.5% glutaraldehyde in 0.2 M cacodylate buffer). Microvessels were disassembled and fully immersed in the same fixative solution for several days. Samples were rinsed in 0.1 M cacodylate buffer then post-fixed using 2% OsO4 in 0.2 M cacodylate buffer followed by another rinse with 0.1 M cacodylate buffer. Sample dehydration was performed using immersions in graded solutions of ethanol, then propylene oxide (PO), before 1:1 PO/Epon 812 (Ted Pella Inc) immersion overnight. Fresh Epon 812 was then exchanged for 2 hours after which the blocks were cured for 48 hours at 60°C. Ultrathin sections (70 nm) were cut from

blocks using a diamond (Diatome US) blade on a Leica EMUC6 ultra-microtome and placed onto grids. Grids were stained with uranyl acetate for 2 hours and lead citrate for 5 minutes. Sections were imaged using a JEOL JEM-1400 Transmission Electron Microscope (JEOL Ltd.) using 100 kV acceleration voltage. Images were acquired with a Gatan Ultrascan 1000XP camera (Gatan, Inc.).

Measurement of microvessel permeability

To measure barrier function of HUVEC only, megakaryocyte co-cultured, and HUVEC with megakaryocyte-conditioned media vessels, 40kD FITC-Dextran (Sigma) was perfused through the microvessels *in situ*. Fluorescent confocal images were acquired at 1 frame/second for 10 minutes. The image sequences were analyzed with Matlab to estimate the permeability coefficient of dextran in collagen based on the model developed in a previous publication from our group [108].

3.4 RESULTS

Megakaryocytes migrate towards the vessel as they mature

To obtain mechanistic insights into the differentiation of specific hematopoietic lineages, we fabricated a marrow VME to specifically study thrombopoiesis. Human CD34+ progenitors, isolated from either umbilical cord blood or mobilized peripheral blood, were differentiated into megakaryocytes [154]. After 10 days of culture, 30-70% of the cells expressed the megakaryocyte marker CD41a (**Appendix B, Supplementary Figure 1A**). CD41a+ megakaryocytes were then purified by flow sorting and embedded in type I collagen (7.5 mg/mL) using lithographic processes described [108–110]. HUVECs were seeded in the lumen of microchannels within the gel and cultured under perfusion. The endothelial cells formed a single-layer vessel with cobble-stone morphology and junctions at regions of cell-cell contact (**Figure 3.1 A**) [108–110]. The microvessels were cultured in endothelial growth medium supplemented with thrombopoietin (TPO) under gravity or syringe pump driven flow for 3 to 14 days. Due to the network geometry, the vessel branches further away from the inlet and outlet have wall shear stress approximately fifty folds lower than the inlet and outlet [155]. The range of flow conditions (averaged to 0.1 dynes/cm^2 in gravity driven conditions, and 3 dynes/cm^2 under syringe pump conditions) mimics the very low wall shear stress in the small arterioles of the marrow, estimated in previous literature to range from 0 to 4.6 dynes/cm^2 [156–158].

After 3 days of culture, endothelial cells formed junctions at regions of cell-cell contact, indicated by CD31 expression (**Figure 3.1 A,B**). Though the majority of CD41a+ megakaryocytes remained in the matrix, some moved to the abluminal side of microvessel, and others appeared on the luminal surface of the vessel (**Figure 3.2 B**). Detailed views of megakaryocytes shown interacting with the endothelial wall reveal intact, CD41a+ cells with internalized lobed nuclei (**Appendix B, Supplementary Figure 1E**). Megakaryocytes close to or in contact with the vessel wall had higher ploidy (3.1 ± 0.3SD) compared to

megakaryocytes distant from the vessel (2.4 ± 0.2 SD lobes, p<0.05; **Figure 4.1 C-E and Appendix B, Supplementary Figure 1 B-C**).

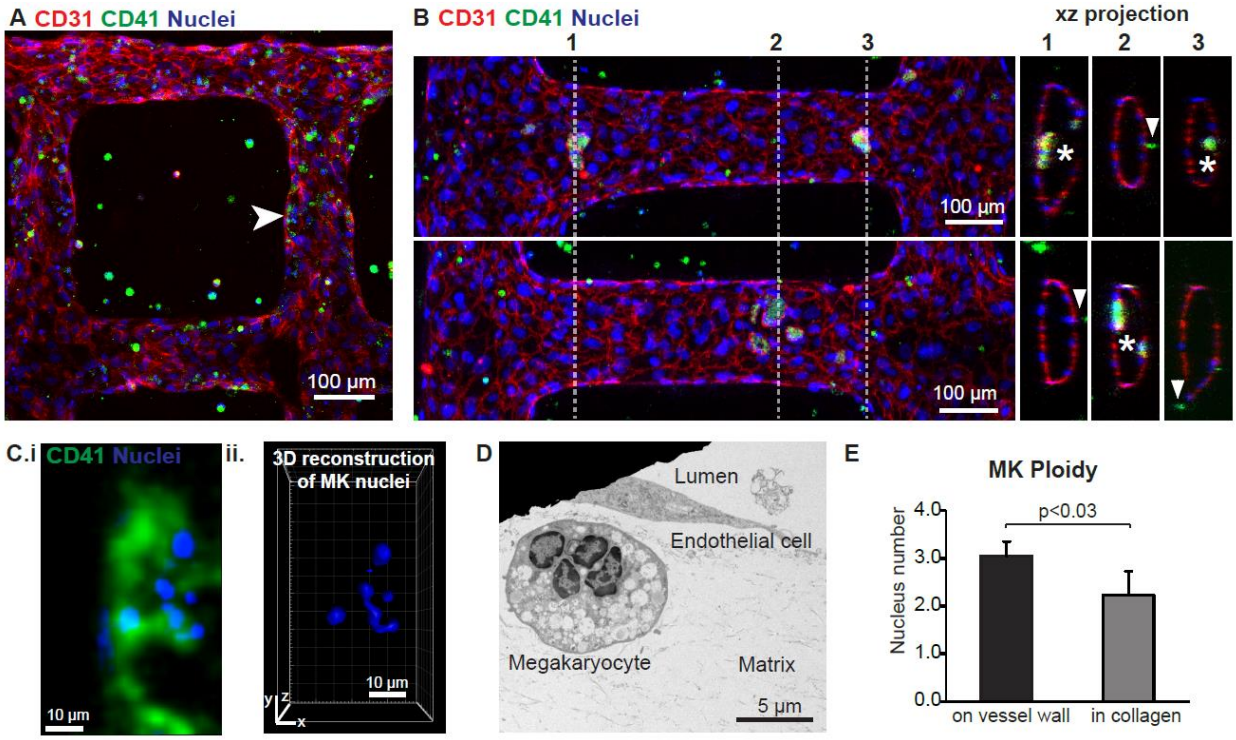

Figure 3.1. Marrow VME for the study of thrombopoiesis *in vitro*. A. Z-stack projection of confocal fluorescence imaging of megakaryocytes co-cultured within a 3D microvascular system. Green: CD41, red: CD31, blue: nuclei. **B**. Enlarged view, z-projection of confocal fluorescence images (left panel) and orthogonal views (right two panels) of locations at dotted lines 1 and 2, showing megakaryocytes interacting with the vessel wall (stars) and in the lumen and on the abluminal vessel wall (arrowheads). Green: CD41, red: CD31, blue: nuclei. **C**. (i) Zoomed view of megakaryocyte indicated in A (arrowhead) showing CD41a+ (green) and nucleus staining (blue) (ii) 3D reconstruction of the nucleus lobes from the megakaryocyte in i. **D**. A TEM image showing a megakaryocyte with four nucleus lobes close to a vessel. **E**. Megakaryocyte lobe counts near and far from the vessel wall shows more mature megakaryocytes are located closer to the vessel wall.

After 3 days of culture, megakaryocyte density increased over three fold near the vessel wall compared to the initial seeding density of 1 million cells/mL (**Figure 4.2 A.i, B** and **Appendix B, Supplementary Figure 1D**). Concurrently, megakaryocyte density decreased to one fifth of the original density at a distance greater than 300 μm (3 times the vessel diameter) from the vessel wall (**Figure 3.2 B**), suggesting that the megakaryocytes moved towards the vessel wall. Live imaging confirmed this phenomenon, as we observed megakaryocytes in the matrix actively migrating towards the vessel wall during culture (**Appendix B, Video 1, 2, and 3**). Canine megakaryocytes showed the same migration pattern. Megakaryocytes isolated from dog marrow were engineered to express GFP under the PF4 promoter and cultured in the same system [159]. After 3 days of culture, the majority of these

megakaryocytes closely associated with the vessel wall (**Appendix B, Supplementary Figure 2A-C**). In contrast, a control human bone marrow stromal cell line (HS5) cultured in the matrix at the same cell density showed no significant change in cell density in relation to the vessel walls throughout culture (**Figure 3.2 B**).

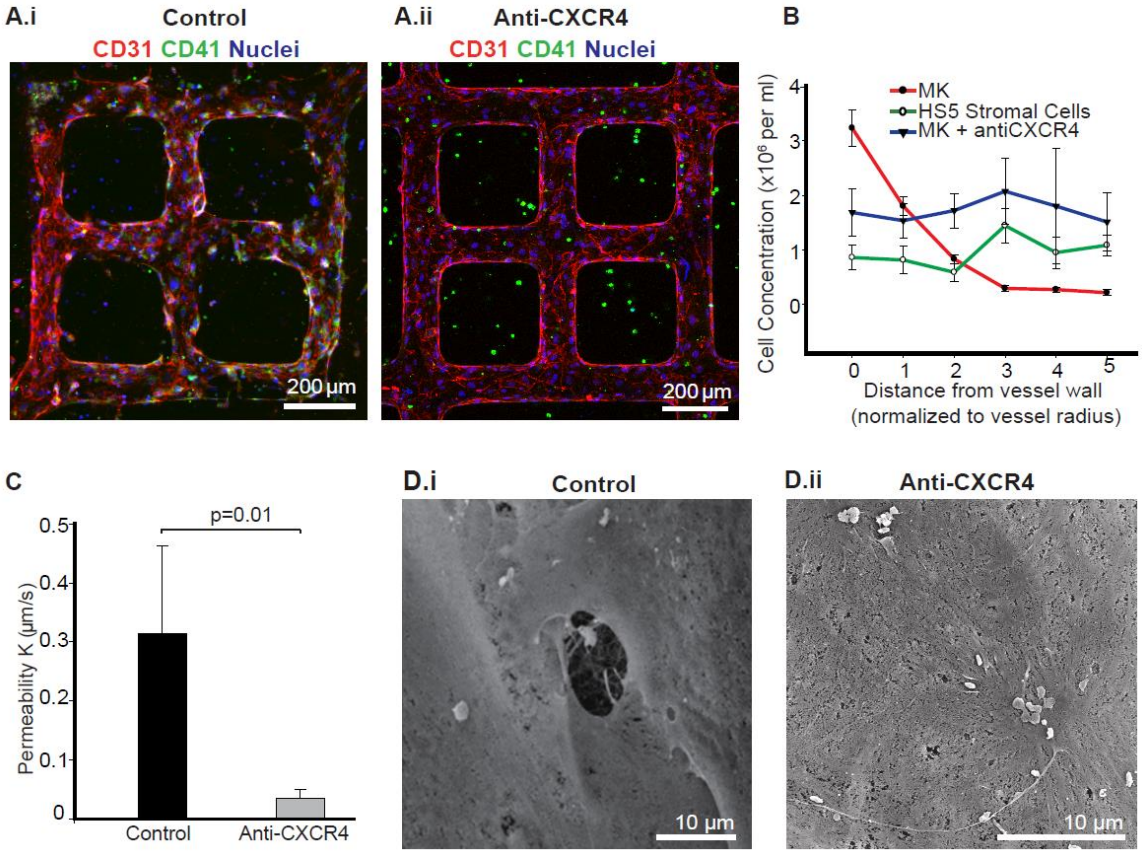

Figure 3.2. CXCR4 mediates MK migration and penetration through the endothelium. A. Z-stack projection of confocal fluorescence image of co-cultured thrombopoietic VME in control media (i) and media supplemented with anti-CXCR4 (ii) after three days. Green: CD41, red: CD31, and blue: nuclei. **B**. Cell density of megakaryocytes and HS5 stromal cells in collagen with respect to distance to microvessel walls after three days of culture. **C**. Permeability coefficient (mean ± S.D., n=3) of megakaryocytes co-cultured microvessels in control and anti-CXCR4 treated conditions. **D**. SEM of microvessel lumen showing holes in the endothelium of MK vessels in control (i), but not in anti-CXCR4 supplemented conditions (ii).

The maturation of megakaryocytes *in vivo* is driven primarily by thrombopoietin (TPO) [64] and stromal cell-derived factor 1 (SDF-1/CXCL12) [67], among other growth factors [66]. As they mature, megakaryocytes upregulate expression of CXCR4 and respond to CXCL12 (SDF-1) signaling, which directs their migration within the hematopoietic microenvironment [62,67,72,78,160,161]. To examine the role of CXCR4/CXCL12 signaling in the migration of megakaryocytes in our system, we studied the effect of a

neutralizing CXCR4 antibody. In anti-CXCR4 treated cultures, megakaryocytes remained in the matrix with no migration after three days of culture (**Figure 4.2 Aii., B**), suggesting that CXCR4/CXCL12 signaling is necessary for megakaryocyte migration and their interactions with the microvessels.

The presence of megakaryocytes in the matrix also affected microvascular permeability. FITC-conjugated 40-kDa dextran was perfused through the microvessels to estimate the permeability coefficient *K* of the endothelium, in an approach similar to one described previously [108]. The presence of megakaryocytes near the vessel increased microvessel permeability, with the permeability coefficient *K* = 0.31 ± 0.15 μm/s, nearly 10 fold higher than in microvessels without megakaryocytes (*K* = 0.032 ± 0.01 μm/s). Megakaryocyte conditioned media in HUVEC-only vessels decreased barrier function minimally (K = 0.11 +/- 0.03 um/s, **Appendix B, Supplementary Figure 3**). Neutralizing CXCR4 antibodies restored the barrier function of the microvessels (*K* = 0.036 ± 0.014 μm/s, $p<0.05$) to a value similar to that of vessels without megakaryocytes (**Figure 3.2 C**) [108]. Scanning electron microscopy and confocal microscopy revealed that pores of 1-10 μm developed in the vessel wall during co-culture with megakaryocytes, similar to those seen in microvessels co-cultured with marrow aspirates. However, these pores are not seen in HUVEC-only vessels with or without conditioned media (**Appendix B, Supplementary Figure 3 B,C**). The pores or fenestrae likely account for the increased vessel permeability (**Figure 3.2 D**).

Megakaryocytes penetrated the vessel wall and released platelet-like particles

In the marrow, megakaryocytes must migrate across or extend processes through the vessel wall into the lumen to release platelets [72,76,162]. However, it is unclear when or how megakaryocytes transmigrate through the endothelium, mainly due to the lack of access to the marrow and complex microenvironment. Our system allowed for close-up examination of the interaction of megakaryocytes and the vessel walls in real time. Megakaryocytes were observed to develop multiple processes that extended towards the vessel wall, migrated into the lumen, and released platelet-like particles (**Appendix B, Video 2**). Confocal and electron microscopy revealed different stages of this process (**Figure 3.3**). Some megakaryocytes resided completely on the abluminal surface of the microvessel (**Figure 3.3 A**). Some other megakaryocytes occupied both the abluminal and luminal space, apparently transmigrating through the endothelium while undergoing membrane demarcation (**Figure 3.3 B**) and fragmentation into clusters or pro-platelet strings on the vessel wall (**Figure 3.3 C**). Large megakaryocyte fragments or whole megakaryocytes were also found on the vessel walls (**Appendix B, Supplementary Figure 4**), where they would be expected to finalize their maturation and fragment into platelets while in circulation.

We next examined the capacity of our marrow VME to generate platelets. We embedded 7–10 × 10^6/mL differentiated megakaryocytes (unsorted after 10 days of differentiation culture) in the collagen matrix for co-culture with HUVEC-lined microvessels under flow. After an initial two days of culture, we collected the effluent perfusate every 24 hours **(Figure 3.4 A**). The released particles/cells ranged from the size of microparticles to that of red blood cells, as defined by the forward-scatter plot of washed platelets and whole blood, along with platelet-specific CD41a and CD42b analysis (**Figure 3.4 B**). Transmission

electron microscopy of platelet-like particles revealed heterogeneous morphology (**Appendix B, Supplementary Figure 6**). The collected perfusate contained an average of 1.82×10^6 platelet-sized particles, regardless of granularity, with over 550,000 CD42b+ particles in approximately 2 mL per thrombopoietic VME device per day. Each device contained microvessels with a surface area of 0.53 cm^2 and a volume of 1.6 µL. Considering that megakaryocytes within 100 µm of the vessel wall were able to generate particles and release them into the circulation, we calculated the yield of CD42b+ platelet-sized particles per megakaryocyte per day to be approximately 27, without counting any particles adhered on the vessel wall. Cytoskeletal rearrangement was evident when particles were activated with 3U/mL thrombin for 5 minutes by immunofluorescence staining of CD41a and β-tubulin (**Figure 3.4 C-D**).

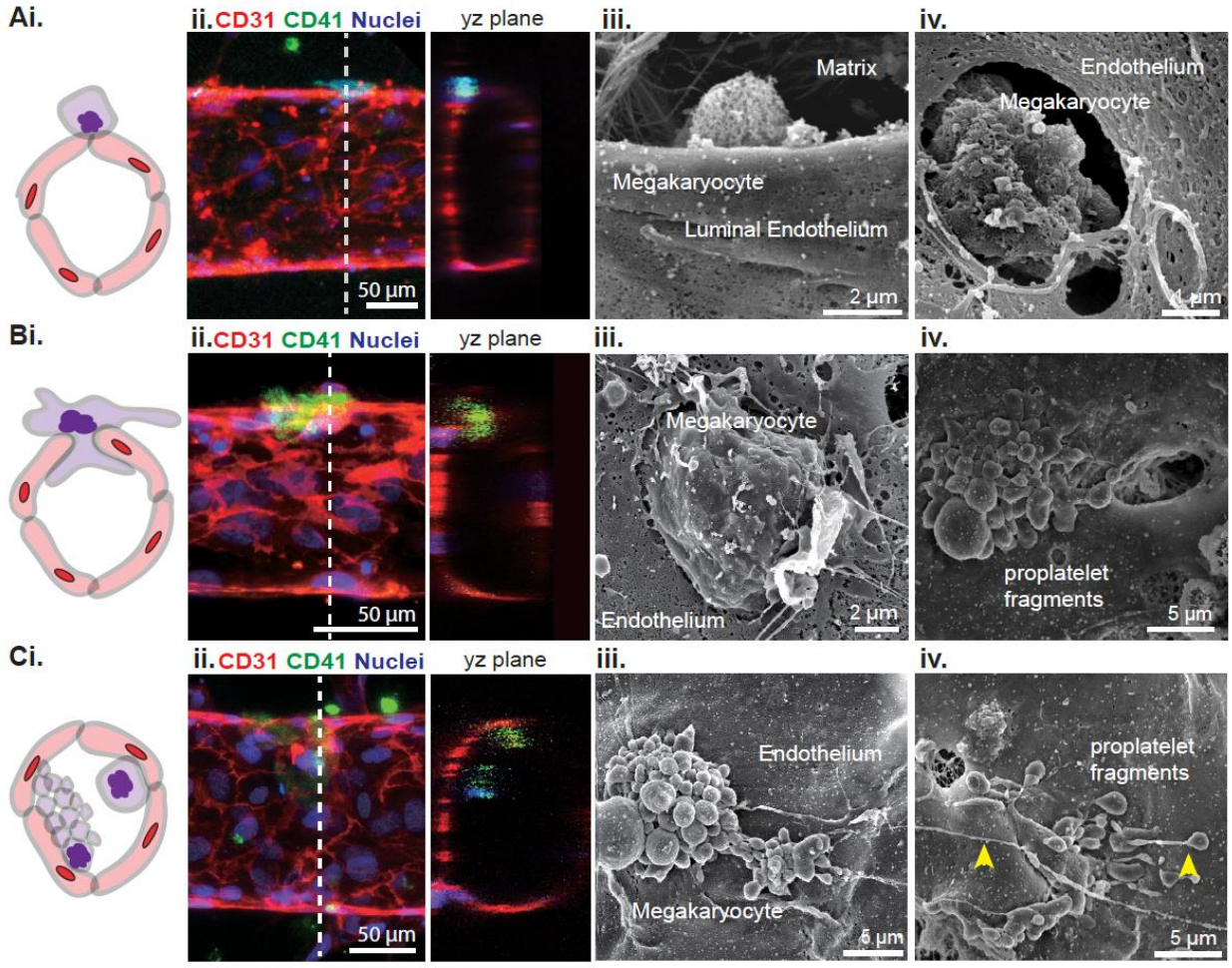

Figure 3.3. Megakaryocytes transmigrate through the endothelium and release platelet-like particles. Megakaryocytes are present in three locations relative to the microvessel wall during the process of transmigration: **A**. abluminal, **B**. transmigrating and **C**. luminal. **Column i**.: Schematics of the relative position of MKs and microvessel. **Column ii**.: z-stack projections and cross-sectional views of MK transmigration acquired through confocal fluorescence imaging. Red: CD31, green: CD41, blue: nuclei. **Columns iii-iv**.: SEM imaging of MKs interacting with the luminal endothelium at different stages, and pro-platelet fragments shedding platelet-like particles along the direction of flow (yellow arrowheads).

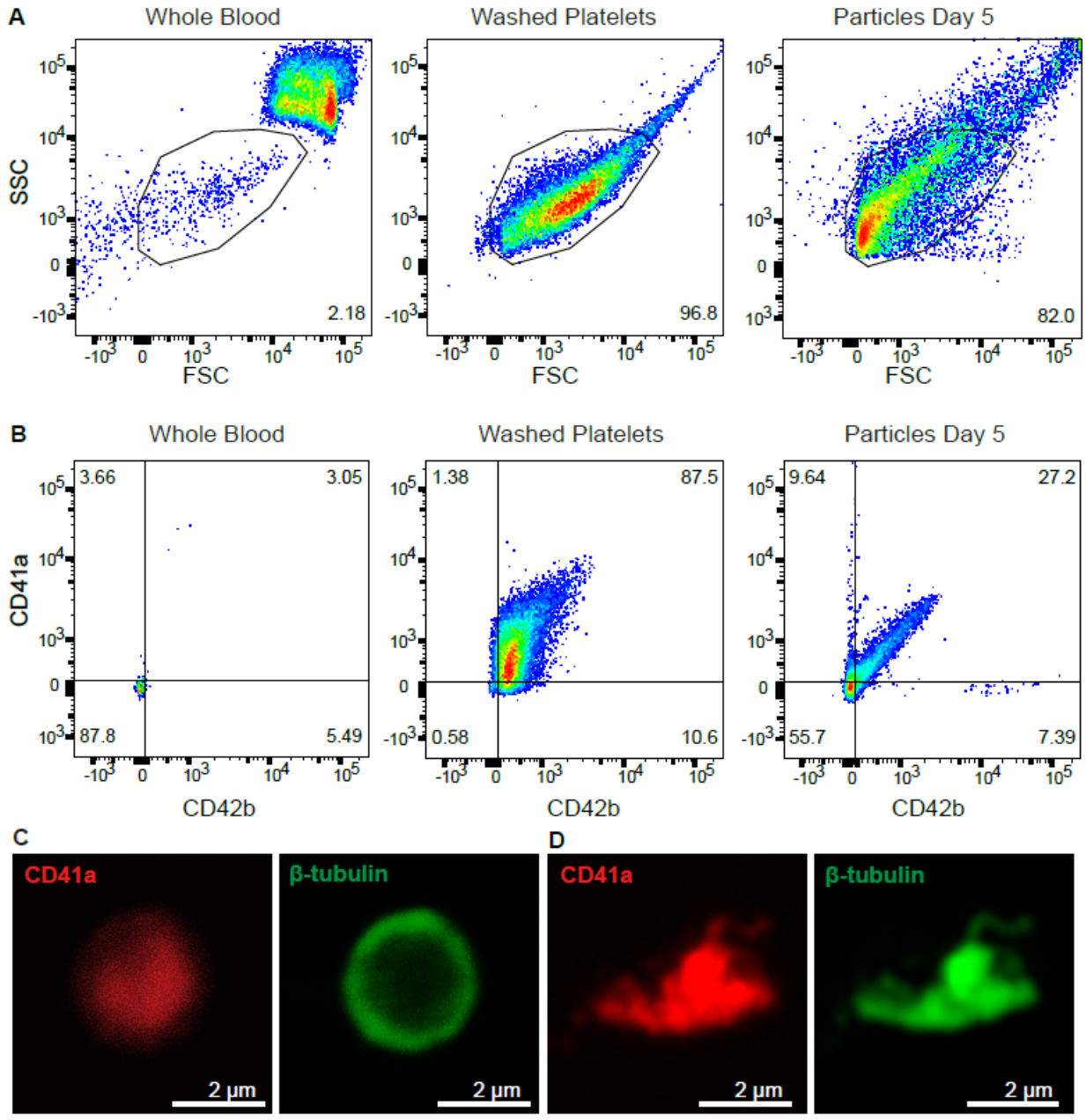

Figure 3.4. Characterization of generated platelet-like particles. A. Flow cytometry of whole blood, washed platelets, and collected particles from MK vessels at day five of culture showing granularity (SSC-A) and size (FSC-A). Gating was based on the platelet population of the whole blood sample. **B.** CD41a and CD42b expression of gated population from whole blood, washed platelets, and collected particles at day five. **C-D.** Immunofluorescence images of un-activated and thrombin-activated particles stained for CD41a and β-tubulin.

3.5 DISCUSSION

The bone marrow is essentially a liquid tissue with heterogeneous population and complex architecture. Stem cell and maturing components are not ordered in recognizable spaces as they are in epithelia. This poses a problem in visualizing hematopoietic differentiation, particularly in the context of large animals. In the past decade, advances have been made to visualize thrombopoiesis in mouse models via intravital microscopy. These studies show that marrow megakaryocytes released pro-platelets into the circulation with an estimated small number of platelets per megakaryocyte to meet the need for physiological platelet turnover [76,162,163]. The process of pro-platelet formation has been recapitulated *in vitro*, and also in this case, low numbers of platelet-like particles per megakaryocyte are produced [78,153,164]. Recently, attention has been paid to finding approaches or mechanisms to enhance the number of platelets generated per megakaryocyte. Under some stress conditions, marrow megakaryocytes were found to generate very large numbers of platelets to meet acute platelet need, potentially releasing them through rupture within the blood vessels, though this phenomena is under debate [77,151].

Here, we used hydrogel matrices to study the close interactions between megakaryocytes and microvessel walls. We showed that purified CD41+ megakaryocytes modified the endothelium of microvessels, interacted with vessel walls, and released platelet-like particles into the lumen. Although this system can benefit from further optimization and biological analysis, it validates the approach of using an engineered microvessel system to model the human marrow VME. For the first time, we detailed the specific interactions of human megakaryocytes with the vessel wall. The combination of three types of imaging data, namely live imaging, immunofluorescence, and scanning electron microscopic images, confirmed that megakaryocytes migrated towards the vessel and created pores in the endothelium, through which they either transmigrated or extended pro-platelets into the vessel lumen to release platelets. We showed that HUVECs, known to form continuous endothelial surfaces in both large vessels [165] and within *in vitro* microvessels [108], were modified by the surrounding megakaryocytes to become discontinuous and leaky. This structural phenotype is found in bone marrow endothelial cells, which are reported to be highly fenestrated [67,117,161,166–168]. The mechanisms behind MK-induced pore formation have been suggested to arise from the matrix-degrading properties of the MK podosome, which are increased in the presence of endothelial basement membrane and SDF1 [45,46,169] In contrast, megakaryocyte conditioned media alone did not change the continuity of HUVEC microvessels. This suggests that the microenvironment can modulate specific endothelial cell phenotypes to adapt to local functional needs, which may be one source of endothelial cell heterogeneity [58,111].

We showed that megakaryocyte migration is mediated in part by CXCR4-CXCL12 signaling, as blocking CXCR4 led to reduced megakaryocyte migration. This provides opportunities to further investigate and modulate the paracrine signaling and cell-cell interactions in thrombopoiesis, particularly in a platform that allows for the migration of cells from large distances away from vasculature. In addition, our system allows for the precise control of flow and perfusion of biochemical cytokines through the microvessels and

particle collection from the outlets. Throughout our culture, flow has been maintained by gravity or syringe pump. The flow rate and resulting wall shear stress mimics a biologically relevant range, which has been reported as extremely low, yielding wall shear stress range between 0 – 4.6 dynes/cm^2 [156–158].

We showed different processes of platelet release, namely pro-platelet territories, platelet-like blebs, and large fragments found in the vessel lumen. Mature megakaryocytes normally release pro-platelets, which are long cytoplasmic extensions with a beaded structure that fragment into platelets in circulation [76,162,170]. We see CD41+ megakaryocytes localize around the vessel wall and extend processes through the endothelium to release particles. The generated platelet-like particles found on the vessel lumen or collected have similar morphology as seen via ultrastructure assessment from electron microscopy and marker expression from immunofluorescence microscopy. Though Nishimura et al show that megakaryocytes can rupture in the presence of inflammatory cues to meet acute platelet need, this phenomena is not widely observed [77,171]. Recent work by Itkin et al. identified different roles of distinct marrow blood vessel types in hematopoiesis: less permeable arterial vessels support a low reactive oxygen species environment, whereas more permeable marrow sinusoids promote the activation of hematopoietic progenitor cells and immature cell trafficking [60]. In our system, endothelial cells appear to be activated and display structural and functional changes, indicating an inflammatory environment. Megakaryocyte-induced permeability could provide sites for immature megakaryocytes or large fragments to migrate across the endothelium, in combination with the lack of mature basement membrane formation. In normal marrow, whole megakaryocytes typically do not transmigrate from the marrow into the venous blood *in vivo*. This may impact the release of megakaryocytes and/or platelets, leading to the multiple types of megakaryocyte fragmentation phenomena observed in our system.

The advantages of our system include controllable cellular composition, matrix, vascular structure, flow, and a 3D geometry, and preserves the capacity for high quality imaging. Nevertheless, there are still improvements that can address technical limitations present in our platform. For example, the vessel wall consists of a single layer of endothelium with a 100 μm diameter, which is larger than the marrow sinusoids. This diameter may induce different stresses and biophysical forces on the vessel walls and affect the cellular interactions between megakaryocytes and the endothelium. Future studies could examine the effect of vessel diameter on thrombopoiesis, ranging from 30 μm, the lower limit of our fabrication technique, to sub millimeter or examine the impact of vessel density on megakaryocyte migration. In addition, we observed large numbers of platelet-like particles adhered to the luminal wall, rather than flowing in the perfused media. It is unclear whether this occurs *in vivo*, and if so, whether physiological mechanisms exist to detach the platelets. It is possible that such adhesion may be an *in vitro* artifact due to high serum content in the media, which activates platelets after their release. In addition, the endothelial cells appeared to have become activated and fenestrated during culture. It would be interesting to re-examine this phenomenon with bone marrow sinusoidal endothelial cells or endothelial cells that do not require serum *in vitro* to better mimic the marrow vasculature [172]. It is also expected that bone marrow endothelial cells have a unique phenotype, representing a less inflammatory and adhesive surface [57,60]. Adhesion blocking reagents

can also be introduced through the vessel wall to allow for better release of particles. Finally, our collected platelet-like particles appeared to lack packaged granules present in human platelets, which could be improved by addition of blood proteins in the media or additional matrix components in biologically relevant gradients, such as laminin, fibronectin, or collagen IV. The production of proper granules could also lead to a more typical morphology in activated particles. These modifications to the culture system could improve the shortcomings of a collagen-based platform and yield more homogenous particles without pre-activation. Nevertheless, our system demonstrated a functional *in vitro* human marrow thrombopoietic VME that lends itself to future mechanistic studies on cell-cell and cell-matrix interactions in the marrow.

Chapter 4.

Hematopoietic cell trafficking in a fibroblast-directed niche

This chapter has been submitted for publication in the following manuscript:

Kotha S.S. et al. “Engineering a Multicellular Vascular Niche to Model Hematopoietic Cell Trafficking” Stem Cell Research & Therapy [Accepted].

4.1 ABSTRACT

The marrow microenvironment and vasculature plays a critical role in regulating hematopoietic cell recruitment, residence, and maturation. Extensive *in vitro* and *in vivo* studies have aimed to understand the marrow cell types that contribute to hematopoiesis and the stem cell environment. Nonetheless, *in vitro* models are limited by the lack of complex multicellular interactions, and cellular interactions are not easily manipulated *in vivo*. Here, we develop an engineered human vascular marrow niche to examine the 3D cell interactions that direct hematopoietic cell trafficking. Using soft lithography and injection molding techniques, fully endothelialized vascular networks were fabricated in type I collagen matrix, and co-cultured under flow with embedded marrow fibroblast cells in the matrix. Marrow fibroblast (MSCs, HS27a, or HS5) interactions with the endothelium were imaged via confocal microscopy and altered endothelial gene expression was analyzed with RT-PCR. Monocytes, hematopoietic progenitor cells, and leukemic cells were perfused through the network and their adhesion and migration was evaluated. HS27a cells and MSCs interact directly with the vessel wall more than HS5 cells, which are not seen to make contact with the endothelial cells. In both HS27a and HS5 co-cultures, endothelial expression of junctional markers was reduced. HS27a co-cultures promote perfused monocytes to adhere and migrate within the vessel network. Hematopoietic progenitors rely on monocyte-fibroblast crosstalk to facilitate preferential recruitment within HS27a co-cultured vessels. In contrast, leukemic cells sense fibroblast differences and are recruited preferentially to HS5 and HS27a co-cultures, but monocytes are able to block this sensitivity. We demonstrate the use of a microvascular platform that incorporates a tunable, multicellular composition to examine differences in hematopoietic cell trafficking. Differential recruitment of hematopoietic cell types to distinct fibroblast microenvironments highlights the complexity of cell-cell interactions within the marrow. This system allows for step-wise incorporation of cellular components to reveal the dynamic spatial and temporal interactions between endothelial cells, marrow-derived fibroblasts, and hematopoietic cells that comprise the marrow vascular niche. Further, this platform has potential for use in testing therapeutics and personalized medicine in both normal and disease contexts.

4.2 INTRODUCTION

Hematopoietic cells dynamically interact with the vasculature and the surrounding microenvironment during recruitment and residence in tissues. Much effort has been made to understand the different endothelial adhesion molecules and soluble factors that regulate recruitment of roving hematopoietic cells, yet it remains unclear which niche components and surrounding stromal cells create permissive vascular environments for transmigration [8,101,173–177]. In particular, the functional contribution of stromal and endothelial phenotypes to hematopoietic recruitment within marrow vascular niche spaces is not fully understood [8,18,32,177]. To date, many individual marrow components, such as mesenchymal stem cells (MSCs), macrophages, and osteoblasts, have been isolated and studied in 2D *in vitro* cultures [177–181]. However, since interactions are dependent on the context of a multicellular environment, more complex models are needed to recapitulate these spaces. Corresponding *in vivo* studies of the functional niche in both healthy and diseased states have been precluded by the complexity of marrow architecture and difficulty of systematic analysis of cell behavior in dense tissue [32,34,177,182]. Intravital microscopy has allowed for single cell visualization of HSPC-endothelial interactions, [8,21,22,182–185] though trafficking events are difficult to capture and the detailed dynamics of multiple niche components are still unclear. It is therefore important to develop new tools that can recapitulate multicellular microvascular environments and allow for functional analysis of hematopoietic cell trafficking.

Cell extravasation across the endothelial wall has been studied extensively for leukocytes, [132,133,186–189] and hematopoietic stem and progenitor cell (HSPC) trafficking has been thought to follow a similar cascade [96,158,190–192]. After vascular inflammation, the release of cytokines signal for the recruitment and arrest of leukocytes on the endothelium [186,190,193]. While *in vitro* and *in vivo* studies have shown that leukocytes transmigrate primarily in response to inflammatory signaling, the specifics about the cues for HSPC trafficking are not completely understood [8,60,158,194]. *In vivo,* HSPCs have been shown to reside in perivascular niche spaces, composed of monocytes/macrophages, stromal fibroblasts, and proximal vasculature [7,32,36,177,178,195]. Monocytes and monocyte-derived macrophages not only reside within these perivascular spaces, they also interact with the endothelial cells and stromal fibroblasts [178,196,197]. In addition, the stromal-endothelial crosstalk results in changes to the local secretion of niche-associated factors to modulate HSPC recruitment [36,128,166,179,181,196,198].

In the marrow, the contribution of monocytes and monocyte-derived macrophages has been noted, but has not been well detailed, particularly in the context of the perivascular niche [35,196,197,199–201]. Previous studies have shown that co-culture of monocytes with marrow derived MSCs has led to diverse outcomes, due to inconsistent definition of the MSC cell type and varying co-culture conditions [176,202,203]. Co-culture of monocytes with a defined human marrow-derived stromal fibroblast line HS27a in 2D cultures results in close associations between the cells, changes in MMP9 secretion, adhesion molecule expression, cytokine secretion, and Notch signaling when compared to each cell cultured alone

[199,204,205]. Meanwhile, co-culture of monocytes with another human marrow fibroblast line HS5 does not change monocyte or HS5 gene expression [35,199]. Taken together, these findings suggest that both the marrow stromal cell type and monocyte co-culture conditions must be carefully juxtaposed to understand cellular crosstalk.

In this study, we utilize a perfusable 3D microvessel system to develop a marrow perivascular niche. We show that marrow-derived fibroblasts modify endothelial phenotype and the vascular microenvironment, which subsequently directs the adhesion and transmigration of perfused monocytes, CD34+ HSPCs, and CD34+ leukemic cells. We show that the circulating monocytes can enter the perivascular niche, interact with fibroblasts, and further change HSPC and leukemic cell trafficking patterns. Our study demonstrates the dynamic multicellular interactions in the marrow microenvironment, and our platform supports spatiotemporal control and monitoring of these dynamics. It also allows for the step-wise addition and subtraction of individual niche elements to further understand the hematopoietic microenvironment in health and disease.

4.3 EXPERIMENTAL METHODS

Cell Sourcing

All experiments were conducted using human umbilical vein endothelial cells (HUVECs, Lonza) between passage 4 and 6, grown and cultured in endothelial growth media (EBM + EGM bullet kit CC-3124, Lonza) until confluent in T-75 flasks prior to use.

Stromal fibroblast cell lines HS5-GFP and HS27a-GFP were generously provided by the Torok-Storb lab [205,206]. These immortalized human marrow stromal lines were cultured in RPMI 1640 medium (Thermo Fisher Scientific) supplemented with L-glutamine (0.4 mg/mL, SAFC Biosciences), sodium pyruvate (1 mM/L), penicillin-streptomycin sulfate (100 µg/mL, Thermo Fisher Scientific), and 10% fetal bovine serum (FBS, Thermo Fisher Scientific). Stromal fibroblasts were cultured to 70% confluence in T-75 flasks and trypsinized prior to embedding in vessels. HS27a conditioned media was removed after 5 days of culture and centrifuged prior to use in vessels for conditioned media experiments. Marrow MSCs were purchased from Lonza. MSCs were cultured in MSCGM (Lonza) in T-75 flasks, and trypsinized prior to use.

Peripheral monocytes were obtained from fresh blood samples under protocols approved by the Institutional Review Board at the Fred Hutchinson Cancer Research Institute. Mononuclear cells were isolated from fresh blood through Ficoll-Paque centrifugation (specific gravity 1.077) at 200 g for 30 minutes at room temperature. Monocytes were isolated from this fraction through incubation with CD14 microbeads (Miltenyi Biotec) for 20 minutes at 4°C, washed with PBS/2% FBS, and purified using magnetic cell sorting (Miltenyi Biotec). The monocytes were then incubated with CD14-PE and CD45-PE (BD Biosciences) for 20 minutes at 4°C and washed twice with PBS/2% FBS prior to use. Healthy and acute myelogenous

(patient-derived) leukemic CD34+ cells were purchased through the Hematopoietic Cell Processing and Repository (DK56465 and DK106829) at Fred Hutchinson Cancer Research Institute under protocols approved by the Institutional Review Board of the Fred Hutchinson Cancer Research Institute. Healthy CD34+ progenitor cells were isolated from GM-CSF-mobilized HSPCs in peripheral blood and stored by the Hematopoietic Cell Processing and Repository. Healthy and leukemic CD34+ cells were allowed to recover overnight after thawing in StemSpan Serum-Free Expansion Medium (StemCell Technologies) supplemented with 10 ng/ml IL-6, 10 ng/ml SCF, 10ng/ml FLT3, 50 ng/ml TPO, and 2 U/ml EPO (Peprotech). Healthy and leukemic CD34+ cells were stained with CD34-APC and CD45-APC (BD Biosciences) for 20 minutes at 4°C, then washed twice with PBS/2% fetal bovine serum prior to use.

Vessel Fabrication

The 3D microfluidic networks were fabricated as described previously [108–110]. Briefly, soft lithography created a PDMS mold patterning a 100 μm-diameter network, and injection molding over the PDMS mold created a 100 μm collagen I gel microvessel which was sealed with a collagen-coated coverslip (**Figure 4.1 A**) [108–110]. MSCs and human bone marrow derived fibroblast cell lines HS27a and HS5 were embedded uniformly in the collagen at 1 million cells per mL. The channels were then perfused with HUVECs, which adhered to the collagen and self-assembled into a functional microvessel with an open lumen. Endothelial cell culture media added to the inlet reservoir flowed through the network driven by gravity, undergoing approximately an 8-fold reduction in flow (~0.1 dyn/cm at minimum). Vessels were cultured for 3-7 days prior to analysis.

Hematopoietic Cell Perfusion through Microvessels

Hematopoietic cells were perfused through vessels that had been cultured for 3-4 days. For single cell perfused vessels, monocytes, healthy CD34+, or leukemic CD34+ cells were added to the inlet of the vessel (100,000 cells in 100 μL PBS/5% FBS) and allowed to perfuse for 30 minutes. Any remaining cell solution was then removed and vessels were washed with media twice for 30 minutes each. In double perfused vessels, monocytes were perfused as above, then 24 hours later, healthy or leukemic CD34+ cells were added to the inlet (100,000 cells in 100 μL PBS/5% FBS) and allowed to perfuse through the vessels for 30 minutes (**Figure 4.1 B**). Excess cell solution was then removed and vessels were washed twice with media (30 minutes each). For VCAM blocking experiments, a VCAM1 blocking antibody (50μg/mL, R&D Systems, clone BBA5) was perfused through the vessels for 1 hour and vessels were briefly washed with media prior to HSPC perfusion. 24 hours after perfusion with cells, vessels were fixed in 3.7% formaldehyde (20 minutes) and washed with PBS three times (20 minutes each).

Immunostaining & Imaging

Prior to immunofluorescence staining, nonspecific binding was blocked with 2% bovine serum albumin (BSA)/0.5% Triton X-100 for 1 hour. Staining for CD31 (Abcam), VE-Cadherin (VE-Cad, Abcam),

von Willebrand Factor (vWF, Abcam), and α-smooth muscle actin (αSMA, Thermo Fisher Scientific) was accomplished through perfusion of immunofluorescence reagents through the microvessel network as described previously [108]. Secondary antibodies with fluorochromes Alexa Fluor 488, 567, or 647 were used. Vessels were imaged on a Nikon A1R confocal microscope.

Scanning Electron Microscopy

After immunofluorescence images of microvessels were taken, microvessels were re-fixed *in situ* with 25% glutaraldehyde for 20 minutes and rinsed three times with PBS. The microvessels were then dissembled into top and bottom parts. The thick top portion of the collagen microvessel was dehydrated in serial ethanol washes (50%, 70%, 85% and 100% ethanol) and further dehydrated by critical point drying (Tousimis). The vessel was then sputter coated with gold-palladium and analyzed by a FEI Sirion scanning electron microscope with an accelerating voltage of 5 kV, spot size 3.

RT-PCR

To harvest RNA lysate from vessels, RLT Buffer was perfused through the network and collected continuously from the vessel outlet for 2 minutes. RNA lysate from the vessels was purified using an RNA purification kit (Qiagen). RNA purification was completed following the provided protocol and quantified using Nanodrop (Thermo Fisher Scientific). RT-PCR was performed (see **Appendix C, Supplementary Table 1** for primer details) and results were normalized to RPL32 expression [207]. Significant differences were determined using Welch's 2 sample, 2 tailed t-test with Bonferroni correction (α= 0.1, n = 3).

Adhesion & Migration Quantification

Quantification of stromal fibroblast location and hematopoietic adhesion and migration with relation to the vessel wall was analyzed using 3-10 confocal images of each vessel (n=3) (Fiji, NIH). Images analyzed were selected from the low flow regions of the vessel (non-inlet or outlet regions). Image stacks of the vessel (120 μm depth) were z-projected to a single plane and coordinates of vessel borders were manually selected. Marrow fibroblast coverage of vessels is presented as percentage of projected vessel area that is masked by fibroblasts. Coordinates of PE-labeled monocytes or APC-labeled CD34+ cells were located via particle analysis on thresholded images. Distances from cells to the vessel were calculated assuming that the cells migrated from the closest vessel wall (**Figure 4.1 C**). Cells that were located within the vessel boundaries were counted as adherent to the vessel wall. Distance from the nearest vessel was normalized to the vessel radius. Cell adhesion and migration data of perfused hematopoietic cells was calculated as a percent of estimated total perfused cells (based on the concentration and volume of cell suspension added to the reservoir and the gravity driven flow rate). A sensitivity analysis of high, middle, and low estimates (75,000, 50,000, and 25,000 cells) was performed, showing no effect of the total number perfused cells on significant differences between groups. Data is presented based on a low estimated

number of perfused cells. Significant differences between groups were determined using 2 Sample, 2 tailed student's t-test. Error bars represent standard error measurements.

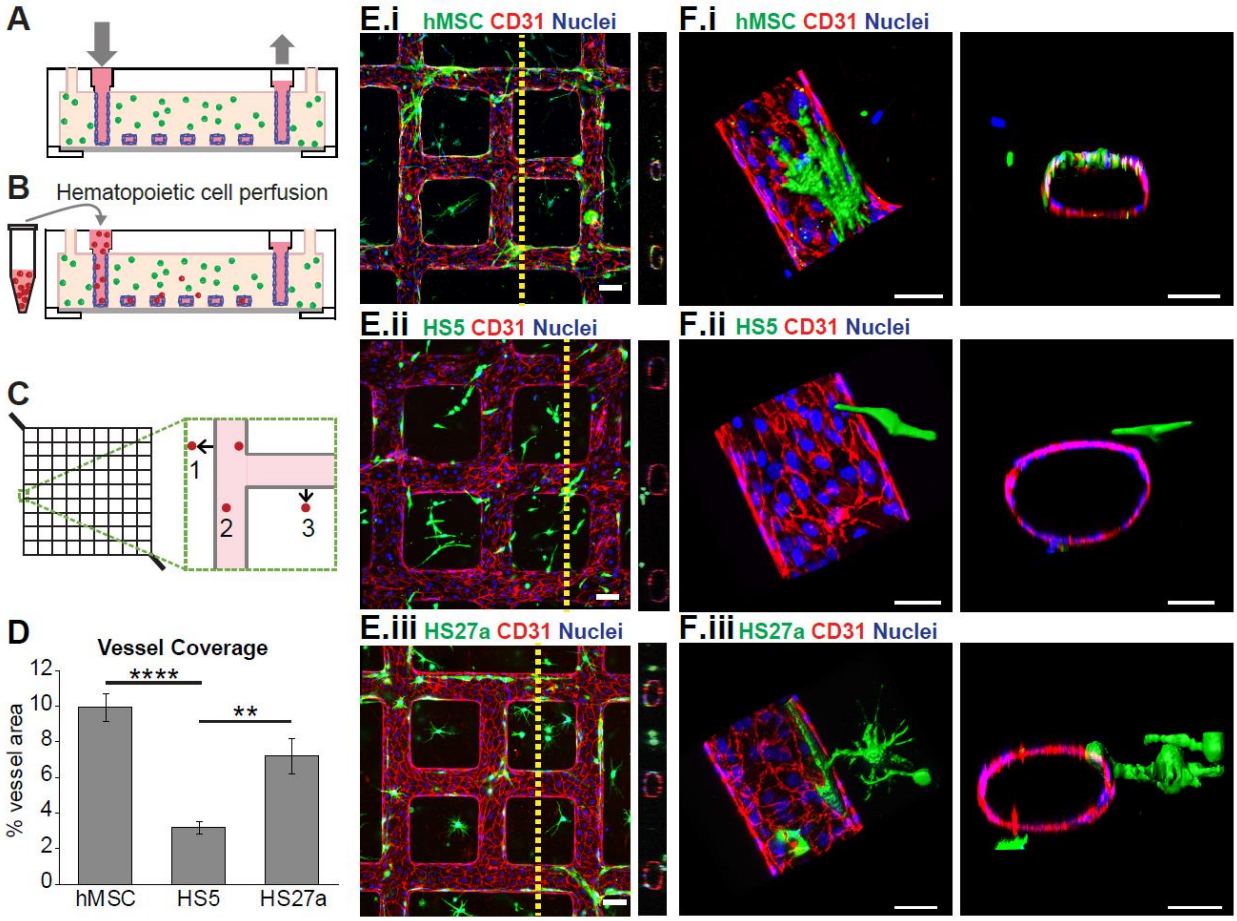

Figure 4.1. Co-culture of marrow fibroblasts with engineered vessels create perfusable marrow microenvironments. (A) Schematic of microvessel platform shows a perfusable network that is then (B) perfused with hematopoietic cells. (C) Perfused hematopoietic cells are identified as migrated (1,3) or adhered (2) within a portion of the vessel network. (D) Quantification of percent vessel coverage by hMSCs and marrow fibroblast types show that hMSCs and HS27a cells coat vessels more than HS5 fibroblasts. **** $p < 0.0001$, ** $p < 0.005$. (E) Co-cultured hMSCs and marrow fibroblasts interact with endothelial vessel walls. Scale bars = 100 μm. (F) 3D reconstruction and orthogonal views of co-cultured microvessels show surface renderings of MSCs, HS5, and HS27a cells interacting with the endothelial wall. Scale bars = 50 μm.

4.4 RESULTS

Stromal cells differentially interact with perfusable microvessels

To recapitulate a 3D perivascular niche *in vivo*, we engineered a 3D microvessel network in collagen gel combining lithography and injection molding processes as described previously [108–110]. The embedded lumens were seeded with human umbilical vein endothelial cells (HUVECs) to form a fully

endothelialized vessel network. Three different stromal fibroblasts, namely MSCs, HS5, and HS27a cell lines, were embedded separately in the collagen gel surrounding the lumen. These co-cultured microvessel devices were maintained in culture under gravity driven flow for up to a week. MSCs are a heterogeneous fibroblast population from the marrow, and have been widely studied for their ability to interact with both the vasculature and hematopoietic cells to define a microenvironment [174,177,178,208]. Here, we consider their function as a stromal fibroblasts sourced from an MSC population. HS5 and HS27a are two marrow-derived stromal fibroblast cell lines that identify distinct functional phenotypes *in vitro* (see **Appendix C, Supplementary Figure 1**). The HS27a cell line is CD146 positive and expresses stem cell niche-associated proteins (SDF-1, angiotensin, osteopontin, and VCAM1, among others) whereas the HS5 line (CD146-) secretes ample amounts of GM-CSF, G-CSF, IL1, IL-8, MCP3, and MIP1a [205,206].

When co-cultured with microvessels under perfusion, the three stromal fibroblasts interact differently with the endothelial cells (**Figure 4.1 D-F**). After six days of culture, both MSCs and HS27a cells displayed pericyte-like close association with the microvessels such that they extended processes and wrapped around the endothelium (**Figure 4.1 D,E.i-ii, F.i-ii**). In contrast, HS5 cells did not associate closely with the microvessels (**Figure 4.1 E.iii, F.iii**), but remain in the matrix. The vessel coverage was significantly increased in the MSCs and HS27a co-cultured microvessels (9.95 ± 0.76% and 7.21 ± 0.35%, respectively) over the HS5 co-cultured vessels (3.18 ± 1.0%) (**Figure 4.1 D**). In all three conditions, the endothelium remained intact with robust junctions at regions of cell-cell contact. We therefore selected the well-defined HS27a and HS5 cell lines in this platform to represent specific marrow stromal contribution (see **Appendix C, Supplementary Figure 1**).

Stromal cells modify endothelial cell phenotype

In addition to differences in coating, the two fibroblast cell lines around the microvessels appeared to modify endothelial phenotypes differently. Endothelial cells displayed uniform cobblestone structure in HS27a co-cultured vessels with homogeneous expression of CD31 and VE-cadherin at regions of cell-cell contact (**Figure 4.2 A**). In HS5 co-cultured microvessels, however, endothelial cells had irregular and heterogeneous shape with varying CD31 and VE-cadherin expression, and were more elongated along the direction of flow (shape index: 0.55 compared to 0.62 with HS27a co-culture, $p<0.05$, **Figure 4.2 A**). In both stromal modified vessels, Von Willebrand Factor expression was low compared to endothelial cell – only vessels, as shown by decreased appearance of Weibel Palade bodies (**Figure 4.2 Aiii, see Appendix C, Supplementary Figure 3**) [155].

RT-PCR on microvessels comparing the HS27a and HS5 stromal co-cultures to vessels with ECs alone showed significant reduction in vWF (75% and 57% reduction in HS5 and HS27a vessels compared to EC only vessels, respectively) and CD31 (59% and 58% reduction in expression in HS5 and HS27a vessels, respectively) expression in microvessels after co-culture. In HS5 co-cultured vessels, TIE2 levels were significantly reduced by 52% from EC only vessels. This combination suggests an activated or inflamed endothelium when co-cultured with HS5 (**Figure 4.2**) [209–212]. No significant change in VCAM1

RNA expression was seen between conditions. Further expression analysis of vessels show that other inflammatory cytokines and endothelial surface markers are modified with co-culture (see **Appendix C, Supplementary Figure 2)**. Together, the stromal fibroblasts around the microvessels modify the endothelial status and direct the formation of a specific tissue microenvironment.

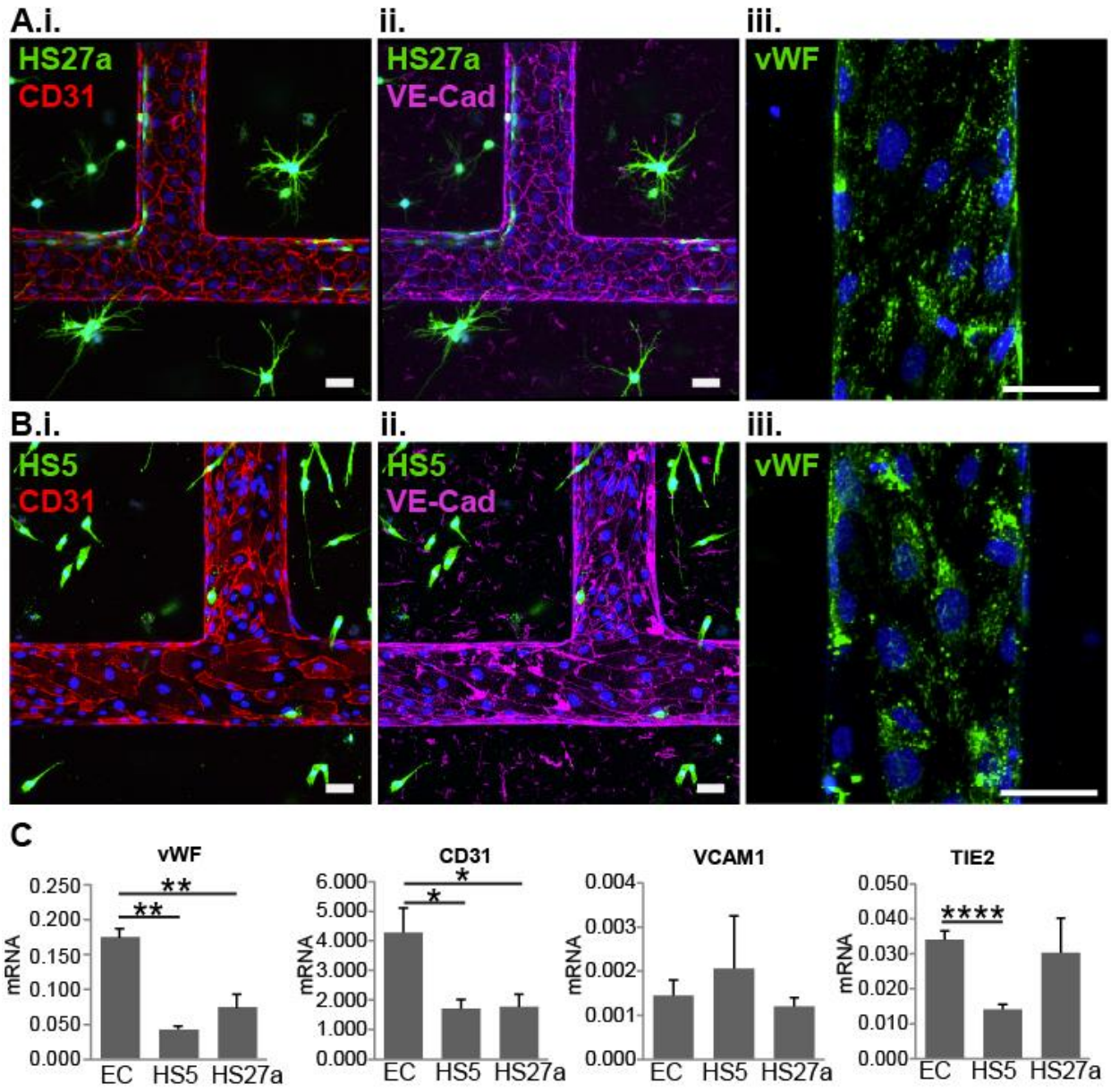

Figure 4.2. Endothelial phenotype changes with stromal cell co-culture. (A) Endothelial staining of HS27a and (B) HS5 co-cultured vessels shows differences in (i) CD31, (ii) VE-cadherin, and (iii) von Willebrand Factor. (C) RNA expression within the co-culture shows differences in endothelial junctional expression and inflammatory marker expression. *p < 0.05, **p < 0.01, *** p <0.001, ****p<0.0001.

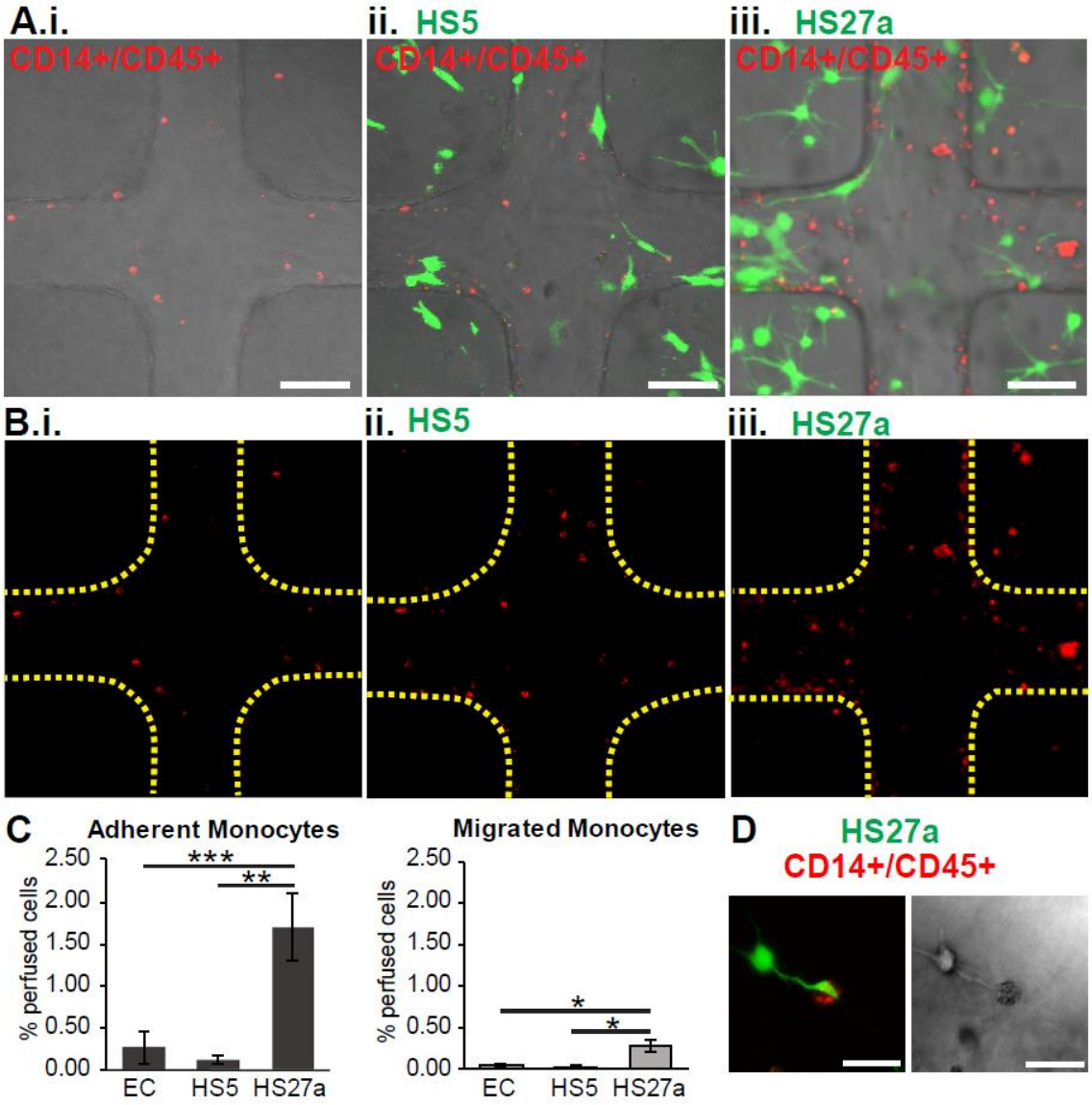

Figure 4.3. Microenvironment cues change perfused monocyte localization. (A) and Monocytes (red) perfused through unmodified, HS5, and HS27a-modified vessels adhere to the endothelium (not stained) and transmigrate into the matrix. Scale bars: 100 µm. (B) Monocytes from (A) are shown alone along with outlines of vessel walls. Scale bars: 100 µm. (C) Quantification of monocyte adhesion and migration shows percentage of cells adhered and migrated within vessels. *$p < 0.05$, **$p < 0.01$, *** $p < 0.001$. (D) An HS27a cell wraps around a monocyte that has transmigrated into the matrix.

Perfused monocytes adhere and transmigrate preferentially in HS27a-modified microvessels

Monocytes are known to circulate through the bloodstream and extravasate through the endothelium towards inflamed regions or tissue repair [213]. To test the functional contribution of the fibroblast-driven endothelial phenotype on monocyte interaction with vasculature, we perfused CD45+/CD14+ labeled monocytes, isolated from human peripheral blood, through the vessels and monitored their adhesion and extravasation in EC only or co-cultured microvessels (**Figure 4.3**). At 24

hours after perfusion, the percentage of monocytes adhered on the vessel wall was significantly more in HS27a co-cultured vessels (1.69 ± 0.40% of perfused cells) than in unmodified (0.26 ± 0.18%) or HS5 co-cultured vessels (0.11 ± 0.04%) (**Figure 4.3 A,B,C**). The percentage of monocytes that transmigrated into the matrix was also significantly increased in the HS27a co-cultured vessels (0.28 ± 0.07% of perfused cells) compared to EC only (0.04 ± 0.02%) and HS5-co-cultured vessels (0.02 ± 0.01%) (**Figure 4.3 C**). In addition, some monocytes that extravasated into the HS27a-seeded matrix appear to make deliberate contact with HS27a cell projections (**Figure 4.3 D**). To examine the source of this interaction, monocyte adhesion within HS27a co-cultured vessels was compared to EC vessels with HS27a-conditioned media (see **Appendix C, Supplementary Figure 4**). Monocytes adhered more in HS27a co-cultured vessels than in those with HS27a-conditioned media, suggesting that the contact-dependent cues rather than soluble factors modulate monocyte adhesion (see **Appendix C, Supplementary Figure 4**). This behavior has been seen *in vivo*, where marrow biopsy samples show the *in vivo* counterpart of HS27a cells, the CD146+ fibroblast, wrapped around marrow vessels and in contact with monocytes/macrophages [33,199]. The direct interaction between monocytes and HS27a fibroblasts indicates cell-cell crosstalk for the development of a complex tissue microenvironment.

Monocytes modify HSPC adhesion and trafficking

During tissue regeneration, HSPC recruitment may be directed by the local microenvironment. We next examined HSPC trafficking across the fibroblast modified microvessels. Labeled CD34+/CD45+ HSPCs were perfused through the microvessel system in EC-only, HS5, and HS27a co-cultures (**Figure 4.4 A,B,C**). Surprisingly, we found no significant differences in adhesion (0.45 ± 0.06%, 0.40 ± 0.08%, and 0.41 ± 0.07% of perfused cells in EC only, HS5, and HS27a vessels respectively) or extravasation (0.10 ± 0.03%, 0.11 ± 0.01%, and 0.10 ± 0.01% for EC only, HS5, and HS27a vessels) among vessels 24 hours post-perfusion. This pattern suggests that the fibroblast-endothelial microenvironments alone do not strongly influence HSPC trafficking (**Figure 4.4 C**)**.** However, when monocytes were perfused 24 hours prior to HSPCs in these same vessel co-cultures, the pattern of HSPC adhesion and extravasation was modified (**Figure 4.5**). When monocytes were present, HSPCs preferentially adhered within the EC and HS27a co-cultured vessels over the HS5 co-cultured vessels (0.35 ± 0.12% and 0.20 ± 0.03% in EC and HS27a vessels, respectively, over 0.05 ± 0.01% in HS5 vessels) (**Figure 4.5 A,B,C**).

Further analysis of data from Iwata et al shows that the direct co-culture of monocytes with HS27a fibroblasts, but not HS5 fibroblasts or conditioned media, resulted in an overall increase in VCAM1 expression, which may partially explain the increased retention of HSPCs in HS27a vessels (see **Appendix C, Supplementary Figure 5**) [199]. The baseline of HSPC adhesion and migration in the EC only context did not change with the inclusion of monocytes (0.45 ± 0.06% HSPCs adhered, 0.10 ± 0.03% migrated without monocytes compared to 0.35 ± 0.12% HSPCs adhered, 0.06 ± 0.02% migrated with monocytes). In contrast, HSPC adhesion within HS5 and HS27a co-cultured vessels was reduced when monocytes were present compared to the corresponding vessels without co-perfused monocytes: adhesion was

reduced from 0.40 ± 0.08% to 0.05 ± 0.01% in HS5 vessels, and from 0.39 ± 0.07% to 0.20 ± 0.04% in HS27a vessels. To explore the role of VCAM1 in HSPC adhesion in these co-perfused vessels, we perfused a VCAM1 blocking antibody after monocyte perfusion in the HS27a co-cultured vessels and prior to HSPC perfusion (**Figure 4.6 A,B**). However, after perfusion of monocytes, blocking VCAM1 did not change adhesion or migration patterns of HSPCs in HS27a co-cultured vessels (**Figure 4.6 C,D**). This data suggests that while monocytes and stromal fibroblasts play a role in modulating HSPC adhesion, VCAM1 is not the adhesion molecule that significantly directs HSPC trafficking. We show that monocytes interact with stromal cells and modify the microvascular environment, which in turn changes HSPC trafficking.

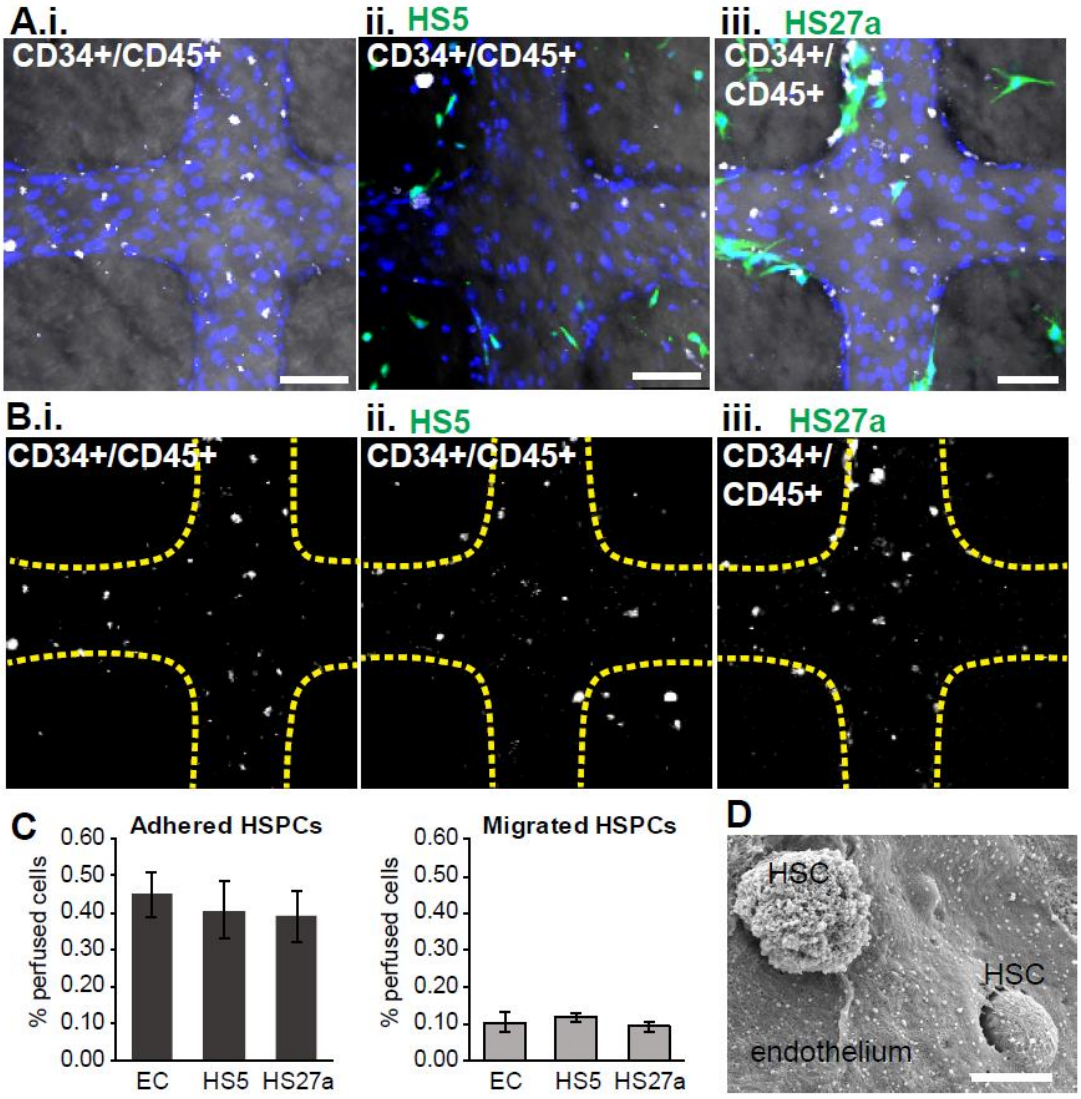

Figure 4.4. Microenvironment cues do not change CD34+ HSPC localization. (A) CD34+ HSPCs perfused through unmodified, HS5, and HS27a-modified vessels adhere to the endothelium (not stained) and transmigrate into the matrix. Scale bars: 100 µm. (B) CD34+ cells from (A) are shown alone with outlines of vessel walls (yellow dotted lines). (C) Quantification of CD34+ HSPC adhesion and migration shows percentage of cells adhered and migrated within vessels. (D) Scanning electron microscopic image of an HSC adhered and transmigrating through the endothelium in a vessel construct.

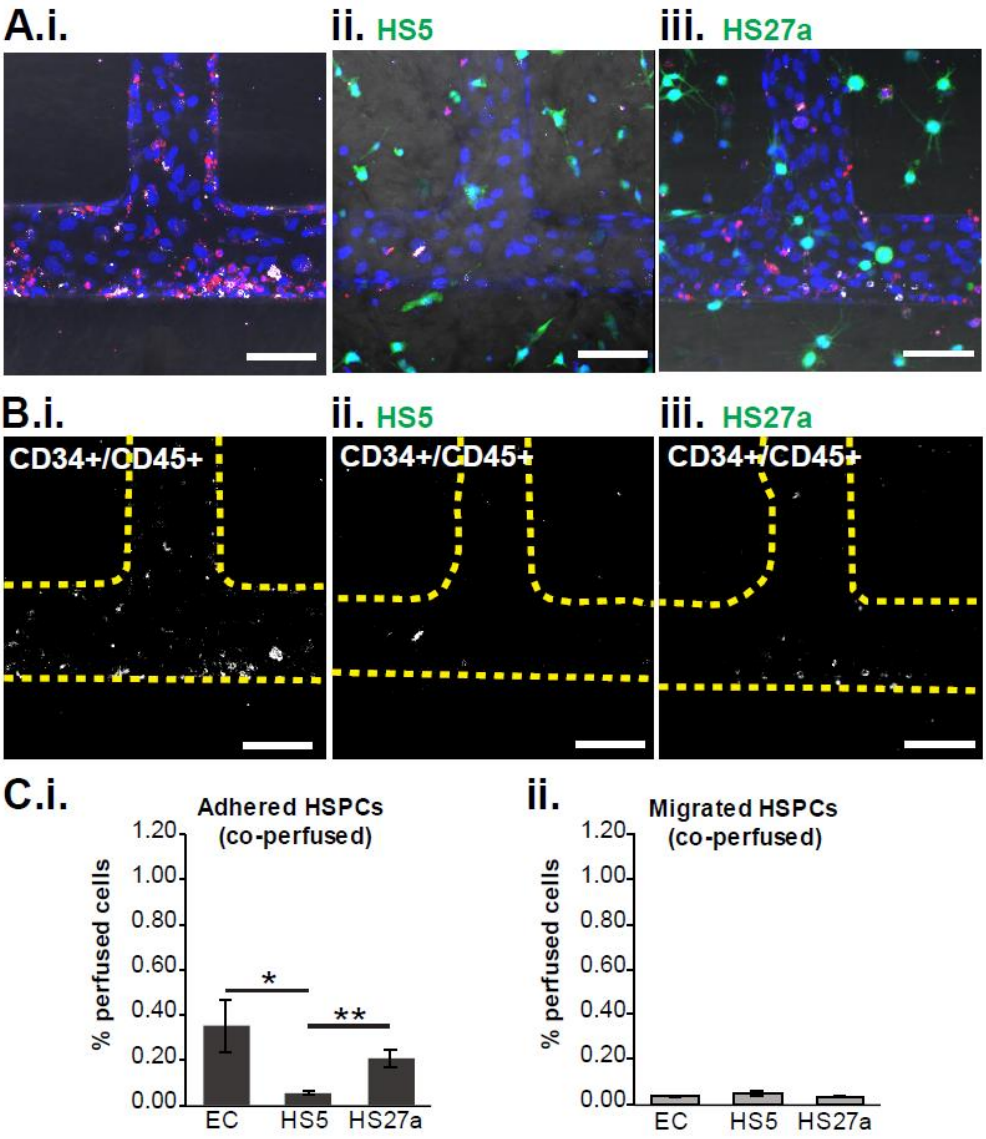

Figure 4.5. When perfused after monocytes, CD34+ cells preferentially adhere in EC and HS27a-modified vessels. (A-C). Healthy CD34+ cells (white) are perfused 24 hours after monocytes (red) in each vessel type. Healthy CD34+ cells and monocytes appear to cluster. Blue = nuclei. (B) Locations of healthy CD34+ cells are seen relative to vessel wall (yellow dotted line). Scale bars: 100 μm. (C) Quantification of CD34+ cells adhesion and migration in vessels. *$p < 0.05$, **$p < 0.01$.

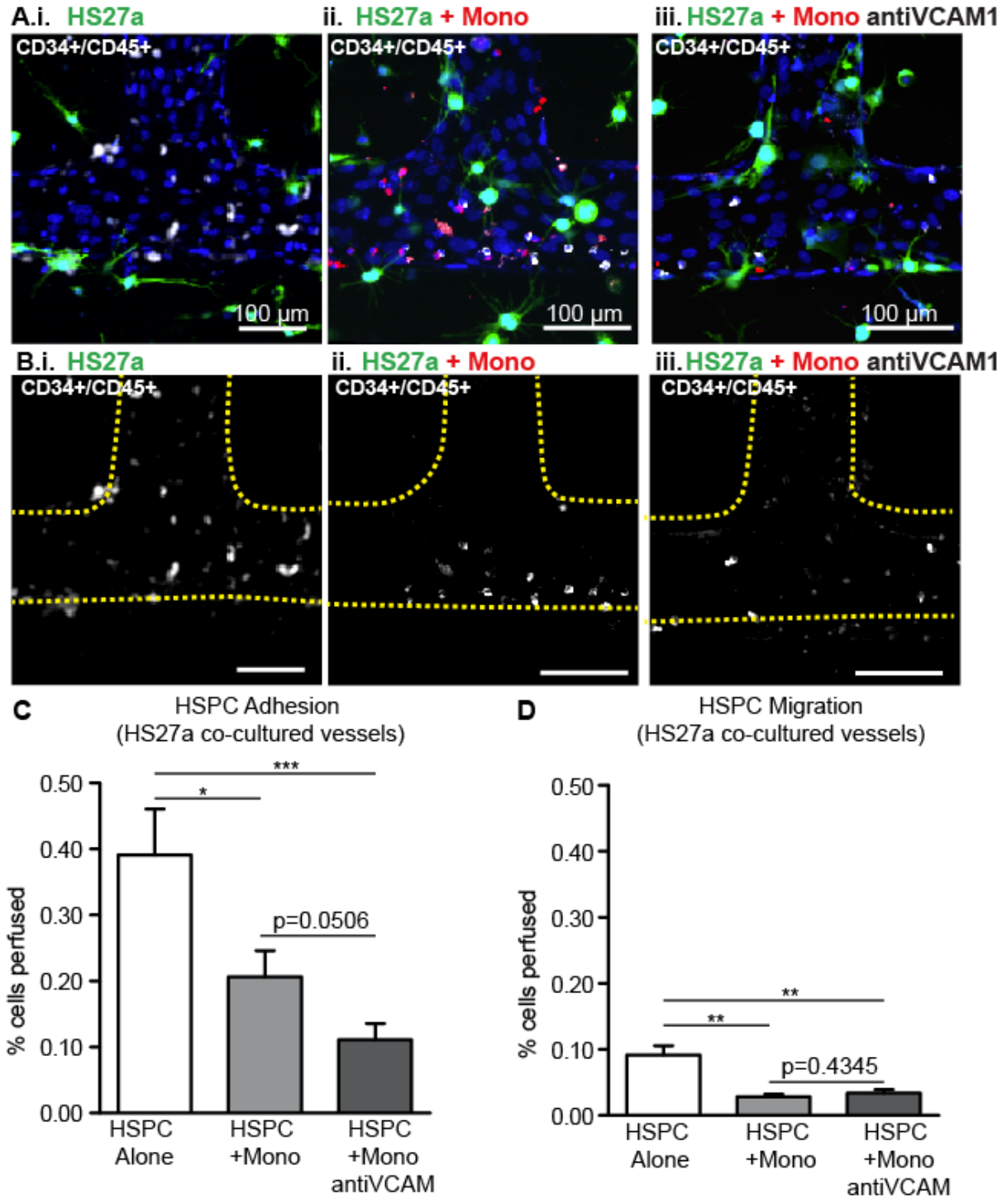

Figure 4.6. Monocytes, not VCAM1, determine HSPC trafficking in HS27a vessels. (A) HSPCs were perfused through HS27a co-cultured vessels (i) alone, (ii) after monocyte perfusion, or (iii) after monocyte and VCAM1 blocking antibody perfusion. (B) HSPCs are shown with the vessel boundary (yellow dotted line). Scale bars: 100 μm. Quantification of (C) HSPC adhesion and (D) migration behavior from these vessels show that monocytes change HSPC adhesion and migration but blocking VCAM1 in the presence of monocytes does not significantly change adhesion and migration. *p < 0.05, **p < 0.01, *** p <0.001.

Leukemic cells show heightened response to fibroblasts without monocytes

The establishment of a fibroblast niche further enables the examination of leukemic cell behavior within the *in vitro* marrow space. The differences between leukemic cells and healthy HSPCs with respect to their interactions with the endothelium are not well understood. In order to examine the affinity of leukemic cells in the fibroblast-directed microenvironments presented here, patient-derived acute myeloid leukemic cells were perfused through unmodified, HS5, or HS27a co-cultured vessels (**Figure 4.7**). The adhesion and migration of leukemic cells was significantly increased in HS27a co-cultured vessels, with 0.77 ± 0.14% of perfused cells adhered in HS27a vessels compared to 0.14 ± 0.04% and 0.33 ± 0.07% of cells perfused through EC only and HS5 co-cultured vessels respectively (**Figure 4.7**). A smaller but significant increase in adhesion was also present in leukemia cells perfused in HS5 co-cultured vessels over EC only vessels (**Figure 4.7 C**). The same trend was present in migrated cells, with significant increases from EC only vessels (0.01 ± < 0.01%) to HS5 vessels (0.02 ± < 0.01%) and from HS5 vessels to HS27a vessels (0.19 ± 0.04%) (**Figure 4.7 C**). Unlike HSPCs perfused alone, patient-derived CD34+ leukemic cells showed a strong fibroblast-directed adhesion and migration pattern (**Figure 4.7 C**).

When leukemic cells are perfused after monocytes, the distribution of leukemic cells is changed compared to perfusion of either cell type alone (**Figure 4.8**). Co-perfused leukemic cells showed no differences in adhesion between the vessel conditions (0.37 ± 0.06%, 0.21 ± 0.05%, 0.45 ± 0.01% in EC only, HS5, and HS27a vessels, respectively) (**Figure 4.8 C**). Transmigration of leukemic cells also showed no significant differences among vessel conditions (0.09 ± 0.02%, 0.04 ± < 0.01%, and 0.05 ± 0.01% in EC, HS5, and HS27a vessels, respectively) (**Figure 4.8 C**). In combination, this suggests that, when monocytes are present, patient-derived leukemic cells lose their responsiveness to fibroblast-specific environments. This system thus differentiates the niche components responsible for dictating patterns of cell adhesion and extravasation.

4.5 DISCUSSION

The vascular microenvironment plays an integral role in hematopoietic cell adhesion, transmigration, and engraftment [31,101,173,191,194,195,214]. Detailed exploration of the dynamics between niche components and the contribution of the fibroblasts, endothelial, and hematopoietic cells is needed to understand marrow function and tissue regeneration [101,215]. Here, we have utilized an engineered microvascular platform to show that fibroblast-directed crosstalk alters hematopoietic cell adhesion and transmigration into the extravascular space.

Through the use of this multicellular co-culture with a perfusable vascular network, we first demonstrated the influence of specific marrow fibroblasts on the endothelium, which subsequently influences monocyte adhesion and extravasation. HS27a and HS5 represent functionally distinct marrow components [205,216]. In 2D cultures, analysis of multicellular interactions with these cells is limited due to overgrowth. However, fibroblasts in 3D collagen are relatively non-mitotic, more closely approximating their

in vivo behavior [215,216]. In our system, both MSCs and HS27a fibroblasts wrapped around the vessel wall while the HS5 fibroblasts did not. The co-cultured vessels displayed different RNA expression, and the interaction of these cells with the endothelium creates a fibroblast-defined vascular niche. Though the use of marrow sinusoidal endothelial cells would be ideal, the availability of this cell type is limited. Here, we show that HUVECs are able to adapt in response to microenvironmental influences from stromal fibroblasts. Functional evidence of these changes are shown through the differential adhesion of monocytes in the fibroblast co-cultured vessels.

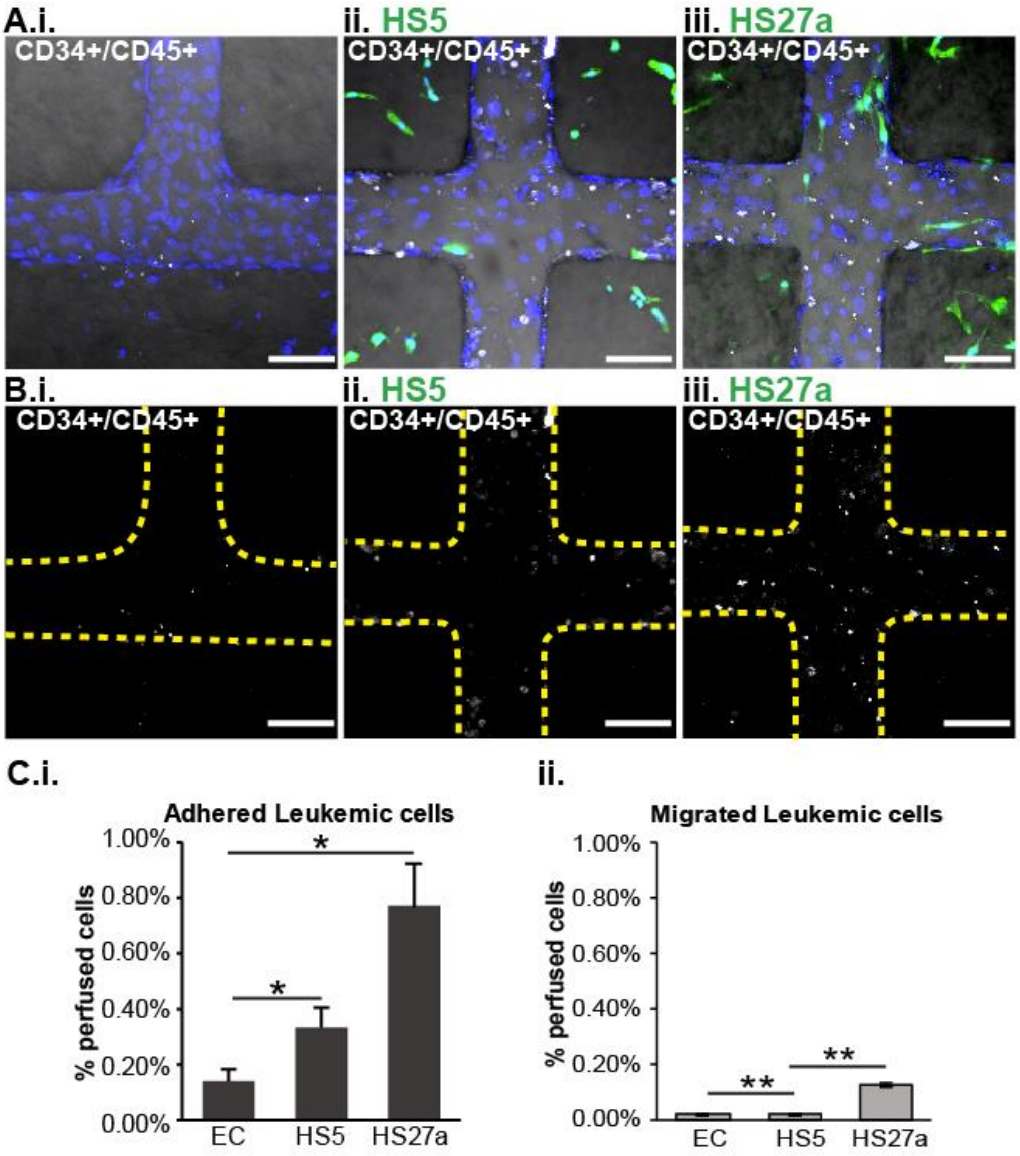

Figure 4.7. Leukemic cells perfused alone respond to microenvironmental cues. (A) Leukemic CD34+ cells perfused through unmodified, HS5, and HS27a-modified vessels adhere and migrate. (B) Visualization of the leukemic cells with regards to the vessel walls (yellow dotted lines). blue = nuclei, scale bars 100 μm. (C) Quantification of adhesion and migration of leukemic cells. Significant differences are shown between unmodified (EC) and stromal conditions unless marked. * $p < 0.05$, ** $p < 0.01$.

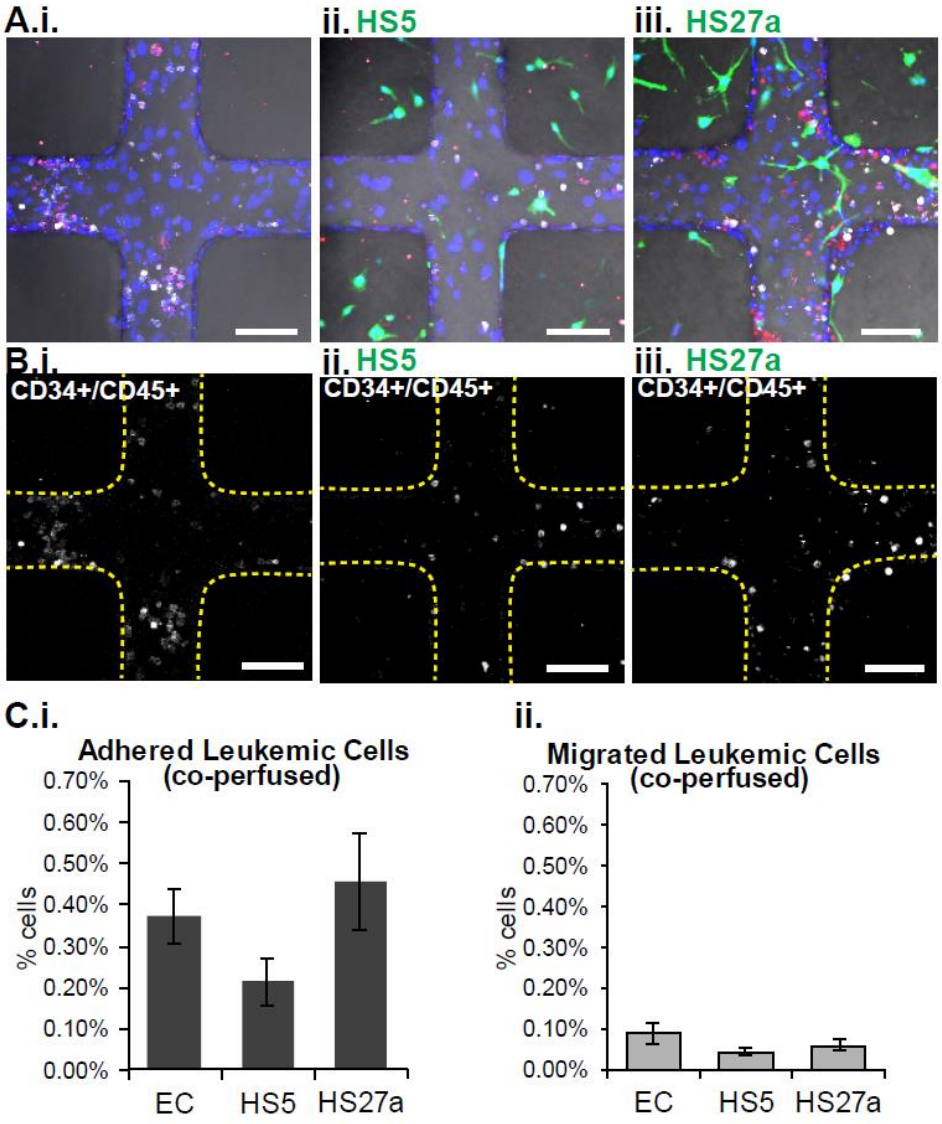

Figure 4.8. Leukemic cells perfused after monocytes do not adhere based on stromal cues. (A) Leukemic CD34+ cells perfused after monocytes in unmodified, HS5, and HS27a-modified vessels. Blue = nuclei. (B) Adhesion and migration of leukemic cells are shown in relation to the vessel walls (yellow dotted lines). Scale bars 100 μm. (C) Quantification of leukemic CD34+ cell adhesion and migration.

Our data further shows that crosstalk between circulating monocytes and fibroblasts modifies the vascular microenvironment. Perfused HSPCs showed no preferential adhesion or extravasation among any co-culture conditions. However, after the perfusion of monocytes, HSPCs demonstrated preferential recruitment into HS27a co-cultured vascular space. Leukemic CD34+ cells, contrastingly, had the opposite trend compared to the healthy HSPCs. Alone, leukemic cells did show preferential migration towards the HS27a co-cultures. Monocyte perfusion removed the leukemic cell preference towards a fibroblast-modified microenvironment. The ability of these cells to sense and respond to differences in the vascular

microenvironment demonstrates the necessity of a specific co-culture system to study hematopoietic recruitment and the niche space.

Previous studies have identified that monocytes/macrophages create a permissive niche for HSPC residence in the marrow, such that the combination of these cells with stromal fibroblasts are necessary to maintain marrow HSPC populations [34,85,175,176,200,201]. Thus, these results suggest that the monocytes recruited to the extravascular space modulate HSPC and leukemic cell adhesion and extravasation through cellular crosstalk [33,85,204]. Healthy HSPCs, then, rely on monocytes to regulate their extravasation in the presence of stromal co-cultures, but not solely through VCAM1-mediated adhesive interactions. However, monocytes block leukemic cell sensitivity to stromal contexts, perhaps due to a loss of adhesive integrin interactions or prevention from adhesive interactions by monocytes that occupy the same binding sites. *In vivo* studies also suggest opposing niche spaces for leukemic and HSPC cells, indicating different components are required to support leukemic or healthy niche spaces [84,217]. The use of three separate acute myeloid leukemia patient samples in this study could have contributed to a wide variation in leukemic cell behavior. Overall, the functional crosstalk between hematopoietic cells and the vascular microenvironment is evident in this platform. Improved microphysiological models for human marrow can greatly mitigate challenges to examining multicellular interactions in hematopoietic biology.

Here, we have shown that different vascular microenvironments created by functionally divergent fibroblast cell types affect hematopoietic trafficking across the vasculature. Understanding these multifaceted cellular interactions within a vascular system provides insight to the endothelial niche. In disease contexts, microenvironmental aberrations have been implicated in the induction of disease phenotypes, particularly in leukemia and other hematopoietic malignancies [81,217–219]. There is significant potential for a tunable system such as this to be used as a tool in preclinical therapeutics testing and precision medicine. With this platform, it is possible to study in further detail the mechanisms behind dynamic spatial and temporal cell-cell interactions within the vascular niche, in both healthy and disease-remodeled marrow spaces.

Chapter 5

In Vitro Modeling of Leukemia-Induced Angiogenic Sprouting

5.1 ABSTRACT

Angiogenesis in the context of cancer occurs in response to nutrient demands and disruption of normal vascular patterning by expanding malignant cells. However, the mechanisms underlying these phenomena have proven to be complex and vary among different cancer types and patients. In myeloid leukemia, examination of patient marrow has shown that some patients have extensive marrow angiogenesis at diagnosis. Therapeutic efforts to block major angiogenic pathways have yielded heterogeneous results, largely due to the variation in leukemia mutation profiles among patients. Increased efforts are needed to understand the varying mechanisms present. Here, we demonstrate, for the first time, *in vitro* platforms to gain insight into leukemia-induced angiogenic sprouting. We demonstrate that out of four malignant cell lines (U937, HL-60, K562, and KG1a), only two (K562 and KG1a) consistently induce sprouting in a monolayer angiogenesis assay. In a 3D microvessel model, we demonstrate the VEGFR2-dependence of KG1a-induced sprouting but not K562-induces sprouting. We demonstrated the utility of 3D culture platforms for examining leukemia-induced sprouting *in vitro.* Further use of such platforms can yield insight into the varying mechanisms present in hematological malignancies and potentially direct therapeutic interventions.

5.2 INTRODUCTION

Acute myeloid leukemia (AML) occurs when neoplasms arise within the myeloid progenitor lineage, preventing the maturation of hematopoietic cells. The abnormal progenitor cells proliferate, accumulate in the marrow and peripheral blood, and inhibit normal hematopoiesis [81–84]**.** Disordered interactions of AML cells with healthy hematopoietic cells drives changes to the marrow microenvironment such as disrupted cell-cell interactions and cytokine secretion [81,84,85]**.** Of particular interest is the ability of leukemic cells to modify the marrow space by remodeling the marrow vasculature [83,88]. Though tumor–induced neoangiogenesis has been observed in great detail for many cancer types, this phenomenon within the marrow is not well understood [220,221].

Analyses of patient biopsies and high contrast MRI on marrow has revealed that marrow vascularity is markedly increased in a large proportion of AML patients [91,92,222–224]. Detection of marrow angiogenesis at diagnosis is used as an indicator of clinical outcome. However, the presence or degree of vascularity do not seem to correlate directly to cell burden or progression stage [91,92]. Detailed characterization of patient cell isolates has revealed that mRNA of pro-angiogenic factors such as VEGF,

bFGF, HIF1α, IL-8, and MMPs are expressed at varying levels among patients [90,223,225,226]. However, the relationship between AML cell factor expression and the amount of vascularity is not seen. Further, the morphology of marrow sprouts in AML marrow is varied, with large dilated vessels found in some biopsies, but smaller, immature sprouts found in others [224]. This heterogeneity in presentation, cell phenotype, and vessel morphology suggests varied mechanisms of leukemia-induced vascular remodeling based on variations in the cytogenetic profile of the AML.

Angiogenesis in the diseased marrow provides nutrient support for leukemic cells, and potentially enables their release into circulation [92,227]**.** Anti-angiogenic therapeutics blocking VEGFA, VEGFR2, and associated factors have had significant clinical impact in many cancer types [228,229]. However, efforts to prevent AML-induced vascular remodeling have been largely mixed. Initial studies on the inclusion of the anti-VEGFA antibody bevicazumab in therapeutic regimes reported improved overall and progression-free survival [230,231]; however, other reports suggest that these antibodies imparted little effect [232,233]. Targeting of other angiogenesis-associated pathways has yielded some improvement [229]. As such, a more detailed understanding of the variation in leukemia-induced angiogenesis can help identify key mechanisms to prevent angiogenic remodeling, potentially allowing for more targeted and effective treatment strategies.

To date, most research on leukemia-induced angiogenesis has occurred through analysis of bone marrow aspirates and biopsies [90–92,234]. Though these provide great insight into the progression and characterization of disease progression, controlled manipulation of cell behavior in this context is not possible. *In vitro* studies on the cancer microenvironment have increasingly begun to rely on 3D cell culture techniques, allowing for the use of human cell types cultured in biologically-relevant geometries [235–239]. Current 3D culture approaches for AML utilize cell spheroids or scaffold-based systems to model the tumor microenvironment [240–242]. Examination of endothelial responses to AML cells largely rely on conditioned media and chemotaxis assays, which measure the migration of endothelial cells across a mesh and not actual sprout formation within a native matrix [223,238,243]. To our knowledge, no platform has been developed to recreate this phenomenon *in vitro* and investigate the interaction of leukemic cells with vasculature.

Here, we present two 3D culture systems with 4 leukemic cell lines to model leukemic influences on endothelial cells and vasculature: a 2D monolayer sprouting assay and a 3D perfusable microvessel platform (**Figure 5.1)** [108–110]. A monolayer angiogenesis assay consists of endothelial cells seeded on top of collagen I matrix embedded with leukemia cells. The endothelial cells can sense secreted cytokines from the leukemia cells in the matrix and are able to remodel the collagen matrix to form sprouts in a natural matrix substrate. This platform has the advantage of high throughput fabrication and culture of leukemia cells in a 3D matrix. The microvessel platform incorporates perfusable vasculature embedded in a collagen matrix [108]. Here, endothelial cells are seeded within the network where they self-assemble into a lumen. Leukemia cells are seeded within the matrix on one side of the vessel, allowing for close cell-cell interactions

and signaling. The advantage of this system lies in the geometry and laminar flow, providing a biologically relevant context for endothelial cells [110].

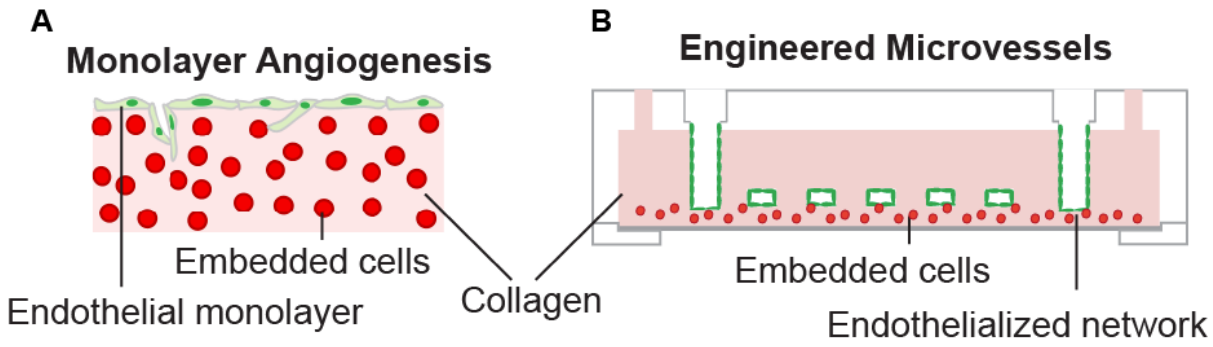

Figure 5.1. *In vitro* platforms to examine leukemia-induced angiogenesis. (A) A monolayer of endothelial cells seeded above a leukemia cell embedded collagen matrix allow sprouting angiogenesis into the matrix. (B) An engineered microvessel platform containing a perfused vascular network contains embedded leukemia cells to visualize angiogenesis from patent vessels.

We demonstrate that the co-culture of leukemic cells in a 3D collagen matrix with a 2D endothelial monolayer (**Figure 1A**) in conjunction with leukemic cells surrounding a perfused 3D microvessel network **(Figure 1B**) can induce VEGF-dependent angiogenic sprouts. These 3D platforms are the first to visualize leukemia-induced vascular remodeling *in vitro*, and have the potential to provide significant insight to the mechanisms involved.

5.3 EXPERIMENTAL METHODS

Leukemia Cell Lines

Leukemia cell lines U937, HL-60, K562, and KG1a were provided as a generous gift from the Torok-Storb lab. All cell lines were transduced to express the mCherry fluorescent protein under the PGK promoter. Viral packaging was performed in 293T cells transfected with 2µg VSV-G (Addgene # 12259), 5 µg (Addgene # 12260), and 10 µg mCherry (modified from Addgene #12252) plasmids per 10cm plate with a standard calcium phosphate transfection protocol. Media was conditioned from 24-48 hours post-transfection and collected, then centrifuged at 4,000g for 24 hours at 4°C. Supernatant was removed, the viral pellet was resuspended, and frozen at -80°C. Protamine sulfate was added to leukemia cell lines to a final concentration of 8µg/ml (4µl/ml) along with the virus. Media (IMDM + 10% fetal bovine serum) was replaced after 16 hours. After 2-3 days of culture, cells were sorted for mCherry expression (BD FACS Aria II). All mCherry-expressing cell populations were expanded and frozen prior to use.

Expression Analysis

RNASeq expression data for U937, HL60, K562, and KG1 leukemia cell lines were obtained from the Cancer Cell Line Encyclopedia (CCLE, Novartis). Pathway enrichment of the top 130 angiogenesis-associated genes was performed via ToppFun Pathway enrichment. Heatmaps of normalized mRNA reads were visualized with MultiExpression Viewer (Center for Cancer Computational Biology, Dana-Farber Cancer Institute). Hierarchical clustering was performed with Pearson's Correlation to measure similarity of genes. RNA from K562 and KG1a cells cultured in collagen for 3 days at 5 million cells per mL was collected through direct lysis of cells in collagen using RNeast Miniprep kit (Qiagen). Synthesis of cDNA was performed using iScript cDNA Synthesis kit (Bio-Rad). Quantitative PCR was performed using Power SYBR Green PCR mix using the 7900HT Fast-Real-time PCR system (Applied Biosystems). Fold change in expression for each primer pair is quantified relative to GAPDH.

Angiogenesis Assays and Microvessel Fabrication

For monolayer angiogenesis assays, leukemic cell lines were embedded in a collagen matrix (6 mg/mL) at 5 million cells/mL and 20 million cells/mL and plated into 4mm PDMS wells. Human umbilical vein endothelial cells (HUVECs) were seeded as a monolayer on the top surface. Well devices were fabricated in triplicate and fed with endothelial growth media (EGM, Lonza).

For microvessel assays, soft lithography and injection molding of collagen I was used to fabricate perfusable networks. Leukemia cells were seeded at 5 million cells/mL on the bottom half of the vessel. To seed microvessels, HUVECs were trypsinized and resuspended at a concentration of 8×10^6 cells/mL [108,110]. After removal of media from the inlet and outlet of the devices, 10uL of HUVEC suspension was added into the inlet of microvessel and allowed to attach at 37°C for 15 min. After attachment, media was added to the inlet reservoir for perfusion culture. Microvessels were perfused with EGM from the inlet reservoir. Media was replaced every 12 hours.

For VEGF blocking studies in angiogenesis assays and microvessels, initial endothelial cell seeding was done with EGM. 24 hours after fabrication, media was changed to EGM supplemented with soluble recombinant human VEGFR2-Fc chimera (200 ng/mL).

Immunofluorescence staining and sprout quantitation

All devices were fixed *in situ* at 3 or 7 days after fabrication with 4% formaldehyde followed by three 15 minute washes with PBS. Immunofluorescence staining of both the angiogenesis assay devices and microvessels were performed to visualize endothelial sprouting. A blocking solution of 2% bovine serum albumin (BSA) and 0.1% Triton X-100 (Invitrogen) was added for 1 hour prior to the addition of rabbit anti-human CD31 (Abcam) primary antibody, which was incubated overnight at 4°C. The devices were washed three times with PBS for 15 minutes each. The goat anti-rabbit Alexa Fluor 647 or Alexa Fluor 488 (Invitrogen) secondary antibody and Hoechst 33342 nuclear counterstain were then added and incubated

at room temperature for one hour, then washed three times for 20 minutes each.

Immunofluorescence z-stack images of angiogenesis assays (step size 3µm, 150µm depth) and microvessels (step size 10µm, 150µm depth) of microvessels were taken with a Nikon A1R confocal microscope with a 10x objective. For angiogenesis assays, z-stacks were resliced to view the y-z plane and z-projections of 20 slices each were created using Image J (National Institutes of Health). Sprouts from each projection were manually quantified. For microvessels, a large image z-stack was acquired to show the full side of the vessel grid. Sprouts were manually quantified from a z-projection. Significant differences between control and anti-VEGF treated conditions were determined using Welch's t-test.

5.4 RESULTS

Leukemic cell lines express varied pro-angiogenic genes

Leukemia cell lines K562, HL-60, and KG1 are derived from patients with different myeloid leukemias, while cell line U937 is derived from histiocytic lymphoma [244–247]. KG1a, the cell type used in further experiments within this study, is a subtype of KG1 discovered after *in vitro* expansion of this cell line [247]. Examination of the mRNA expression profile of the U937, HL60, K562, and KG1 cell lines was performed from RNASeq data made available by the Cancer Cell Line Encyclopedia (Novartis). Pathway enrichment and hierarchical clustering of angiogenesis-associated genes showed varied expression of potent angiogenic regulators such as VEGFA, VEGFB, angiopoietin 1, and angiopoietin 2, and inflammatory cytokines such as IL-1β, IL-6, and IL-8 (**Figure 5.2**). VEGFA, known to signal through endothelial VEGFR2, and VEGFB, which signals through VEGFR1, are known as the primary regulators of sprouting angiogenesis [228]. Angiogenic factors are known to induce changes to EC function and sprouting [228]. Preliminary data on KG1a (a subtype of the KG1 cell line) and K562 cells cultured in collagen further demonstrate differences in proangiogenic factor expression (**Appendix D, Supplementary Figure 1**). KG1a cells express more VEGFA and VEGFB but less ANGPT2 and MMP2 than K562 cells. Variation in pro-angiogenic factors could determine the mechanisms inducing endothelial remodeling and sprouting by the leukemic cell lines in this study. Leukemia cell lines that express high levels of angiogenic factors have the potential to induce endothelial sprouting *in vitro.*

Leukemia cell lines induce varying amounts of angiogenesis

To investigate the effect of leukemic cells on endothelial remodeling, each cell line (U937, HL60, K562, and KG1a) was co-cultured with endothelial cells in an angiogenesis assay. Prior to seeding, leukemia cell lines were transduced to express the mCherry fluorescent protein for ease of visualization. The cells were then embedded within a collagen I matrix at 5 million cells/mL and 20 million cells/mL, with a human umbilical vein endothelial cell (HUVEC) monolayer seeded on the top of the matrix. Collagen matrices with endothelial cells but no leukemia cells embedded were used as controls. After 3 and 7 days

of co-culture, constructs were fixed and stained for CD31, an endothelial junctional marker, to examine angiogenic sprouting into the matrix.

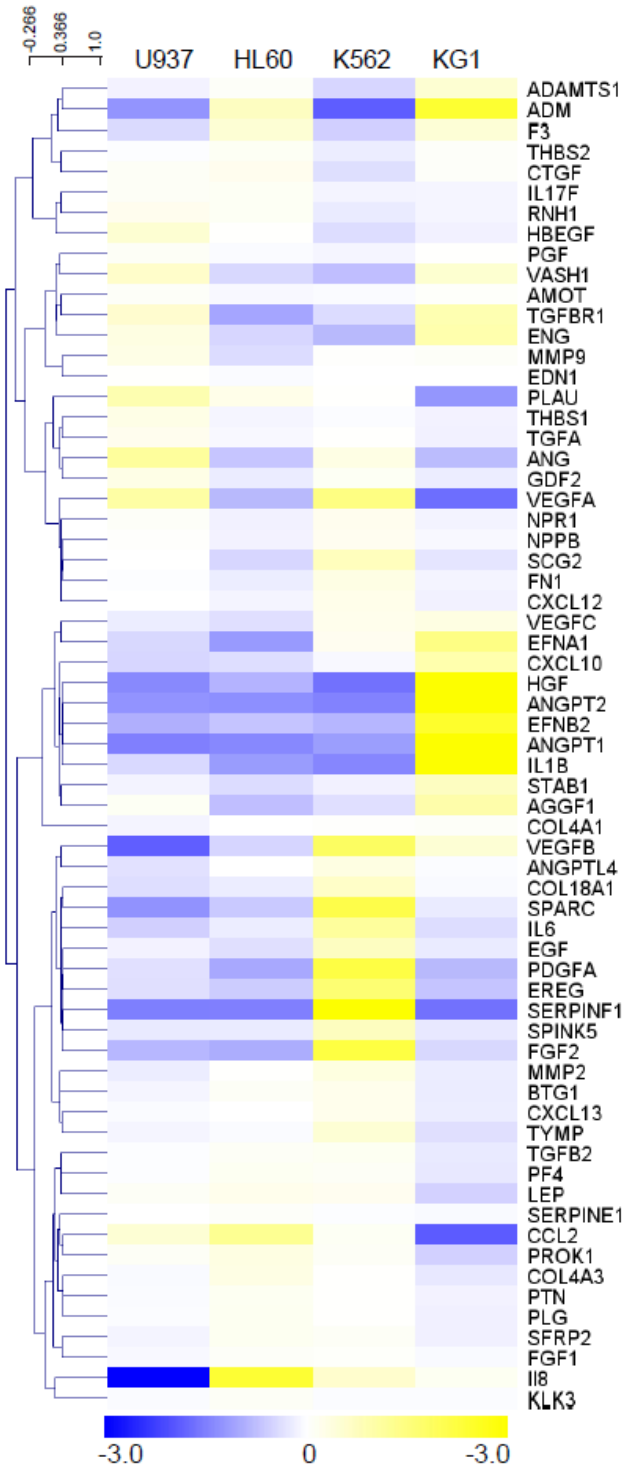

Figure 5.2. Hierarchical clustering of angiogenesis-associated genes in U937, HL60, K562 and KG1 cell lines. Yellow indicates higher than average expression, while blue indicates lower than average expression.

After 3 days, all four leukemia cell lines seeded at 5 million cells/mL induced a significant number of sprouts per field of view compared to the EC only condition (**Figure 5.3 A**). At day 7, U937, K562, and KG1a maintained a significant increase in sprout number compared to the EC-only condition, while HL60 did not induce a significantly higher number of sprouts (**Figure 5.3B**). Confocal imaging of the constructs at day 3 showed intact endothelial CD31 junctional staining in the EC-only condition, but heterogeneous and diffuse CD31 expression in the KG1a constructs. This pattern of expression suggests an unstable and inflamed endothelium [248,249].

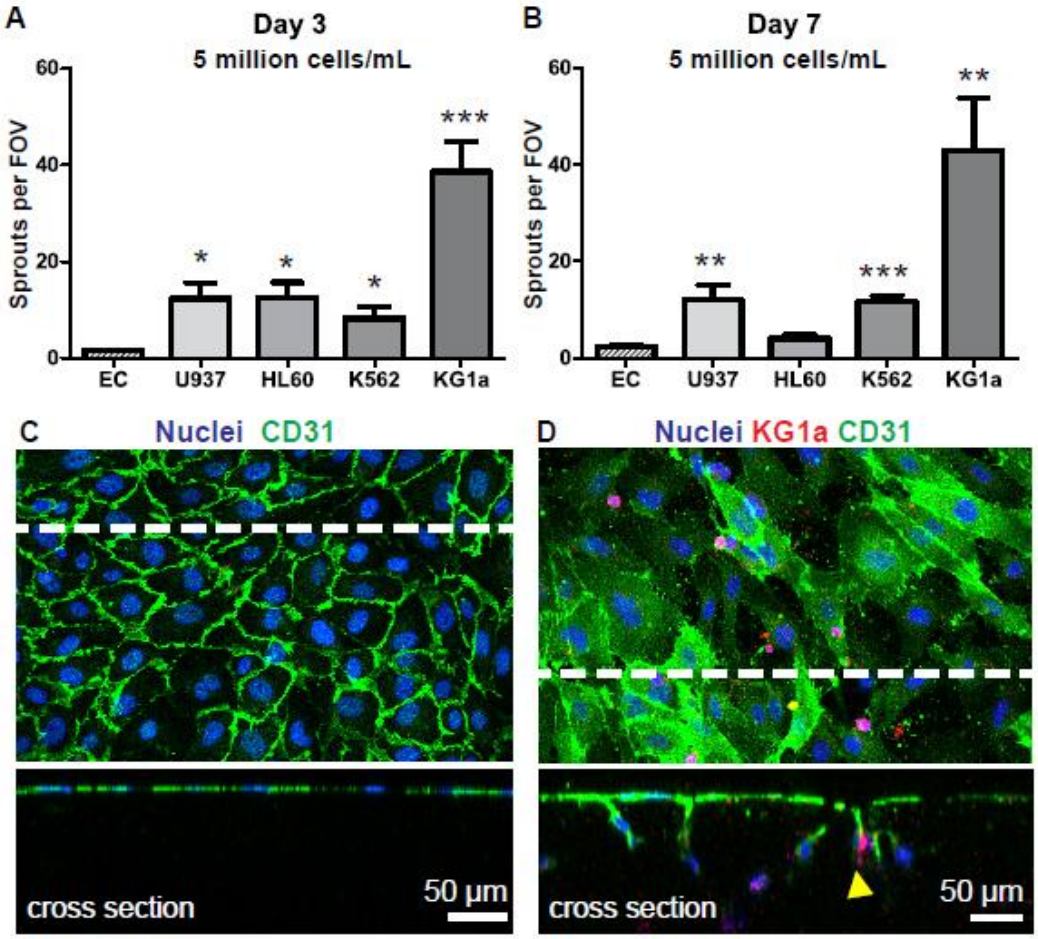

Figure 5.3. Leukemic cell lines induce endothelial sprouting into the matrix. (A) Leukemic cells seeded at 5 million cells per mL induced endothelial sprouting at day 3 and (B) day 7 of co-culture. (C) immunofluorescence confocal imaging shows CD31 junctional staining on EC-only cultures and (D) sprouting in KG1a -EC co-cultures. cross sectional views around the dashed lined are shown. Yellow arrowheads indicate KG1a cells co-localized with a sprout. * $p < 0.05$, ** $p < 0.01$, *** $p < 0.001$.

Leukemia cells seeded at a high density in collagen matrix (20 million cells/mL) also induced endothelial sprouting after 3 and 7 days. At 3 days, K562 and KG1a induced more sprouts per field of view than in the EC condition (**Figure 5.4 A**). After 7 days of culture, HL60, K562, and KG1a induced a significantly increased number of sprouts from the EC-only condition (**Figure 5.4 B**). The overall number of sprouts induced by these cell lines nearly doubled compared to the 5 million cells/mL condition. Immunofluorescence staining of endothelial CD31 shows strong junctions in ECs cultured alone, but diffuse staining in KG1a-EC co-cultures (**Figure 5.4 C,D**). In addition, within the KG1a co-cultures some EC lumens appear within matrix, suggesting sprouts that may have become disconnected from the monolayer. These co-cultures reveal the varied effects of myeloid leukemia and lymphoma-derived cell lines on an *in vitro* EC monolayer.

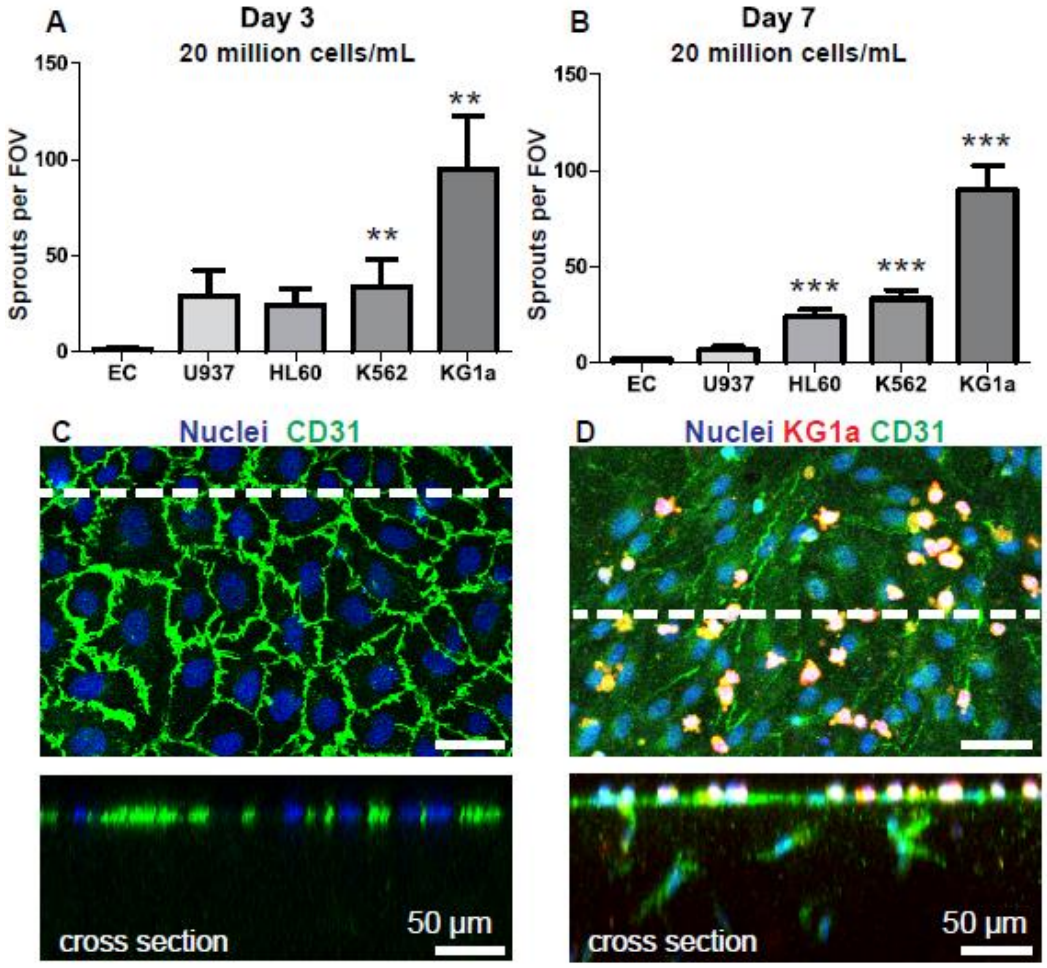

Figure 5.4. Leukemic cell lines seeded at high density induce endothelial sprouting into the matrix. (A) Leukemic cells seeded at 20 million cells per mL induced endothelial sprouting at day 3 and (B) day 7 of co-culture. (C) immunofluorescence confocal imaging shows CD31 junctional staining on EC-only cultures and (D) sprouting in KG1a -EC co-cultures. Cross sectional views around the dashed lined are shown. ** $p < 0.01$, *** $p< 0.001$.

VEGFR2 blockade does not change sprouting in monolayer angiogenesis assays

To gain insight into the mechanisms behind the leukemia cell-induced sprouting, we performed a VEGFR2 blocking study. The two cell lines that displayed sustained increases in angiogenic sprouts, K562 and KG1a, were seeded at 5 million cells/mL in the monolayer angiogenesis assay platform. The media was supplemented with a recombinant soluble VEGFR2/Fc chimera (200 ng/mL) known to block the VEGFR2 receptor and inhibit VEGFA-induced angiogenesis [229]. After 3 days of culture, there was a significant decrease in the number of sprouts in K562 co-cultured endothelial monolayers but, surprisingly, no change in the number of KG1a-induced sprouts when the VEGFR2 blocking antibody was added to the media (**Figure 5.5 A)**. After 7 days of culture, the effect of the antiVEGFR2 on K562 was lost, and KG1a maintains no change to the number of sprouts (**Figure 5.5 B)**. These results show that blocking VEGFR2 can have varying effects that are not only based on cell type, but also over time.

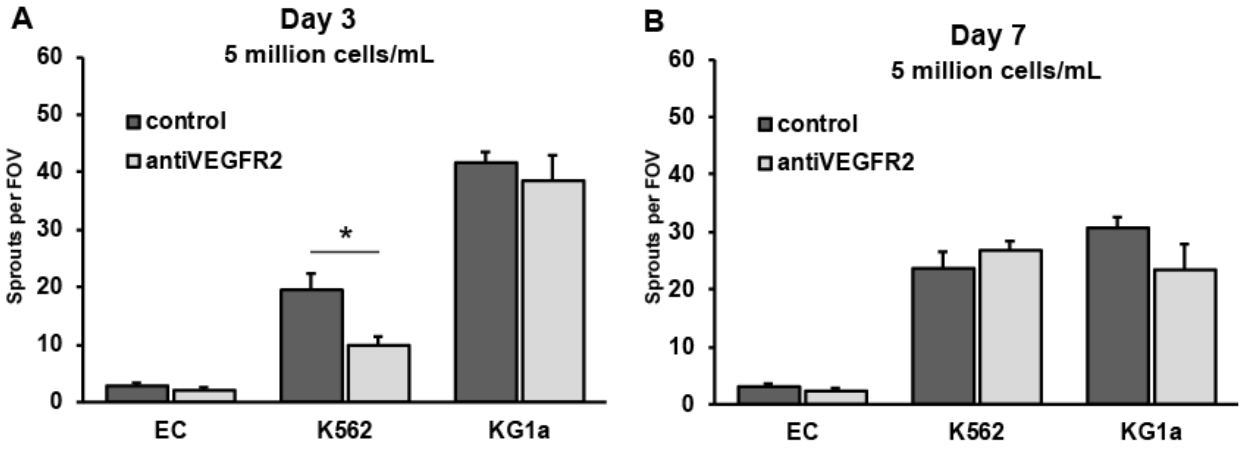

Figure 5.5. K562 and KG1a co-cultured endothelial monolayers show muted response to VEGFR2 blocking. (A) After 3 days of co-culture, K562 co-cultured endothelial cells treated with a VEGFR2 antibody show decreased numbers of sprouts per field of view. (B) K562 and KG1a show no differences between VEGFR2 blocked co-cultures and control after 7 days. * $p < 0.05$.

VEGFR2 mediates KG1a-induced sprouting in microvessels

In vivo, leukemia-induced vascular remodeling and angiogenesis occur in the marrow vasculature, which are continually perfused. As such, leukemia-induced angiogenesis would be more optimally studied in a 3D culture system that allows for intact, perfusable vasculature. Engineered microvessels were fabricated as described previously [108–110]. Briefly, injection molding of collagen I onto a PDMS stamp forms a top piece with an imprinted network pattern. A flat layer of collagen was seeded with leukemia cell lines K562 or KG1a at 5 million cells/mL. After collagen gelation, the PDMS stamp was removed from the

top piece and the imprinted network was sealed with the cell-embedded flat collagen layer to create perfusable, cell-seeded microvessels. Previous work with this system has shown that the microvessels respond to inflammatory stimuli and can sprout when exposed to VEGF [108].

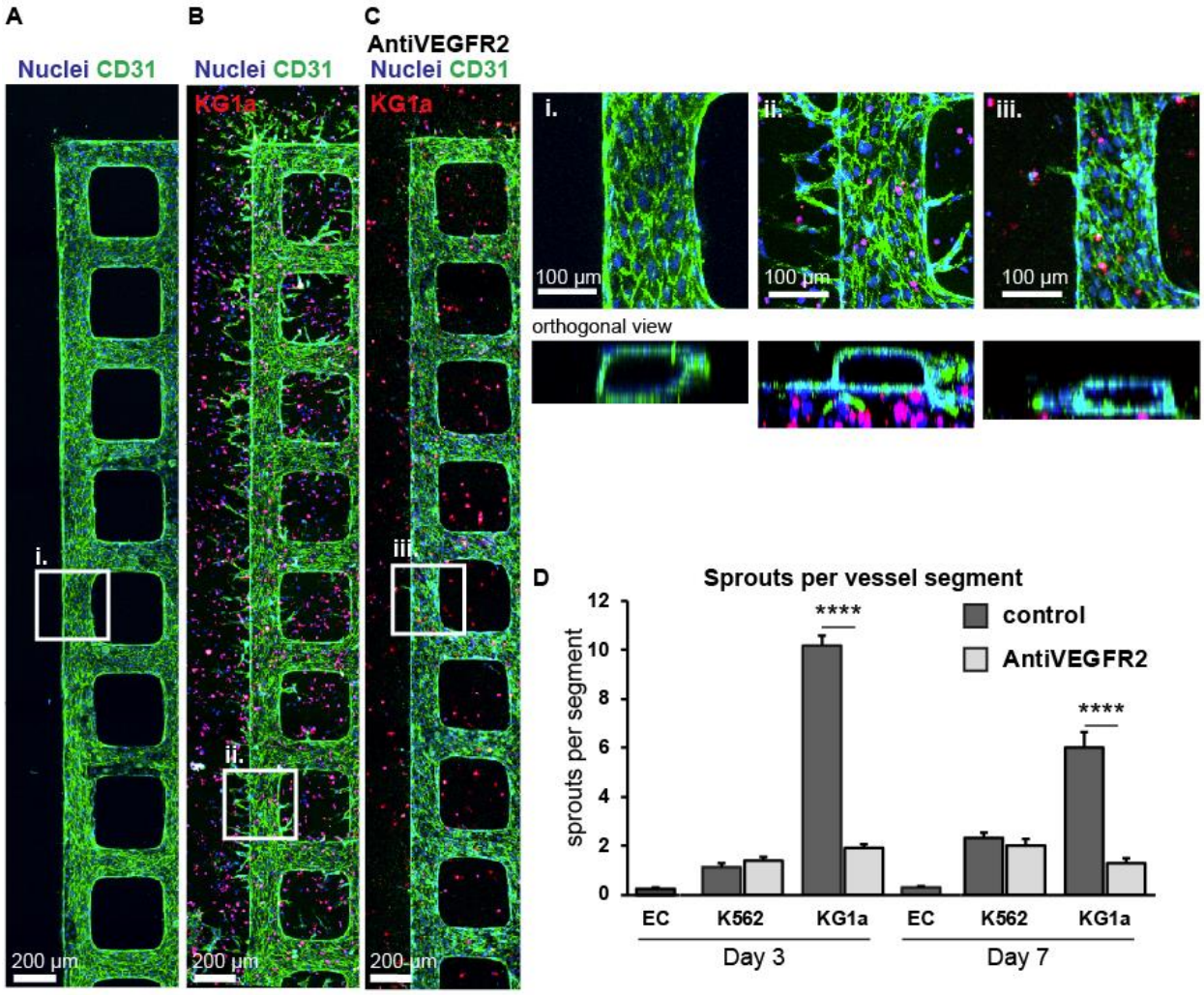

Figure 5.6. KG1a induced microvessel sprouting is reduced with VEGFR2 blocking. Confocal immunofluorescence imaging shows endothelial CD31 junctions in (A) EC only vessels (B) KG1a co-cultured vessels, and (C) KG1a co-cultured vessels with VEGFR2 blocking. Zoomed views of boxed regions from A, B, and C are shown in i, ii, and iii, respectively. Orthogonal views are shown below, showing lateral and downward sprouts towards the leukemia-seeded collagen. (D) Quantification of the number of sprouts per segment in EC only, K562 co-cultured, and KG1a co-cultured vessels shows a significant decrease in KG1a induced sprouts in VEGFR2 blocked vessels. **** $p < 0.0001$.

Vessels seeded with or without leukemia cell lines K562 or KG1a were cultured in the microvessel platform for 3 to 7 days **(Figure 5.6 A-C)**. In the microvessels, unlike the monolayer assays, endothelial CD31 remained at the junctions, and heterogeneous or membrane expression in KG1a co-cultures was not observed **(Figure 5.6 A-C)**. At either time point, K562 co-cultured vessels displayed no significant differences in the number of sprouts per segment of the grid network in control or antiVEGFR2-treated vessels **(Figure 5.6 D)**. In contrast, the KG1a co-cultured vessels demonstrated a significant decrease in the number of sprouts per segment with antiVEGFR2 at both 3 and 7 days of culture **(Figure 5.6 D)**. The microvessel platform represents a more physiologically relevant geometry for the assessment of leukemia-induced angiogenesis and highlights divergent responses to VEGFR2 blockade in leukemic cell line co-cultures.

5.5 DISCUSSION

In this study, we demonstrate the first use of *in vitro* platforms to model leukemia-induced angiogenesis with two collagen-based systems: a monolayer angiogenesis assay and 3D microvessel platform. Four leukemic cell lines, U937, HL60, K562, and KG1a were shown to induce angiogenic sprouting in endothelial monolayers. When leukemia cells are seeded at high concentration in the matrix, lines K562 and KG1a induced consistently high numbers of sprouts per FOV. This platform demonstrates endothelial sprouting from a monolayer into a collagen matrix induced by leukemia cell-secreted signaling.

When a neutralizing antibody to VEGFR2 was introduced to the media, the effects on the K562 and KG1a-induced sprouts were varied. In the monolayer angiogenesis assay, we observed an initial decrease in sprouts induced by K562 on day 3, but the effect was not present by day 7. In contrast, there appeared to be no effect on KG1a-induced sprouting. This can potentially be explained by a reduction in endothelial viability due to a destabilized monolayer after 7 days, but further analysis is needed to confirm this hypothesis. In the microvessel platform, however, the effect of a VEGFR2 antibody was much more pronounced. K562 co-cultured vessels showed no significant differences between treated and untreated vessels at days 3 and 7, while KG1a co-cultured microvessels demonstrated a significant reduction in sprouting with VEGFR2 blockade at both 3 and 7 days.

The varied outcomes with the K562 and KG1a cell lines demonstrates the complexity of angiogenic signaling and the type of culture platform used. Expression data from the CCLE and RT-PCR data from cell lines cultured in collagen can potentially indicate mechanistic differences leading to the sprouting outcomes observed. KG1a cells expressed more VEGFA than K562 cells, though blocking VEGFR2, the receptor for VEGFA, did not consistently block endothelial sprouting in monolayer co-cultures. Both cell lines also express VEGFB, a factor that signals through endothelial VEGFR1 to induce migration and sprouting [228,229]. It is possible that blocking VEGFR2 alone was not sufficient to prevent pro-angiogenic effects on endothelial cells, as sprouting was not completely abrogated in either the monolayer or microvessel co-cultures. The differences in results from the monolayer angiogenesis assay and 3D microvessel cultures

highlight the importance of relevant culture platforms. Further, in the microvessel platform, orthogonal views of the lumen clarify that the induced sprouting is directional, with the majority of sprouts extending laterally or down into the leukemia cell-seeded collagen layer. While 2D angiogenesis platforms provide a convenient screening platform, detailed examination of endothelial behavior may be better studied in a more *in vivo*-like setting incorporating laminar flow through a lumen.

Though studies on the role of VEGF in AML disagree on the relationship between marrow angiogenesis and progression stage [91,92], there is broad agreement that increased marrow angiogenesis is an independent indicator for poor outcomes [222–224,250]. Clinical efforts to pursue treatments using VEGFA antibodies or VEGFR2 inhibitors have had varied success in AML, particularly due to the heterogeneity of cytogenetic abnormalities and the complex microenvironmental effects of hematopoietic angiogenic factor crosstalk. Improvements to the 3D culture platforms outlined in this study could enable more detailed analysis of clinically relevant phenomena, such as alternate mechanisms responsible for angiogenic sprouting or mobilization potential. For example, though antiVEGFR2 caused a significant decrease in the number of sprouts per segment in KG1a co-cultured microvessels, a baseline number of sprouts remained. Alternate receptors for proangiogenic pathways such as VEGFR1 or FGFR could be examined for their contribution to sprouting observed in these co-cultures [91,223]. Additionally, factors involved in endothelial destabilization, proliferation, and migration such as MMPs and angiopoietins could also be explored to better understand endothelial remodeling in leukemic cell co-cultures. With increased insight into potential pathways responsible, patient cells could also be seeded in these platforms to examine their effect on endothelial cells *in vitro*. This would be particularly useful for both exploratory research into the diversity of mechanisms present in different leukemias and in the context of personalized medicine. Combinations of relevant therapeutics, including antibody therapies, can be tested within this platform to inform clinical care.

Here, we demonstrate that the co-culture of various leukemic cell lines from myeloid malignancies (HL60, K562, an KG1a) and histiocytic lymphoma (U937) can induce angiogenic sprouting from endothelial monolayers and microvessels. We further demonstrate variable responses to VEGFR2 blockade from K562 and KG1a co-culture. With this platform, the influence of leukemic cell types on endothelial morphology and remodeling can be examined *in vitro*, allowing for a controlled comparison of AML cell subtypes. Further, these platforms have to potential to provide patient-specific characterization of angiogenesis, which could subsequently direct personalized treatment strategies.

CONCLUSIONS AND FUTURE DIRECTIONS

The platforms outlined in this dissertation describe 3D microvessels studying the interaction of marrow endothelial cells, stromal fibroblasts, hematopoietic stem cells, and terminally differentiated hematopoietic cells. This work addresses challenges in the recapitulation of the marrow microenvironment, with a focus on the interaction of endothelial cells with surrounding cells. In chapter 2, we demonstrate the fabrication of an organ-specific vascular microenvironment and characterize marrow-derived endothelial cells. In chapter 3, close examination of megakaryocyte migration and differentiation shows endothelial structural changes during platelet release. In chapter 4, the influence of stromal fibroblasts on perfused hematopoietic cells demonstrates the role of microenvironment on HSPC trafficking. In chapter 5, leukemic cells are shown to modify intact vasculature and induce angiogenesis.

The major advantages of the microvessel model for recapitulation of the marrow lie in the matrix and the perfusable network geometry. Matrix-embedded cells are able to remodel their surroundings, migrate through the matrix, and interact with other cells present. Endothelial cells seeded within the network can sense surrounding cells and their structure can be altered in response to microenvironmental signaling. Hematopoietic cell egress into the circulation can rely on shear stresses for proper release, as in proplatelet and platelet formation, supporting the use of perfusion culture conditions similar to the sinusoidal regions of the marrow. The branched network geometries further enable examination of higher and lower shear stresses within a single platform.

In each of these co-culture systems, further improvements in the cell types used, culture conditions, and manipulation of signaling could enable deeper insight into the cell-cell interactions present. Optimization of the endothelial cell populations used is necessary for organ-specific recapitulation of the marrow space. In chapter 2, hBMECs are compared to HUVECs in both monolayer and microvessel cultures. However, limitations exist currently to the use of hBMECs in broader applications due to donor variability and limited expansion potential of isolated cells. Methods to prevent senescence or immortalize the isolated hBMEC cell populations would allow for the use of all marrow-specific cells in microvessel co-cultures. This type of manipulation has been demonstrated in HUVECs, where adenoviral E4ORF1 enables long term survival through MAPK-independent activation of Akt signaling [172]. These cells maintain their angiogenic potential and can be cultured in the absence of serum. Similar manipulation of isolated hBMECs would allow cell expansion and promote their broader use.

Serum-free culture conditions are particularly important in hematopoietic stem and differentiation cultures, where the presence of chemically undefined components can alter cell fate and phenotype. For example, platelets are activated by components in serum. In chapter 3, HUVECs were used in the creation of a thrombopoietic niche, necessitating the use of serum during co-culture. Collected platelet-like particles from this thrombopoietic niche were partially pre-activated. Though there may be other causes, including activation from exposed collagen, the presence of serum could have contributed to platelet-like particle

activation. The use of serum-free culture conditions could allow better particle collection and more appropriate culture conditions for stem and progenitor cells.

The extracellular matrix composition of the marrow includes collagen IV, fibronectin, laminin, and other components that line the marrow vasculature and play roles in hematopoietic differentiation. RNASeq results from chapter 2, comparing the expression of extracellular matrix associated genes in hBMECs and HUVECs show significantly higher expression of various collagens and laminin, suggesting that hBMECs contribute directly to their surrounding matrix environment. hBMEC expression patterns suggest key roles for extracellular matrix and matrix-associated factors not only in vessel structure, but also in interactions with hematopoietic cells. For example, matrix composition has been demonstrated to impact megakaryocyte maturation and platelet granule formation during thrombopoiesis. Inclusion of additional matrix components to the collagen I microvessel platform can be accomplished through perfusion of collagens through the vessel network prior to cell seeding, manipulation of endothelial cell populations to allow additional matrix secretion at the vessel wall, and incorporation of additional matrix components directly in the collagen. Gradients in matrix composition can more accurately recapitulate differences in hematopoietic niche spaces in the marrow. Advancements in patterning matrix within the platform could enable further understanding of hematopoietic cell-matrix interactions during migration and differentiation.

Improvements in the control of cell-cell interactions could further the utility of an *in vitro* human marrow niche. We have demonstrated that treatment of the system with antagonists such as CXCR4 or VEGFR2 antibodies yields insight into major signaling pathways between cell types in the context of thrombopoiesis and leukemia-induced vascular remodeling. Further analysis of hematopoietic trafficking can be performed through manipulation of CXCR4 signaling in other contexts. For example, in chapter 2, unfractionated marrow cell populations are co-cultured within the microvessel platform and migration into the lumen is visualized via scanning electron microscopy. More detailed examination of CXCR4 or other signaling pathways in this context could provide more insight into how specific cell populations are retained or released from the marrow space. Cell responses to additional mobilization factors, such as G-CSF, which is used clinically in hematopoietic stem cell mobilization for transplant, can also be explored. Signaling can also be manipulated through overexpression or knockdown of genes in the endothelial population. In the studies described here, manipulation of chemoattractants and hematopoietically active cytokines could provide additional insight into endothelial contributions to cell function, maturation, and migration. Additional biochemical manipulation of specific cell types or vascular regions within a complex cell population would yield insight into cell-cell interactions within the vascular niche.

Overall, this dissertation demonstrates the functionality of multiple *in vitro* marrow platforms in examining marrow cell interactions. With additional spatiotemporal control of matrix interactions and cell-cell signaling, these co-culture platforms can improve our understanding of the role of vasculature in the marrow.

REFERENCES

1. Sender R, Fuchs S, Milo R. Revised Estimates for the Number of Human and Bacteria Cells in the Body. PLOS Biol. Cold Spring Harbor Labs Journals; 2016;14: e1002533. doi:10.1371/journal.pbio.1002533
2. Wang LD, Wagers AJ. Dynamic niches in the origination and differentiation of haematopoietic stem cells. Nat Rev Mol Cell Biol. Nature Publishing Group, a division of Macmillan Publishers Limited. All Rights Reserved.; 2011;12: 643–55. doi:10.1038/nrm3184
3. R Schofield. The Relationship Between the Spleen Colony-Forming Cell and the Haematopoietic Stem Cell. Blood. 1978;4: 7–25.
4. Coskun S, Hirschi KK. Establishment and regulation of the HSC niche: Roles of osteoblastic and vascular compartments. Birth Defects Res C Embryo Today. 2010;90: 229–42. doi:10.1002/bdrc.20194
5. Center for International Blood and Marrow Transplant Research, a contractor for the C.W. Bill Young Cell Transplantation Program operated through the U. S. Department of Health and Human Services, Health Resources and Services Administration HSB. Transplant Activity Report Covering 2009-2013 [Internet]. 2013. Available: http://bloodcell.transplant.hrsa.gov/research/transplant_data/transplant_activity_report/summary-total_tx_by_year.pdf
6. Heazlewood SY, Oteiza A, Cao H, Nilsson SK. Analyzing hematopoietic stem cell homing, lodgment, and engraftment to better understand the bone marrow niche. Ann N Y Acad Sci. 2014;1310: 119–28. doi:10.1111/nyas.12329
7. Kunisaki Y, Bruns I, Scheiermann C, Ahmed J, Pinho S, Zhang D, et al. Arteriolar niches maintain haematopoietic stem cell quiescence. Nature. Nature Publishing Group; 2013;502: 637–643. doi:10.1038/nature12612
8. Bixel MG, Kusumbe AP, Ramasamy SK, Sivaraj KK, Butz S, Vestweber D, et al. Flow Dynamics and HSPC Homing in Bone Marrow Microvessels. Cell Rep. 2017;18: 1804–1816. doi:10.1016/j.celrep.2017.01.042
9. Nombela-Arrieta C, Manz MG. Quantification and three-dimensional microanatomical organization of the bone marrow. Blood Adv. 2017;1: 407–416. doi:10.1182/bloodadvances.2016003194
10. Dexter TM, Allen TD, Lajtha LG. Conditions controlling the proliferation of haemopoietic stem cells in vitro. J Cell Physiol. 1977;91: 335–44. doi:10.1002/jcp.1040910303
11. Gartner S, Kaplan HS. Long-term culture of human bone marrow cells. Proc Natl Acad Sci U S A. 1980;77: 4756–9. Available: http://www.pubmedcentral.nih.gov/articlerender.fcgi?artid=349925&tool=pmcentrez&rendertype=abstract
12. Tsai S, Emerson SG, Sieff CA, Nathan DG. Isolation of a human stromal cell strain secreting hemopoietic growth factors. J Cell Physiol. 1986;127: 137–45. doi:10.1002/jcp.1041270117
13. Ho MSH, Medcalf RL, Livesey SA, Traianedes K. The dynamics of adult haematopoiesis in the bone and bone marrow environment. Br J Haematol. 2015;170: 472–486. doi:10.1111/bjh.13445
14. Köhler A, Geiger H, Gunzer M. Imaging hematopoietic stem cells in the marrow of long bones in vivo. Methods Mol Biol. 2011;750: 215–224. doi:10.1007/978-1-61779-145-1_15
15. Fliedner TMM, Graessle D, Paulsen C, Reimers K. Structure and function of bone marrow hemopoiesis: mechanisms of response to ionizing radiation exposure. Cancer Biother Radiopharm. 2002;17: 405–426. doi:10.1089/108497802760363204
16. Catlin SN, Busque L, Gale RE, Guttorp P, Abkowitz JL. The replication rate of human hematopoietic stem cells in vivo. Blood. American Society of Hematology; 2011;117: 4460–6. doi:10.1182/blood-2010-08-303537

17. Challen GA, Boles N, Lin KK-Y, Goodell MA. Mouse hematopoietic stem cell identification and analysis. Cytometry A. 2009;75: 14–24. doi:10.1002/cyto.a.20674

18. Winkler IG, Barbier V, Wadley R, Zannettino ACW, Williams S, Lévesque J-P. Positioning of bone marrow hematopoietic and stromal cells relative to blood flow in vivo: serially reconstituting hematopoietic stem cells reside in distinct nonperfused niches. Blood. American Society of Hematology; 2010;116: 375–85. doi:10.1182/blood-2009-07-233437

19. Notta F, Doulatov S, Laurenti E, Poeppl A, Jurisica I, Dick JE. Isolation of Single Human Hematopoietic Stem Cells Capable of Long-Term Multilineage Engraftment. Science (80-). American Association for the Advancement of Science; 2011;333: 218–221. doi:10.1126/science.1201219

20. Ivanova NB, Dimos JT, Schaniel C, Hackney JA, Moore KA, Lemischka IR. A stem cell molecular signature. Science. 2002;298: 601–4. doi:10.1126/science.1073823

21. Köhler A, Schmithorst V, Filippi M-D, Ryan MA, Daria D, Gunzer M, et al. Altered cellular dynamics and endosteal location of aged early hematopoietic progenitor cells revealed by time-lapse intravital imaging in long bones. Blood. American Society of Hematology; 2009;114: 290–8. doi:10.1182/blood-2008-12-195644

22. Lo Celso C, Fleming HE, Wu JW, Zhao CX, Miake-Lye S, Fujisaki J, et al. Live-animal tracking of individual haematopoietic stem/progenitor cells in their niche. Nature. Nature Publishing Group; 2009;457: 92–6. doi:10.1038/nature07434

23. Haylock DN, Williams B, Johnston HM, Liu MCP, Rutherford KE, Whitty G a, et al. Hemopoietic Stem Cells with Higher Hemopoietic Potential Reside at the Bone Marrow Endosteum. Stem Cells. 2007;25: 1062–1069. doi:10.1634/stemcells.2006-0528

24. Nilsson SK, Johnston HM, Coverdale J a. Spatial localization of transplanted hemopoietic stem cells: Inferences for the localization of stem cell niches. Blood. American Society of Hematology; 2001;97: 2293–2299. doi:10.1182/blood.V97.8.2293

25. Calvi LM, Adams GB, Weibrecht KW, Weber JM, Olson DP, Knight MC, et al. Osteoblastic cells regulate the haematopoietic stem cell niche. Nature. 2003;425: 841–846. doi:10.1038/nature02040

26. Jiwang Zhang, Chao Niu, Ling Ye, Haiyang Huang, Xi He, Wei-Gang Tong, Jason Ross, Jeff Haug, Teri Johnson, Jian Q. Feng, Stephen Harris, Leanne M. Wiedemann YM& LL. Identification of the haematopoietic stem cell niche and control of the niche size. Nature. 2003;425: 836. doi:10.1038/nature02064.1.

27. Visnjic D, Kalajzic Z, Rowe DW, Katavic V, Lorenzo J, Aguila HL. Hematopoiesis is severely altered in mice with an induced osteoblast deficiency. Blood. 2004;103: 3258–3264. doi:10.1182/blood-2003-11-4011

28. Kiel MJ, Morrison SJ. Maintaining hematopoietic stem cells in the vascular niche. Immunity. 2006;25: 862–4. doi:10.1016/j.immuni.2006.11.005

29. Morrison SJ, Scadden DT. The bone marrow niche for haematopoietic stem cells. Nature. 2014;505: 327–34. doi:10.1038/nature12984

30. Silberstein LE, Lin CP. A New Image of the Hematopoietic Stem Cell Vascular Niche. Cell Stem Cell. 2013;13: 514–516. doi:10.1016/j.stem.2013.10.012

31. Nombela-Arrieta C, Pivarnik G, Winkel B, Canty KJ, Harley B, Mahoney JE, et al. Quantitative imaging of haematopoietic stem and progenitor cell localization and hypoxic status in the bone marrow microenvironment. Nat Cell Biol. Nature Publishing Group, a division of Macmillan Publishers Limited. All Rights Reserved.; 2013;15: 533–43. doi:10.1038/ncb2730

32. Tamplin OJ, Durand EM, Carr LA, Childs SJ, Hagedorn EJ, Li P, et al. Hematopoietic Stem Cell Arrival Triggers Dynamic Remodeling of the Perivascular Niche. Cell. 2015;160: 241–252. doi:10.1016/j.cell.2014.12.032

33. Tormin A, Li O, Brune JC, Walsh S, Schutz B, Ehinger M, et al. CD146 expression on primary

nonhematopoietic bone marrow stem cells is correlated with in situ localization. Blood. 2011;117: 5067–5077. doi:10.1182/blood-2010-08-304287

34. Sacchetti B, Funari A, Michienzi S, Di Cesare S, Piersanti S, Saggio I, et al. Self-Renewing Osteoprogenitors in Bone Marrow Sinusoids Can Organize a Hematopoietic Microenvironment. Cell. 2007;131: 324–336. doi:10.1016/j.cell.2007.08.025

35. Iwata M, Awaya N, Graf L, Kahl C, Torok-Storb B. Human marrow stromal cells activate monocytes to secrete osteopontin, which down-regulates Notch1 gene expression in CD34+ cells. Blood. 2004;103: 4496–4502. doi:10.1182/blood-2004-01-0256

36. Ding L, Saunders TL, Enikolopov G, Morrison SJ. Endothelial and perivascular cells maintain haematopoietic stem cells. Nature. Nature Publishing Group; 2012;481: 457–462. doi:10.1038/nature10783

37. Schroeder MA, DiPersio JF. Mobilization of hematopoietic stem and leukemia cells. J Leukoc Biol. 2012;91: 47–57. doi:10.1189/jlb.0210085

38. Arai F, Hirao A, Ohmura M, Sato H, Matsuoka S, Takubo K, et al. Tie2/angiopoietin-1 signaling regulates hematopoietic stem cell quiescence in the bone marrow niche. Cell. 2004;118: 149–161. doi:10.1016/j.cell.2004.07.004

39. Peled A, Grabovsky V, Habler L, Sandbank J, Arenzana-Seisdedos F, Petit I, et al. The chemokine SDF-1 stimulates integrin-mediated arrest of CD34+ cells on vascular endothelium under shear flow. J Clin Invest. 1999;104: 1199–1211. doi:10.1172/JCI7615

40. Orkin SH, Zon LI. Hematopoiesis: An Evolving Paradigm for Stem Cell Biology. Cell. 2008;132: 631–644. doi:10.1016/j.cell.2008.01.025

41. Birbrair A, Frenette PS. Niche heterogeneity in the bone marrow. Ann N Y Acad Sci. NIH Public Access; 2016;1370: 82–96. doi:10.1111/nyas.13016

42. ZAMBONI L, PEASE DC. The vascular bed of red bone marrow. J Ultrastruct Res. 1961;5: 65–85. Available: http://www.ncbi.nlm.nih.gov/pubmed/13787795

43. Simionescu M, Simionescu N, Palade GE. Morphometric data on the endothelium of blood capillaries. J Cell Biol. Rockefeller University Press; 1974;60: 128–52. doi:10.1083/JCB.60.1.128

44. Becker RP, De Bruyn PP. The transmural passage of blood cells into myeloid sinusoids and the entry of platelets into the sinusoidal circulation; a scanning electron microscopic investigation. Am J Anat. 1976;145: 183–205. doi:10.1002/aja.1001450204

45. Schachtner H, Calaminus SDJ, Sinclair A, Monypenny J, Blundell MP, Leon C, et al. Megakaryocytes assemble podosomes that degrade matrix and protrude through basement membrane. Blood. American Society of Hematology; 2013;121: 2542–52. doi:10.1182/blood-2012-07-443457

46. French DL. Megakaryocytes put a foot through the door. Blood. 2013;121: 2379–80. doi:10.1182/blood-2013-02-479022

47. Yokoyama T, Etoh T, Kitagawa H, Tsukahara S, Kannan Y. Migration of erythroblastic islands toward the sinusoid as erythroid maturation proceeds in rat bone marrow. J Vet Med Sci. 2003;65: 449–52. Available: http://www.ncbi.nlm.nih.gov/pubmed/12736425

48. Chasis JA, Mohandas N. Erythroblastic islands: niches for erythropoiesis. Blood. 2008;112: 470–8. doi:10.1182/blood-2008-03-077883

49. Tsou C-L, Peters W, Si Y, Slaymaker S, Aslanian AM, Weisberg SP, et al. Critical roles for CCR2 and MCP-3 in monocyte mobilization from bone marrow and recruitment to inflammatory sites. J Clin Invest. American Society for Clinical Investigation; 2007;117: 902–9. doi:10.1172/JCI29919

50. Furze RC, Rankin SM. Neutrophil mobilization and clearance in the bone marrow. Immunology. Wiley-Blackwell; 2008;125: 281–8. doi:10.1111/j.1365-2567.2008.02950.x

51. Ludin A, Gur-Cohen S, Golan K, Kaufmann KB, Itkin T, Medaglia C, et al. Reactive oxygen species regulate hematopoietic stem cell self-renewal, migration and development, as well as their

bone marrow microenvironment. Antioxid Redox Signal. 2014;21: 1605–19. doi:10.1089/ars.2014.5941

52. Ito K, Hirao A, Arai F, Takubo K, Matsuoka S, Miyamoto K, et al. Reactive oxygen species act through p38 MAPK to limit the lifespan of hematopoietic stem cells. Nat Med. Nature Publishing Group; 2006;12: 446–451. doi:10.1038/nm1388

53. Rafii S, Shapiro F, Pettengell R, Ferris B, Nachman RL, Moore M a, et al. Human bone marrow microvascular endothelial cells support long-term proliferation and differentiation of myeloid and megakaryocytic progenitors. Blood. 1995;86: 3353–63. Available: http://www.bloodjournal.org/content/86/9/3353.abstract

54. Winkler IG, Barbier V, Nowlan B, Jacobsen RN, Forristal CE, Patton JT, et al. Vascular niche E-selectin regulates hematopoietic stem cell dormancy, self renewal and chemoresistance. Nat Med. 2012;18. doi:10.1038/nm.2969

55. Rafii S, Shapiro F, Rimarachin J, Nachman RL, Ferris B, Weksler B, et al. Isolation and characterization of human bone marrow microvascular endothelial cells: hematopoietic progenitor cell adhesion. Blood. 1994;84: 10–19.

56. Schweitzer KM, Dräger AM, van der Valk P, Thijsen SF, Zevenbergen A, Theijsmeijer AP, et al. Constitutive expression of E-selectin and vascular cell adhesion molecule-1 on endothelial cells of hematopoietic tissues. Am J Pathol. American Society for Investigative Pathology; 1996;148: 165–75. Available: http://www.ncbi.nlm.nih.gov/pubmed/8546203

57. Schweitzer CM, van der Schoot CE, Dräger AM, van der Valk P, Zevenbergen A, Hooibrink B, et al. Isolation and culture of human bone marrow endothelial cells. Exp Hematol. 1995;23: 41–8. Available: http://www.ncbi.nlm.nih.gov/pubmed/7995370

58. Nolan D, Ginsberg M, Israely E, Palikuqi B, Poulos MG, James D, et al. Molecular Signatures of Tissue-Specific Microvascular Endothelial Cell Heterogeneity in Organ Maintenance and Regeneration. Dev Cell. Elsevier Inc.; 2013;26: 204–219. doi:10.1016/j.devcel.2013.06.017

59. Kusumbe AP, Ramasamy SK, Adams RH. Coupling of angiogenesis and osteogenesis by a specific vessel subtype in bone. Nature. Nature Publishing Group, a division of Macmillan Publishers Limited. All Rights Reserved.; 2014;507: 323–8. doi:10.1038/nature13145

60. Itkin T, Gur-Cohen S, Spencer JA, Schajnovitz A, Ramasamy SK, Kusumbe AP, et al. Distinct bone marrow blood vessels differentially regulate haematopoiesis. Nature. Nature Publishing Group, a division of Macmillan Publishers Limited. All Rights Reserved.; 2016;advance on. doi:10.1038/nature17624

61. Ramasamy SK, Kusumbe AP, Schiller M, Zeuschner D, Bixel MG, Milia C, et al. Blood flow controls bone vascular function and osteogenesis. Nat Commun. 2016;7. doi:10.1038/ncomms13601

62. Machlus KR, Italiano JE. The incredible journey: From megakaryocyte development to platelet formation. J Cell Biol. 2013;201: 785–796. doi:10.1083/jcb.201304054

63. Arai F, Suda T. Maintenance of quiescent hematopoietic stem cells in the osteoblastic niche. Ann N Y Acad Sci. 2007;1106: 41–53. doi:10.1196/annals.1392.005

64. Kaushansky K, Broudy VC, Lin N, Jorgensen MJ, McCarty J, Fox N, et al. Thrombopoietin, the Mp1 ligand, is essential for full megakaryocyte development. Proc Natl Acad Sci. 1995;92: 3234–3238. doi:10.1073/pnas.92.8.3234

65. Kaushansky K. Thrombopoietin: The primary regulator of platelet production [Internet]. Trends in Endocrinology and Metabolism. 1997. pp. 45–50. doi:10.1016/S1043-2760(96)00269-X

66. Kuter DJ. New thrombopoietic growth factors [Internet]. Blood. 2007. pp. 4607–4616. doi:10.1182/blood-2006-10-019315

67. Hamada T, Möhle R, Hesselgesser J, Hoxie J, Nachman RL, Moore MAS, et al. Transendothelial migration of megakaryocytes in response to stromal cell-derived factor 1 (SDF-1) enhances platelet formation. J Exp Med. 1998;188: 539–48. doi:10.1084/jem.188.3.539

68. Wang JF, Liu ZY, Groopman JE. The alpha-chemokine receptor CXCR4 is expressed on the megakaryocytic lineage from progenitor to platelets and modulates migration and adhesion. Blood. 1998;92: 756–64. Available: http://www.ncbi.nlm.nih.gov/pubmed/9680341

69. Rivière C, Subra F, Cohen-Solal K, Cordette-Lagarde V, Letestu R, Auclair C, et al. Phenotypic and functional evidence for the expression of CXCR4 receptor during megakaryocytopoiesis. Blood. 1999;93: 1511–23. Available: http://www.ncbi.nlm.nih.gov/pubmed/10029579

70. Pitchford SC, Lodie T, Rankin SM. VEGFR1 stimulates a CXCR4-dependent translocation of megakaryocytes to the vascular niche, enhancing platelet production in mice. Blood. 2012;120. Available: http://www.bloodjournal.org/content/120/14/2787.long?sso-checked=true

71. Niswander LM, Fegan KH, Kingsley PD, McGrath KE, Palis J, Jackson C. SDF-1 dynamically mediates megakaryocyte niche occupancy and thrombopoiesis at steady state and following radiation injury. Blood. American Society of Hematology; 2014;124: 277–86. doi:10.1182/blood-2014-01-547638

72. Avecilla ST, Hattori K, Heissig B, Tejada R, Liao F, Shido K, et al. Chemokine-mediated interaction of hematopoietic progenitors with the bone marrow vascular niche is required for thrombopoiesis. Nat Med. 2004;10: 64–71. doi:10.1038/nm973

73. Larson MK, Watson SP. Regulation of proplatelet formation and platelet release by integrin alpha IIb beta3. Blood. 2006;108: 1509–14. doi:10.1182/blood-2005-11-011957

74. Semeniak D, Kulawig R, Stegner D, Meyer I, Schwiebert S, Bösing H, et al. Proplatelet formation is selectively inhibited by collagen type I through Syk-independent GPVI signaling. J Cell Sci. 2016;129: 3473–3484. doi:10.1242/jcs.187971

75. Aguilar A, Pertuy F, Eckly A, Strassel C, Collin D, Gachet C, et al. Importance of environmental stiffness for megakaryocyte differentiation and proplatelet formation. Blood. 2016;128: 2022–2032. doi:10.1182/blood-2016-02-699959

76. Junt T, Schulze H, Chen Z, Massberg S, Goerge T, Krueger A, et al. Dynamic visualization of thrombopoiesis within bone marrow. Science. 2007;317: 1767–1770. doi:10.1126/science.1146304

77. Nishimura S, Nagasaki M, Kunishima S, Sawaguchi A, Sakata A, Sakaguchi H, et al. IL-1α induces thrombopoiesis through megakaryocyte rupture in response to acute platelet needs. J Cell Biol. 2015;209: 453–466. doi:10.1083/jcb.201410052

78. Di Buduo CA, Wray LS, Tozzi L, Malara A, Chen Y, Ghezzi CE, et al. Programmable 3D silk bone marrow niche for platelet generation ex vivo and modeling of megakaryopoiesis pathologies. Blood. American Society of Hematology; 2015;125: 2254–2264. doi:10.1182/blood-2014-08-595561

79. Avanzi MP, Izak M, Oluwadara OE, Mitchell WB. Actin Inhibition Increases Megakaryocyte Proplatelet Formation through an Apoptosis-Dependent Mechanism. Mandal M, editor. PLoS One. Public Library of Science; 2015;10: e0125057. doi:10.1371/journal.pone.0125057

80. Dunois-Lardé C, Capron C, Fichelson S, Bauer T, Cramer-Bordé E, Baruch D. Exposure of human megakaryocytes to high shear rates accelerates platelet production. Blood. American Society of Hematology; 2009;114: 1875–83. doi:10.1182/blood-2009-03-209205

81. Colmone A, Amorim M, Pontier AL, Wang S, Jablonski E, Sipkins D a. Leukemic cells create bone marrow niches that disrupt the behavior of normal hematopoietic progenitor cells. Science. 2008;322: 1861–1865. doi:10.1126/science.1164390

82. Ninomiya M, Abe a, Katsumi a, Xu J, Ito M, Arai F, et al. Homing, proliferation and survival sites of human leukemia cells in vivo in immunodeficient mice. Leuk Off J Leuk Soc Am Leuk Res Fund, UK. 2007;21: 136–142. doi:10.1038/sj.leu.2404432

83. Konopleva MY, Jordan CT. Leukemia stem cells and microenvironment: Biology and therapeutic targeting. J Clin Oncol. 2011;29: 591–599. doi:10.1200/JCO.2010.31.0904

84. Lane SW, Scadden DT, Gilliland DG. The leukemic stem cell niche: Current concepts and

therapeutic opportunities. Blood. 2009;114: 1150–1157. doi:10.1182/blood-2009-01-202606

85. Ramakrishnan A, Torok-Storb BJ. The role of the marrow microenvironment in hematopoietic stem cell transplantation. Cell Ther Transplant. 2010;2: 7–12. doi:10.3205/ctt-2009-en-000072.01

86. Jensen PO, Mortensen BT, Hodgkiss RJ, Iversen A PO, Christensen IJ, Helledie N, et al. Increased cellular hypoxia and reduced proliferation of both normal and leukaemic cells during progression of acute myeloid leukaemia in rats. Cell Prolif. 2000;33: 381–395. doi:10.1046/j.1365-2184.2000.00183.x

87. Wellmann S, Guschmann M, Griethe W, Eckert C, von Stackelberg A, Lottaz C, et al. Activation of the HIF pathway in childhood ALL, prognostic implications of VEGF. Leukemia. Nature Publishing Group; 2004;18: 926–33. doi:10.1038/sj.leu.2403332

88. Ayala F, Dewar R, Kieran M, Kalluri R. Contribution of bone microenvironment to leukemogenesis and leukemia progression. Leukemia. Nature Publishing Group; 2009;23: 2233–2241. doi:10.1038/leu.2009.175

89. Hicklin DJ, Ellis LM. Role of the vascular endothelial growth factor pathway in tumor growth and angiogenesis. J Clin Oncol. 2005;23: 1011–1027. doi:10.1200/JCO.2005.06.081

90. Ghannadan M, Wimazal F, Simonitsch I, Sperr WR, Mayerhofer M, Sillaber C, et al. Immunohistochemical Detection of VEGF in the Bone Marrow of Patients With Acute Myeloid Leukemia. Am J Clin Pathol. 2003;119: 663–671. doi:10.1309/331QX7AXKWFJFKXM

91. Hussong JW, Rodgers GM, Shami PJ. Evidence of increased angiogenesis in patients with acute myeloid leukemia. Blood. American Society of Hematology; 2000;95: 309–13. Available: http://www.bloodjournal.org/content/95/1/309.abstract

92. Padró T, Ruiz S, Bieker R, Bürger H, Steins M, Kienast J, et al. Increased angiogenesis in the bone marrow of patients with acute myeloid leukemia. Blood. 2000;95: 2637–2644. doi:10.1016/S0002-9440(10)61111-X

93. Lemoli RM, de Vivo A, Damiani D, Isidori A, Tani M, Bonini A, et al. Autologous transplantation of granulocyte colony-stimulating factor-primed bone marrow is effective in supporting myeloablative chemotherapy in patients with hematologic malignancies and poor peripheral blood stem cell mobilization. Blood. American Society of Hematology; 2003;102: 1595–600. doi:10.1182/blood-2003-02-0440

94. De Clercq E. Recent advances on the use of the CXCR4 antagonist plerixafor (AMD3100, Mozobil) and potential of other CXCR4 antagonists as stem cell mobilizers [Internet]. Pharmacology and Therapeutics. Elsevier Inc.; 2010. pp. 509–518. doi:10.1016/j.pharmthera.2010.08.009

95. Uy GL, Rettig MP, Cashen AF. Plerixafor, a CXCR4 antagonist for the mobilization of hematopoietic stem cells. Expert Opin Biol Ther. Taylor & Francis; 2008;8: 1797–804. doi:10.1517/14712598.8.11.1797

96. Frenette PS, Subbarao S, Mazo IB, von Andrian UH, Wagner DD. Endothelial selectins and vascular cell adhesion molecule-1 promote hematopoietic progenitor homing to bone marrow. Proc Natl Acad Sci U S A. 1998;95: 14423–14428. doi:10.1073/pnas.95.24.14423

97. Avigdor A, Goichberg P, Shivtiel S, Dar A, Peled A, Samira S, et al. CD44 and hyaluronic acid cooperate with SDF-1 in the trafficking of human CD34+ stem/progenitor cells to bone marrow. Blood. 2004;103: 2981–2989. doi:10.1182/blood-2003-10-3611

98. Scott LM, Priestley G V., Papayannopoulou T. Deletion of alpha4 Integrins from Adult Hematopoietic Cells Reveals Roles in Homeostasis, Regeneration, and Homing. Mol Cell Biol. 2003;23: 9349–9360. doi:10.1128/MCB.23.24.9349-9360.2003

99. Dar A, Goichberg P, Shinder V, Kalinkovich A, Kollet O, Netzer N, et al. Chemokine receptor CXCR4-dependent internalization and resecretion of functional chemokine SDF-1 by bone marrow endothelial and stromal cells. Nat Immunol. 2005;6: 1038–1046. doi:10.1038/ni1251

100. Voermans C, Rood PM, Hordijk PL, Gerritsen WR, van der Schoot CE. Adhesion molecules

involved in transendothelial migration of human hematopoietic progenitor cells. Stem Cells. 2000;18: 435–43. doi:10.1634/stemcells.18-6-435

101. Ellis SL, Grassinger J, Jones A, Borg J, Camenisch T, Haylock D, et al. The relationship between bone, hemopoietic stem cells, and vasculature. Blood. 2011;118: 1516–1524. doi:10.1182/blood-2010-08-303800

102. Honczarenko M, Le Y, Swierkowski M, Ghiran I, Glodek AM, Silberstein LE. Human bone marrow stromal cells express a distinct set of biologically functional chemokine receptors. Stem Cells. 2006;24: 1030–1041. doi:10.1634/stemcells.2005-0319

103. Wilson A, Trumpp A. Bone-marrow haematopoietic-stem-cell niches. Nat Rev Immunol. 2006;6: 93–106. doi:10.1038/nri1779

104. Di Maggio N, Piccinini E, Jaworski M, Trumpp A, Wendt DJ, Martin I. Toward modeling the bone marrow niche using scaffold-based 3D culture systems. Biomaterials. Elsevier Ltd; 2011;32: 321–329. doi:10.1016/j.biomaterials.2010.09.041

105. Lutolf MP, Hubbell J a. Synthetic biomaterials as instructive extracellular microenvironments for morphogenesis in tissue engineering. Nat Biotechnol. 2005;23: 47–55. doi:10.1038/nbt1055

106. Lutolf MP, Doyonnas R, Havenstrite K, Koleckar K, Blau HM. Perturbation of single hematopoietic stem cell fates in artificial niches. Integr Biol (Camb). 2009;1: 59–69. doi:10.1039/b815718a

107. Braccini A, Wendt D, Jaquiery C, Jakob M, Heberer M, Kenins L, et al. Three-dimensional perfusion culture of human bone marrow cells and generation of osteoinductive grafts. Stem Cells. 2005;23: 1066–72. doi:10.1634/stemcells.2005-0002

108. Zheng Y, Chen J, Craven M, Choi NW, Totorica S, Diaz-Santana A, et al. In vitro microvessels for the study of angiogenesis and thrombosis. Proc Natl Acad Sci U S A. 2012;109: 9342–7. doi:10.1073/pnas.1201240109

109. Ligresti G, Nagao RJ, Xue J, Choi YJ, Xu J, Ren S, et al. A Novel Three-Dimensional Human Peritubular Microvascular System. J Am Soc Nephrol. 2015; 1–12. doi:10.1681/ASN.2015070747

110. Roberts MA, Kotha SS, Phong KT, Zheng Y. Micropatterning and Assembly of 3D Microvessels. J Vis Exp. 2016; e54457–e54457. doi:10.3791/54457

111. Aird WC. Phenotypic heterogeneity of the endothelium: I. Structure, function, and mechanisms. Circ Res. 2007;100: 158–73. doi:10.1161/01.RES.0000255691.76142.4a

112. Auerbach R, Alby L, Morrissey LW, Tu M, Joseph J. Expression of organ-specific antigens on capillary endothelial cells. Microvasc Res. 1985;29: 401–411. doi:10.1016/0026-2862(85)90028-7

113. Butcher EC, Scollay RG, Weissman IL. Organ specificity of lymphocyte migration: mediation by highly selective lymphocyte interaction with organ-specific determinants on high endothelial venules. Eur J Immunol. WILEY-VCH Verlag GmbH; 1980;10: 556–561. doi:10.1002/eji.1830100713

114. Kumar S, West DC, Ager A. Heterogeneity in endothelial cells from large vessels and microvessels. Differentiation. 1987;36: 57–70. doi:10.1111/j.1432-0436.1987.tb00181.x

115. Molema G. Heterogeneity in Endothelial Responsiveness to Cytokines, Molecular Causes, and Pharmacological Consequences. Semin Thromb Hemost. © Thieme Medical Publishers; 2010;36: 246–264. doi:10.1055/s-0030-1253448

116. Minami T, Aird WC. Endothelial cell gene regulation. Trends Cardiovasc Med. 2005;15: 174–184. doi:10.1016/j.tcm.2005.06.002

117. Hooper AT, Butler JM, Nolan DJ, Kranz A, Iida K, Kobayashi M, et al. Engraftment and Reconstitution of Hematopoiesis Is Dependent on VEGFR2-Mediated Regeneration of Sinusoidal Endothelial Cells. Cell Stem Cell. Elsevier; 2009;4: 263–274. doi:10.1016/j.stem.2009.01.006

118. Stan R V, Kubitza M, Palade GE. PV-1 is a component of the fenestral and stomatal diaphragms in fenestrated endothelia. Proc Natl Acad Sci U S A. National Academy of Sciences; 1999;96: 13203–7. doi:10.1073/PNAS.96.23.13203

119. Braet F, Wisse E, Wisse E, Widmann J, Cotran R, Fahimi H, et al. Structural and functional aspects of liver sinusoidal endothelial cell fenestrae: a review. Comp Hepatol. BioMed Central; 2002;1: 1. doi:10.1186/1476-5926-1-1

120. Candal FJ, Rafii S, Parker JT, Ades EW, Ferris B, Nachman RL, et al. BMEC-1: a human bone marrow microvascular endothelial cell line with primary cell characteristics. Microvasc Res. 1996;52: 221–234. doi:10.1006/mvre.1996.0060

121. Lee J, Heckl D, Parekkadan B. Multiple genetically engineered humanized microenvironments in a single mouse. Biomater Res. BioMed Central; 2016;20: 19. doi:10.1186/s40824-016-0066-2

122. Gori JL, Butler JM, Chan Y-Y, Chandrasekaran D, Poulos MG, Ginsberg M, et al. Vascular niche promotes hematopoietic multipotent progenitor formation from pluripotent stem cells. J Clin Invest. 2015;125: 1243–54. doi:10.1172/JCI79328

123. Katayama Y, Battista M, Kao WM, Hidalgo A, Peired AJ, Thomas S a., et al. Signals from the sympathetic nervous system regulate hematopoietic stem cell egress from bone marrow. Cell. 2006;124: 407–421. doi:10.1016/j.cell.2005.10.041

124. Orelio C, Haak E, Peeters M, Dzierzak E. Interleukin-1-mediated hematopoietic cell regulation in the aorta-gonad-mesonephros region of the mouse embryo. Blood. American Society of Hematology; 2008;112: 4895–904. doi:10.1182/blood-2007-12-123836

125. Nemeth MJ, Topol L, Anderson SM, Yang Y, Bodine DM. Wnt5a inhibits canonical Wnt signaling in hematopoietic stem cells and enhances repopulation. Proc Natl Acad Sci. 2007;104: 15436–15441. doi:10.1073/pnas.0704747104

126. Schreck C, Istvánffy R, Ziegenhain C, Sippenauer T, Ruf F, Henkel L, et al. Niche WNT5A regulates the actin cytoskeleton during regeneration of hematopoietic stem cells. J Exp Med. 2017;214: 165–181. doi:10.1084/jem.20151414

127. Lee Y, Gotoh A, Kwon HJ, You M, Kohli L, Mantel C, et al. Enhancement of intracellular signaling associated with hematopoietic progenitor cell survival in response to SDF-1/CXCL12 in synergy with other cytokines. Blood. 2002;99: 4307–4317. doi:10.1182/blood.V99.12.4307

128. Sugiyama T, Kohara H, Noda M, Nagasawa T. Maintenance of the Hematopoietic Stem Cell Pool by CXCL12-CXCR4 Chemokine Signaling in Bone Marrow Stromal Cell Niches. Immunity. 2006;25: 977–988. doi:10.1016/j.immuni.2006.10.016

129. Yoon K-A, Cho H-S, Shin H-I, Cho J-Y. Differential Regulation of CXCL5 by FGF2 in Osteoblastic and Endothelial Niche Cells Supports Hematopoietic Stem Cell Migration. Stem Cells Dev. Mary Ann Liebert, Inc. 140 Huguenot Street, 3rd Floor New Rochelle, NY 10801 USA ; 2012;21: 3391–3402. doi:10.1089/scd.2012.0128

130. Sugimura R, He XC, Venkatraman A, Arai F, Box A, Semerad C, et al. Noncanonical Wnt signaling maintains hematopoietic stem cells in the niche. Cell. 2012;150: 351–365. doi:10.1016/j.cell.2012.05.041

131. Stan R V. Endothelial stomatal and fenestral diaphragms in normal vessels and angiogenesis. J Cell Mol Med. 2007;11: 621–643. doi:10.1111/j.1582-4934.2007.00075.x

132. Barzilai S, Yadav SK, Morrell S, Zemel A, Nourshargh S, Correspondence RA, et al. Leukocytes Breach Endothelial Barriers by Insertion of Nuclear Lobes and Disassembly of Endothelial Actin Filaments. Cell Rep. ElsevierCompany.; 2017;18: 685–699. doi:10.1016/j.celrep.2016.12.076

133. Bevilacqua MP, Pober JS, Wheeler ME, Cotran RS, Gimbrone MA. Interleukin 1 acts on cultured human vascular endothelium to increase the adhesion of polymorphonuclear leukocytes, monocytes, and related leukocyte cell lines. J Clin Invest. American Society for Clinical Investigation; 1985;76: 2003–2011. doi:10.1172/JCI112200

134. Luscinskas FW, Gerszten RE, Garcia-Zepeda E a, Lim YC, Yoshida M, Ding H a, et al. C-C and C-X-C chemokines trigger firm adhesion of monocytes to vascular endothelium under flow conditions. Ann N Y Acad Sci. 2000;902: 288–293. doi:10.1038/19546

135. Allport JR, Muller W a., Luscinskas FW. Monocytes induce reversible focal changes in vascular

endothelial cadherin complex during transendothelial migration under flow. J Cell Biol. 2000;148: 203–216. doi:10.1083/jcb.148.1.203

136. Poulos MG, Crowley MJP, Gutkin MC, Ramalingam P, Schachterle W, Thomas J-L, et al. Vascular Platform to Define Hematopoietic Stem Cell Factors and Enhance Regenerative Hematopoiesis. Stem cell reports. 2015;5: 881–94. doi:10.1016/j.stemcr.2015.08.018

137. Stan R V., Tse D, Deharvengt SJ, Smits NC, Xu Y, Luciano MR, et al. The Diaphragms of Fenestrated Endothelia: Gatekeepers of Vascular Permeability and Blood Composition. Dev Cell. 2012;23: 1203–1218. doi:10.1016/j.devcel.2012.11.003

138. Rantakari P, Jäppinen N, Lokka E, Mokkala E, Gerke H, Peuhu E, et al. Fetal liver endothelium regulates the seeding of tissue-resident macrophages. Nature. Nature Publishing Group; 2016;538: 392–396. doi:10.1038/nature19814

139. Minshall RD, Sessa WC, Stan R V., Anderson RGW, Malik AB. Caveolin regulation of endothelial function. Am J Physiol Cell Mol Physiol. 2003;285: L1179–L1183. doi:10.1152/ajplung.00242.2003

140. García-Cardeña G, Martasek P, Masters BS, Skidd PM, Couet J, Li S, et al. Dissecting the interaction between nitric oxide synthase (NOS) and caveolin. Functional significance of the nos caveolin binding domain in vivo. J Biol Chem. American Society for Biochemistry and Molecular Biology; 1997;272: 25437–40. doi:10.1074/JBC.272.41.25437

141. Pober JS, Cotran RS. Cytokines and endothelial cell biology. Physiol Rev. 1990;70: 427–51. doi:10.1152/physrev.1990.70.2.427

142. Nilsson SK, Debatis ME, Dooner MS, Madri JA, Quesenberry PJ, Becker PS. Immunofluorescence Characterization of Key Extracellular Matrix Proteins in Murine Bone Marrow In Situ. J Histochem Cytochem. SAGE PublicationsSage CA: Los Angeles, CA; 1998;46: 371–377. doi:10.1177/002215549804600311

143. Malara A, Gruppi C, Pallotta I, Spedden E, Tenni R, Raspanti M, et al. Extracellular matrix structure and nano-mechanics determine megakaryocyte function. Blood. 2011;118. Available: http://www.bloodjournal.org/content/118/16/4449.long?sso-checked=true

144. Dominietto A, Raiola AM, Van Lint MT, Lamparelli T, Gualandi F, Berisso G, et al. Factors influencing haematological recovery after allogeneic haemopoietic stem cell transplants: graft-versus-host disease, donor type, cytomegalovirus infections and cell dose. Br J Haematol. Blackwell Science Ltd; 2001;112: 219–227. doi:10.1046/J.1365-2141.2001.02468.X

145. Ramírez P, Brunstein CG, Miller B, DeFor T, Weisdorf D. Delayed platelet recovery after allogeneic transplantation: a predictor of increased treatment-related mortality and poorer survival. Bone Marrow Transplant. Nature Publishing Group; 2011;46: 981–986. doi:10.1038/bmt.2010.218

146. Zijlmans JM, Visser JW, Laterveer L, Kleiverda K, Heemskerk DP, Kluin PM, et al. The early phase of engraftment after murine blood cell transplantation is mediated by hematopoietic stem cells. Proc Natl Acad Sci U S A. National Academy of Sciences; 1998;95: 725–9. Available: http://www.ncbi.nlm.nih.gov/pubmed/9435260

147. Uchida N, Tsukamoto A, He D, Friera AM, Scollay R, Weissman IL. High doses of purified stem cells cause early hematopoietic recovery in syngeneic and allogeneic hosts. J Clin Invest. 1998;101: 961–966. doi:10.1172/JCI1681

148. Butler JM, Nolan DJ, Vertes EL, Varnum-Finney B, Kobayashi H, Hooper AT, et al. Endothelial cells are essential for the self-renewal and repopulation of Notch-dependent hematopoietic stem cells. Cell Stem Cell. 2010;6: 251–64. doi:10.1016/j.stem.2010.02.001

149. Doan PL, Russell JL, Himburg HA, Helms K, Harris JR, Lucas J, et al. Tie2(+) bone marrow endothelial cells regulate hematopoietic stem cell regeneration following radiation injury. Stem Cells. 2013;31: 327–37. doi:10.1002/stem.1275

150. Huang H, Cantor AB. Common features of megakaryocytes and hematopoietic stem cells: what's the connection? J Cell Biochem. 2009;107: 857–64. doi:10.1002/jcb.22184

151. Stegner D, VanEeuwijk JMM, Angay O, Gorelashvili MG, Semeniak D, Pinnecker J, et al.

Thrombopoiesis is spatially regulated by the bone marrow vasculature. Nat Commun. 2017;8: 127. doi:10.1038/s41467-017-00201-7

152. Thon JN, Dykstra BJ, Beaulieu LM. Platelet bioreactor: accelerated evolution of design and manufacture. Platelets. Taylor & Francis; 2017;28: 472–477. doi:10.1080/09537104.2016.1265922

153. Thon JN, Mazutis L, Wu S, Sylman JL, Ehrlicher A, Machlus KR, et al. Platelet bioreactor-on-a-chip. Blood. American Society of Hematology; 2014;124: 1857–1867. doi:10.1182/blood-2014-05-574913

154. Sun S, Wang W, Latchman Y, Gao D, Aronow B, Reems J-A. Expression of plasma membrane receptor genes during megakaryocyte development. Physiol Genomics. 2013;45: 217–227. doi:10.1152/physiolgenomics.00056.2012

155. Zheng Y, Chen J, López JA. Flow-driven assembly of VWF fibres and webs in in vitro microvessels. Nat Commun. 2015;6: 7858. doi:10.1038/ncomms8858

156. Brånemark P-I. Vital microscopy of bone marrow in rabbit. Scand J Clin Lab Invest. 1959;38: 1–82. Available: http://www.worldcat.org/title/vital-microscopy-of-bone-marrow-in-rabbit/oclc/14623239

157. Brookes M, Revell WJ. Blood Supply of Bone : Scientific Aspects. Springer London; 1998.

158. Mazo IB, Gutierrez-Ramos JC, Frenette PS, Hynes RO, Wagner DD, von Andrian UH. Hematopoietic progenitor cell rolling in bone marrow microvessels: parallel contributions by endothelial selectins and vascular cell adhesion molecule 1. J Exp Med. 1998;188: 465–474. doi:10.1084/jem.188.3.465

159. Kufrin D, Eslin DE, Bdeir K, Murciano J-C, Kuo A, Kowalska MA, et al. Antithrombotic thrombocytes: ectopic expression of urokinase-type plasminogen activator in platelets. Blood. 2003;102. Available: http://www.bloodjournal.org/content/102/3/926.long?sso-checked=true

160. Pang L, Weiss MJ, Poncz M. Megakaryocyte biology and related disorders. J Clin Invest. American Society for Clinical Investigation; 2005;115: 3332–8. doi:10.1172/JCI26720

161. Pallotta I, Lovett M, Kaplan DL, Balduini A. Three-Dimensional System for the *In Vitro* Study of Megakaryocytes and Functional Platelet Production Using Silk-Based Vascular Tubes. Tissue Eng Part C Methods. Mary Ann Liebert, Inc. 140 Huguenot Street, 3rd Floor New Rochelle, NY 10801 USA ; 2011;17: 1223–1232. doi:10.1089/ten.tec.2011.0134

162. Zhang L, Urtz N, Gaertner F, Legate KR, Petzold T, Lorenz M, et al. Sphingosine kinase 2 (Sphk2) regulates platelet biogenesis by providing intracellular sphingosine 1-phosphate (S1P). Blood. 2013;122: 791–802. doi:10.1182/blood-2012-12-473884

163. Vinet L, Zhedanov A. A “missing” family of classical orthogonal polynomials. J Exp Med. 2010;209: 2165–81. doi:10.1088/1751-8113/44/8/085201

164. Thon JN, Macleod H, Begonja AJ, Zhu J, Lee K-C, Mogilner A, et al. Microtubule and cortical forces determine platelet size during vascular platelet production. Nat Commun. Nature Publishing Group, a division of Macmillan Publishers Limited. All Rights Reserved.; 2012;3: 852. doi:10.1038/ncomms1838

165. Baudin B, Bruneel A, Bosselut N, Vaubourdolle M. A protocol for isolation and culture of human umbilical vein endothelial cells. Nat Protoc. Nature Publishing Group; 2007;2: 481–485. doi:10.1038/nprot.2007.54

166. Kopp H-G, Avecilla ST, Hooper AT, Rafii S. The bone marrow vascular niche: home of HSC differentiation and mobilization. Physiology (Bethesda). 2005;20: 349–356. doi:10.1152/physiol.00025.2005

167. Malara A, Currao M, Gruppi C, Celesti G, Viarengo G, Buracchi C, et al. Megakaryocytes contribute to the bone marrow-matrix environment by expressing fibronectin, type IV collagen, and laminin. Stem Cells. 2014;32: 926–937. doi:10.1002/stem.1626

168. Hagiwara T, Nagasawa T, Nagahisa H, Takizawa M, Osada M, Abe T. Expression of adhesion molecules on cytoplasmic processes of human megakaryocytes. Exp Hematol. 1996;24: 690–5.

Available: http://www.ncbi.nlm.nih.gov/pubmed/8635524

169. Sabri S, Foudi A, Boukour S, Franc B, Charrier S, Jandrot-Perrus M, et al. Deficiency in the Wiskott-Aldrich protein induces premature proplatelet formation and platelet production in the bone marrow compartment. Blood. American Society of Hematology; 2006;108: 134–40. doi:10.1182/blood-2005-03-1219

170. Italiano JE, Patel-Hett S, Hartwig JH. Mechanics of proplatelet elaboration. J Thromb Haemost. 2007;5 Suppl 1: 18–23. doi:10.1111/j.1538-7836.2007.02487.x

171. Dütting S, Gaits-Iacovoni F, Stegner D, Popp M, Antkowiak A, van Eeuwijk JMM, et al. A Cdc42/RhoA regulatory circuit downstream of glycoprotein Ib guides transendothelial platelet biogenesis. Nat Commun. 2017;8: 15838. doi:10.1038/ncomms15838

172. Seandel M, Butler JM, Kobayashi H, Hooper AT, White IA, Zhang F, et al. Generation of a functional and durable vascular niche by the adenoviral E4ORF1 gene. Proc Natl Acad Sci U S A. 2008;105: 19288–93. doi:10.1073/pnas.0805980105

173. Kiel MJ, Morrison SJ. Uncertainty in the niches that maintain haematopoietic stem cells. Nat Rev Immunol. Nature Publishing Group; 2008;8: 290–301. doi:10.1038/nri2279

174. Méndez-Ferrer S, Michurina T V, Ferraro F, Mazloom AR, Macarthur BD, Lira S a, et al. Mesenchymal and haematopoietic stem cells form a unique bone marrow niche. Nature. 2010;466: 829–834. doi:10.1038/nature09262

175. Huang M, Zhu J. The Regulation of Normal and Leukemic Hematopoietic Stem Cells by Niches. Cancer Microenviron. 2012;5: 295–305. doi:10.1007/s12307-012-0114-y

176. Frenette PS, Pinho S, Lucas D, Scheiermann C. Mesenchymal stem cell: keystone of the hematopoietic stem cell niche and a stepping-stone for regenerative medicine [Internet]. Annual Review of Immunology. Annual Reviews ; 2013. doi:10.1146/annurev-immunol-032712-095919

177. Kfoury Y, Scadden DT. Mesenchymal cell contributions to the stem cell niche. Cell Stem Cell. Elsevier; 2015;16: 239–253. doi:10.1016/j.stem.2015.02.019

178. Winkler IG, Sims NA, Pettit AR, Barbier V, Nowlan B, Helwani F, et al. Bone marrow macrophages maintain hematopoietic stem cell (HSC) niches and their depletion mobilizes HSCs. Blood. 2010;116: 4815–4828. doi:10.1182/blood-2009-11-253534

179. Villars F, Bordenave L, Bareille R, Amédée J. Effect of human endothelial cells on human bone marrow stromal cell phenotype: Role of VEGF? J Cell Biochem. John Wiley & Sons, Inc.; 2000;79: 672–685. doi:10.1002/1097-4644(20001215)79:4<672::AID-JCB150>3.0.CO;2-2

180. Grellier M, Bordenave L, Amédée J. Cell-to-cell communication between osteogenic and endothelial lineages: implications for tissue engineering. Trends Biotechnol. 2009;27: 562–571. doi:10.1016/j.tibtech.2009.07.001

181. Bidarra SJ, Barrias CC, Barbosa MA, Soares R, Amédée J, Granja PL. Phenotypic and proliferative modulation of human mesenchymal stem cells via crosstalk with endothelial cells. Stem Cell Res. 2011;7: 186–197. doi:10.1016/j.scr.2011.05.006

182. Hidalgo A, Weiss L a., Frenette PS. Functional selectin ligands mediating human CD34+ cell interactions with bone marrow endothelium are enhanced postnatally. J Clin Invest. 2002;110: 559–569. doi:10.1172/JCI200214047

183. Khorshed RA, Hawkins ED, Duarte D, Scott MK, Akinduro OA, Rashidi NM, et al. Automated Identification and Localization of Hematopoietic Stem Cells in 3D Intravital Microscopy Data. Stem Cell Reports. Elsevier; 2015;5: 139–153. doi:10.1016/j.stemcr.2015.05.017

184. Sipkins D a, Wei X, Wu JW, Runnels JM, Côté D, Means TK, et al. In vivo imaging of specialized bone marrow endothelial microdomains for tumour engraftment. Nature. 2005;435: 969–973. doi:10.1038/nature03703

185. Xie Y, Yin T, Wiegraebe W, He XC, Miller D, Stark D, et al. Detection of functional haematopoietic stem cell niche using real-time imaging. Nature. Macmillan Publishers Limited. All rights reserved; 2009;457: 97–101. doi:10.1038/nature07639

186. Ley K, Laudanna C, Cybulsky MI, Nourshargh S. Getting to the site of inflammation: the leukocyte adhesion cascade updated. Nat Rev Immunol. Nature Publishing Group; 2007;7: 678–689. doi:10.1038/nri2156

187. Muller WA. Mechanisms of Leukocyte Transendothelial Migration. Annu Rev Pathol Mech Dis. 2011;6: 323–344. doi:10.1146/annurev-pathol-011110-130224

188. Sampath R, Kukielka GL, Smith CW, Eskin SG, McIntire L V. Shear stress-mediated changes in the expression of leukocyte adhesion receptors on human umbilical vein endothelial cells in vitro. Ann Biomed Eng. 1995;23: 247–256.

189. Yeh Y-T, Serrano R, François J, Chiu J-J, Li Y-SJ, Del Álamo JC, et al. Three-dimensional forces exerted by leukocytes and vascular endothelial cells dynamically facilitate diapedesis. Proc Natl Acad Sci U S A. National Academy of Sciences; 2017; 201717489. doi:10.1073/pnas.1717489115

190. Möhle R, Rafii S, Moore M a. The role of endothelium in the regulation of hematopoietic stem cell migration. Stem Cells. 1998;16 Suppl 1: 159–65. doi:10.1002/stem.5530160819

191. Méndez-Ferrer S, Frenette PS. Hematopoietic stem cell trafficking: Regulated adhesion and attraction to bone marrow microenvironment. Annals of the New York Academy of Sciences. 2007. pp. 392–413. doi:10.1196/annals.1402.086

192. Gazitt Y. Homing and mobilization of hematopoietic stem cells and hematopoietic cancer cells are mirror image processes, utilizing similar signaling pathways and occurring concurrently: circulating cancer cells constitute an ideal target for concurrent treatment wi. Leuk Off J Leuk Soc Am Leuk Res Fund, UK. 2004;18: 1–10. doi:10.1038/sj.leu.2403173

193. Romano M, Sironi M, Toniatti C, Polentarutti N, Fruscella P, Ghezzi P, et al. Role of IL-6 and its soluble receptor in induction of chemokines and leukocyte recruitment. Immunity. 1997;6: 315–325. doi:10.1016/S1074-7613(00)80334-9

194. Alvarez P, Carrillo E, Vélez C, Hita-Contreras F, Martínez-Amat A, Rodríguez-Serrano F, et al. Regulatory Systems in Bone Marrow for Hematopoietic Stem/Progenitor Cells Mobilization and Homing. Biomed Res Int. 2013;2013: 1–12. doi:10.1155/2013/312656

195. Acar M, Kocherlakota KS, Murphy MM, Peyer JG, Oguro H, Inra CN, et al. Deep imaging of bone marrow shows non-dividing stem cells are mainly perisinusoidal. Nature. Nature Research; 2015;526: 126–130. doi:10.1038/nature15250

196. Ehninger A, Trumpp A. The bone marrow stem cell niche grows up: mesenchymal stem cells and macrophages move in. J Exp Med. 2011;208: 421–428. doi:10.1084/jem.20110132

197. Shi C, Jia T, Mendez-Ferrer S, Hohl TM, Serbina N V., Lipuma L, et al. Bone Marrow Mesenchymal Stem and Progenitor Cells Induce Monocyte Emigration in Response to Circulating Toll-like Receptor Ligands. Immunity. Elsevier Inc.; 2011;34: 590–601. doi:10.1016/j.immuni.2011.02.016

198. Lo Celso C, Scadden DT. The haematopoietic stem cell niche at a glance. J Cell Sci. 2011;124: 3529–35. doi:10.1242/jcs.074112

199. Iwata M, Sandstrom RS, Delrow JJ, Stamatoyannopoulos J a, Torok-Storb B. Functionally and phenotypically distinct subpopulations of marrow stromal cells are fibroblast in origin and induce different fates in peripheral blood monocytes. Stem Cells Dev. 2014;23: 729–40. doi:10.1089/scd.2013.0300

200. Chow A, Lucas D, Hidalgo A, Méndez-Ferrer S, Hashimoto D, Scheiermann C, et al. Bone marrow CD169+ macrophages promote the retention of hematopoietic stem and progenitor cells in the mesenchymal stem cell niche. J Exp Med. 2011;208: 261–271. doi:10.1084/jem.20101688

201. Winkler IG, Sims NA, Pettit AR, Barbier V, Nowlan B, Helwani F, et al. Bone marrow macrophages maintain hematopoietic stem cell (HSC) niches and their depletion mobilizes HSCs. Blood. 2010;116: 4815–4828. doi:10.1182/blood-2009-11-253534

202. Lin R-Z, Moreno-Luna R, Zhou B, Pu WT, Melero-Martin JM. Equal modulation of endothelial cell function by four distinct tissue-specific mesenchymal stem cells. Angiogenesis. Springer

Netherlands; 2012;15: 443–455. doi:10.1007/s10456-012-9272-2

203. Rasmusson I. Immune modulation by mesenchymal stem cells. Exp Cell Res. 2006;312: 2169–2179. doi:10.1016/j.yexcr.2006.03.019

204. Pillai MM, Iwata M, Awaya N, Graf L, Torok-Storb B. Monocyte-derived CXCL7 peptides in the marrow microenvironment. Blood. 2006;107: 3520–3526. doi:10.1182/blood-2005-10-4285

205. Graf L. Gene expression profiling of the functionally distinct human bone marrow stromal cell lines HS-5 and HS-27a. Blood. 2002;100: 1509–1511. doi:10.1182/blood-2002-03-0844

206. Roecklein B a, Torok-Storb B. Functionally distinct human marrow stromal cell lines immortalized by transduction with the human papilloma virus E6/E7 genes. Blood. 1995;85: 997–1005.

207. Mar D, Gharib SA, Zager RA, Johnson A, Denisenko O, Bomsztyk K. Heterogeneity of epigenetic changes at ischemia/reperfusion- and endotoxin-induced acute kidney injury genes. Kidney Int. 2015;88: 734–744. doi:10.1038/ki.2015.164

208. Böhrnsen F, Schliephake H. Supportive angiogenic and osteogenic differentiation of mesenchymal stromal cells and endothelial cells in monolayer and co-cultures. Int J Oral Sci. Nature Publishing Group; 2016;8: 223–230. doi:10.1038/ijos.2016.39

209. Horvath B, Hegedus D, Szapary L, Marton Z, Alexy T, Koltai K, et al. Measurement of von Willebrand factor as the marker of endothelial dysfunction in vascular diseases. Exp Clin Cardiol. 2004;9: 31–34.

210. Shen Y, Winkler IG, Barbier V, Sims N a., Hendy J, Lévesque JP. Tissue inhibitor of metalloproteinase-3 (TIMP-3) regulates hematopoiesis and bone formation in vivo. PLoS One. 2010;5: 1–13. doi:10.1371/journal.pone.0013086

211. Vielhauer V, Cullere X, Mayadas T, Lowenstein CJ, Morrell CN, Yamakuchi M. Endothelial Biomedicine [Internet]. Aird WC, editor. Cambridge: Cambridge University Press; 2007. doi:10.1017/CBO9780511546198

212. Fiedler U, Scharpfenecker M, Koidl S, Hegen A, Grunow V, Schmidt JM, et al. The Tie-2 ligand Angiopoietin-2 is stored in and rapidly released upon stimulation from endothelial cell Weibel-Palade bodies. Blood. 2004;103: 4150–4156. doi:10.1182/blood-2003-10-3685

213. Ingersoll MA, Platt AM, Potteaux S, Randolph GJ. Monocyte trafficking in acute and chronic inflammation [Internet]. Trends in Immunology NIH Public Access; Oct, 2011 pp. 470–477. doi:10.1016/j.it.2011.05.001

214. Kiel MJ, Yilmaz ÖH, Iwashita T, Yilmaz OH, Terhorst C, Morrison SJ. SLAM family receptors distinguish hematopoietic stem and progenitor cells and reveal endothelial niches for stem cells. Cell. 2005;121: 1109–1121. doi:10.1016/j.cell.2005.05.026

215. Zhou BO, Yue R, Murphy MM, Peyer JG, Morrison SJ. Leptin-Receptor-Expressing Mesenchymal Stromal Cells Represent the Main Source of Bone Formed by Adult Bone Marrow. Cell Stem Cell. 2014;15: 154–168. doi:10.1016/j.stem.2014.06.008

216. Iwata M, Torok-Storb B, Wayner EA, Carter WG. CDCP1 Identifies a CD146 Negative Subset of Marrow Fibroblasts Involved with Cytokine Production. Mezey E, editor. PLoS One. 2014;9: e109304. doi:10.1371/journal.pone.0109304

217. Boyd AL, Campbell CJ V, Hopkins CI, Fiebig-comyn A, Russell J, Ulemek J, et al. Niche displacement of human leukemic stem cells uniquely allows their competitive replacement with healthy HSPCs. J Exp Med. 2014;211: 1925–35. doi:10.1084/jem.20140131

218. Ramakrishnan A, Deeg HJ. A novel role for the marrow microenvironment in initiating and sustaining hematopoietic disease. Expert Opin Biol Ther. 2009;9: 21–28. doi:10.1517/14712590802603093

219. Kaplan RN, Psaila B, Lyden D. Niche-to-niche migration of bone-marrow-derived cells. Trends Mol Med. 2007;13: 72–81. doi:10.1016/j.molmed.2006.12.003

220. Kumar R, Kuniyasu H, Bucana CD, Wilson MR, Fidler IJ. Spatial and temporal expression of

angiogenic molecules during tumor growth and progression. Oncol Res. 1998;10: 301–311.

221. Algire GH, Chalkley HW, Legallais FY, Park HD. Vascular reactions of normal and malignant tissues in vivo. i. vascular reactions of mice to wounds and to normal and neoplastic transplants. J Natl Cancer Inst. Oxford University Press; 1945;6: 73–85. doi:10.1093/jnci/6.1.73

222. Shih T, Hou H, Liu C, Chen B. Marrow Angiogenesis Magnetic Resonance Imaging in Patients With Acute Myeloid Leukemia: Peak Enhancement Ratio Is an Independent Predictor for Overall Survival. Blood. 2009;113: 3161–3167. doi:10.1182/blood-2008-08-173104.

223. de Bont E, Rosati S, Jacobs S, Kamps WA, Vellenga E. Increased bone marrow vascularization in patients with acute myeloid leukaemia: a possible role for vascular endothelial growth factor. Br J Haematol. Blackwell Science Ltd; 2001;113: 296–304. doi:10.1046/j.1365-2141.2001.02722.x

224. Weidenaar AC, ter Elst A, Koopmans-Klein G, Rosati S, den Dunnen WFA, Meeuwsen-de Boer T, et al. High Acute Myeloid Leukemia derived VEGFA levels are associated with a specific vascular morphology in the leukemic bone marrow. Cell Oncol. Springer Netherlands; 2011;34: 289–296. doi:10.1007/s13402-011-0017-9

225. Fiedler W, Graeven U, Ergün S, Verago S, Kilic N, Stockschläder M, et al. Vascular endothelial growth factor, a possible paracrine growth factor in human acute myeloid leukemia. Blood. American Society of Hematology; 1997;89: 1870–5. Available: http://www.bloodjournal.org/content/89/6/1870.abstract

226. Watarai M, Miwa H, Shikami M, Sugamura K, Wakabayashi M, Satoh A, et al. Expression of endothelial cell-associated molecules in AML cells. Leukemia. Nature Publishing Group; 2002;16: 112–9. doi:10.1038/sj.leu.2402326

227. Lévesque J-P, Winkler IG, Hendy J, Williams B, Helwani F, Barbier V, et al. Hematopoietic Progenitor Cell Mobilization Results in Hypoxia with Increased Hypoxia-Inducible Transcription Factor-1α and Vascular Endothelial Growth Factor A in Bone Marrow. Stem Cells. 2007;25: 1954–1965. doi:10.1634/stemcells.2006-0688

228. Ferrara N, Davis-Smyth T. The Biology of Vascular Endothelial Growth Factor. Endocr Rev. Oxford University Press; 1997;18: 4–25. doi:10.1210/edrv.18.1.0287

229. Ferrara N, Adamis AP. Ten years of anti-vascular endothelial growth factor therapy. Nat Rev Drug Discov. Nature Publishing Group; 2016;15: 385–403. doi:10.1038/nrd.2015.17

230. Tallman MS. New strategies for the treatment of acute myeloid leukemia including antibodies and other novel agents. Hematol Am Soc Hematol Educ Progr. American Society of Hematology; 2005;2005: 143–50. doi:10.1182/asheducation-2005.1.143

231. Karp JE, Gojo I, Pili R, Gocke CD, Greer J, Guo C, et al. Targeting vascular endothelial growth factor for relapsed and refractory adult acute myelogenous leukemias: therapy with sequential 1-beta-d-arabinofuranosylcytosine, mitoxantrone, and bevacizumab. Clin Cancer Res. American Association for Cancer Research; 2004;10: 3577–85. doi:10.1158/1078-0432.CCR-03-0627

232. Chauncey TR, Gundacker H, Shadman M, List AF, Dakhil SR, Erba HP, et al. Sequential phase II Southwest Oncology Group studies (S0112 and S0301) of daunorubicin and cytarabine by continuous infusion, without and with ciclosporin, in older patients with previously untreated acute myeloid leukaemia. Br J Haematol. Blackwell Publishing Ltd; 2010;148: 48–58. doi:10.1111/j.1365-2141.2009.07919.x

233. Ossenkoppele GJ, Stussi G, Maertens J, van Montfort K, Biemond BJ, Breems D, et al. Addition of bevacizumab to chemotherapy in acute myeloid leukemia at older age: a randomized phase 2 trial of the Dutch-Belgian Cooperative Trial Group for Hemato-Oncology (HOVON) and the Swiss Group for Clinical Cancer Research (SAKK). Blood. American Society of Hematology; 2012;120: 4706–11. doi:10.1182/blood-2012-04-420596

234. Perez-Atayde AR, Sallan SE, Tedrow U, Connors S, Allred E, Folkman J. Spectrum of tumor angiogenesis in the bone marrow of children with acute lymphoblastic leukemia. Am J Pathol. 1997;150: 815–21. Available: http://www.pubmedcentral.nih.gov/articlerender.fcgi?artid=1857903&tool=pmcentrez&rendertype=

abstract

235. Hutmacher DW, Sittinger M, Risbud M V. Scaffold-based tissue engineering: Rationale for computer-aided design and solid free-form fabrication systems. Trends Biotechnol. 2004;22: 354–362. doi:10.1016/j.tibtech.2004.05.005

236. Fischbach C, Kong HJ, Hsiong SX, Evangelista MB, Yuen W, Mooney DJ. Cancer cell angiogenic capability is regulated by 3D culture and integrin engagement. Proc Natl Acad Sci U S A. 2009;106: 399–404. doi:10.1073/pnas.0808932106

237. Ghajar CM, Bissell MJ. Tumor engineering: the other face of tissue engineering. Tissue Eng Part A. 2010;16: 2153–6. doi:10.1089/ten.TEA.2010.0135

238. Zhang J, Ye J, Ma D, Liu N, Wu H, Yu S, et al. Cross-talk between leukemic and endothelial cells promotes angiogenesis by VEGF activation of the Notch/Dll4 pathway. Carcinogenesis. 2013;34: 667–77. doi:10.1093/carcin/bgs386

239. Miller CM, Tsuchida C, Zheng Y, Himmelfarb J, Akilesh S. A 3D human renal cell carcinoma on a chip for the study of tumor angiogenesis. Revis. 2017;

240. Ong S-M, Zhao Z, Arooz T, Zhao D, Zhang S, Du T, et al. Engineering a scaffold-free 3D tumor model for in vitro drug penetration studies. Biomaterials. 2010;31: 1180–1190. doi:10.1016/j.biomaterials.2009.10.049

241. Ghajar CM, Peinado H, Mori H, Matei IR, Evason KJ, Brazier H, et al. The perivascular niche regulates breast tumour dormancy. Nat Cell Biol. Nature Publishing Group, a division of Macmillan Publishers Limited. All Rights Reserved.; 2013;15: 807–17. doi:10.1038/ncb2767

242. Verbridge SS, Choi NW, Zheng Y, Brooks DJ, Stroock AD, Fischbach C. Oxygen-controlled three-dimensional cultures to analyze tumor angiogenesis. Tissue Eng Part A. Mary Ann Liebert, Inc. 140 Huguenot Street, 3rd Floor New Rochelle, NY 10801 USA; 2010;16: 2133–41. doi:10.1089/ten.TEA.2009.0670

243. He R, Liu B, Yang C, Yang RC, Tobelem G, Han ZC. Inhibition of K562 leukemia angiogenesis and growth by expression of antisense vascular endothelial growth factor (VEGF) sequence. Cancer Gene Ther. Nature Publishing Group; 2003;10: 879–86. doi:10.1038/sj.cgt.7700645

244. Connolly DT, Olander J V, Heuvelman D, Nelson R, Monsell R, Siegel N, et al. Human vascular permeability factor. Isolation from U937 cells. J Biol Chem. 1989;264: 20017–24. Available: http://www.ncbi.nlm.nih.gov/pubmed/2584205

245. Birnie GD. The HL60 cell line: a model system for studying human myeloid cell differentiation. Br J Cancer Suppl. Nature Publishing Group; 1988;9: 41–5. Available: http://www.ncbi.nlm.nih.gov/pubmed/3076064

246. Klein E, Vánky F, Ben-Bassat H, Neumann H, Ralph P, Zeuthen J, et al. Properties of the K562 cell line, derived from a patient with chronic myeloid leukemia. Int J Cancer. Wiley Subscription Services, Inc., A Wiley Company; 1976;18: 421–431. doi:10.1002/ijc.2910180405

247. Furley AJ, Reeves BR, Mizutani S, Altass LJ, Watt SM, Jacob MC, et al. Divergent molecular phenotypes of KG1 and KG1a myeloid cell lines. Blood. 1986;68: 1101–7. Available: http://www.ncbi.nlm.nih.gov/pubmed/3094604

248. Romer LH, McLean N V, Yan HC, Daise M, Sun J, DeLisser HM. IFN-gamma and TNF-alpha induce redistribution of PECAM-1 (CD31) on human endothelial cells. J Immunol. American Association of Immunologists; 1995;154: 6582–92. Available: http://www.ncbi.nlm.nih.gov/pubmed/7759892

249. Ozaki H, Ishii K, Horiuchi H, Kawamoto T, Okawa K, Kita T. Cutting Edge: Combined Treatment of TNF-α and IFN-γ Causes Redistribution of Junctional Adhesion Molecule in Human Endothelial Cells. J Immunol. 1999;163: 553–7.

250. Aguayo A, Estey E, Kantarjian H, Mansouri T, Gidel C, Keating M, et al. Cellular vascular endothelial growth factor is a predictor of outcome in patients with acute myeloid leukemia. Blood. 1999;94: 3717–3721. Available: http://www.ncbi.nlm.nih.gov/pubmed/10572084

Appendix A

Supplement to Chapter 2

List of Supplementary Figures

Appendix A, Supplementary Figures to Chapter 2.

Supplementary Figure 1

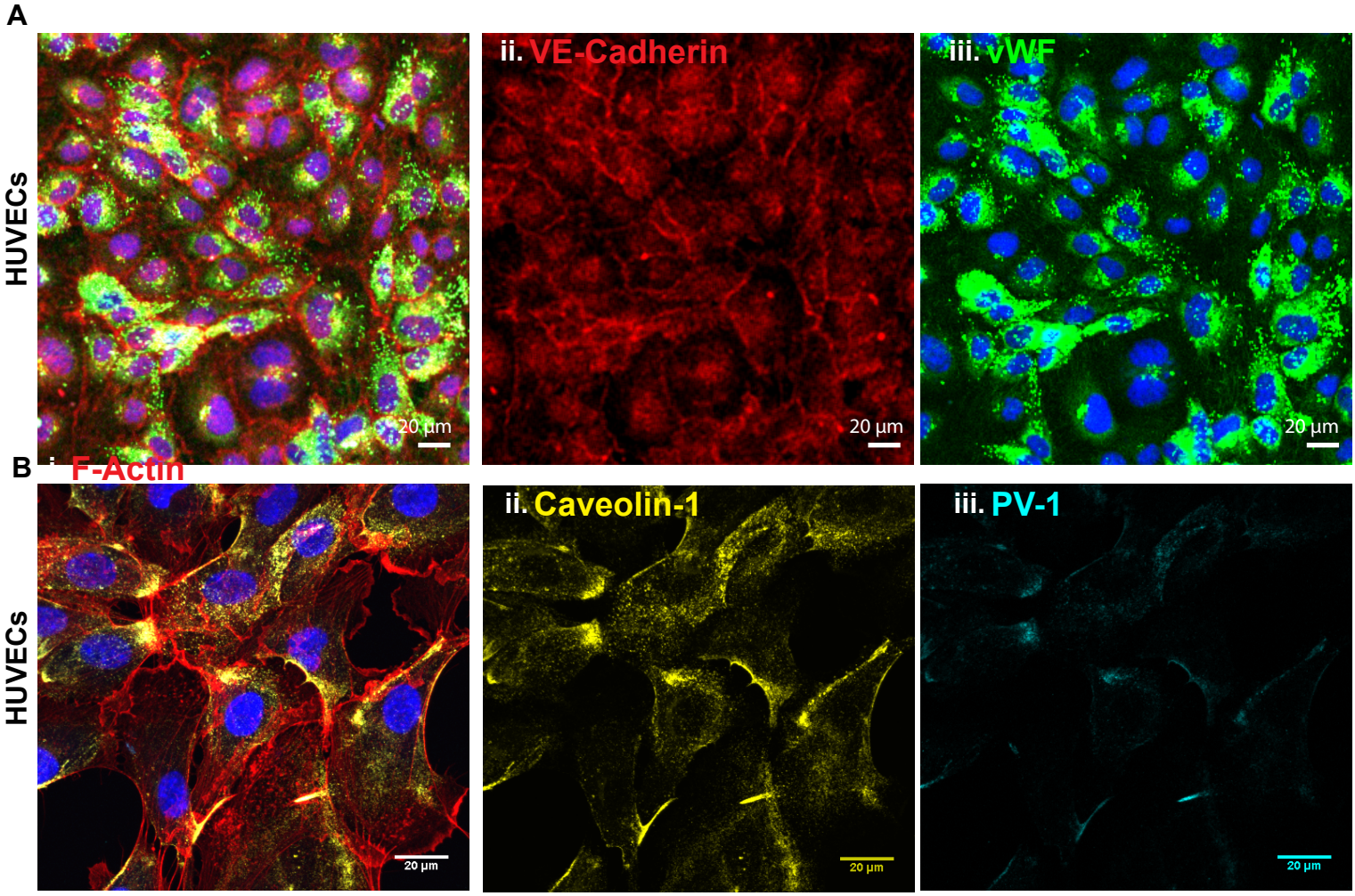

Supplementary Figure 1. Immunofluorescence staining of HUVECs. (A) Immunofluorescence staining of VE-Cadherin (ii) and von Willebrand Factor (iii). (B) Immunofluorescence staining of F-actin, caveolin-1 (ii), and PV-1 staining (iii).

Appendix A, Supplementary Figures to Chapter 2.

Supplementary Figure 2

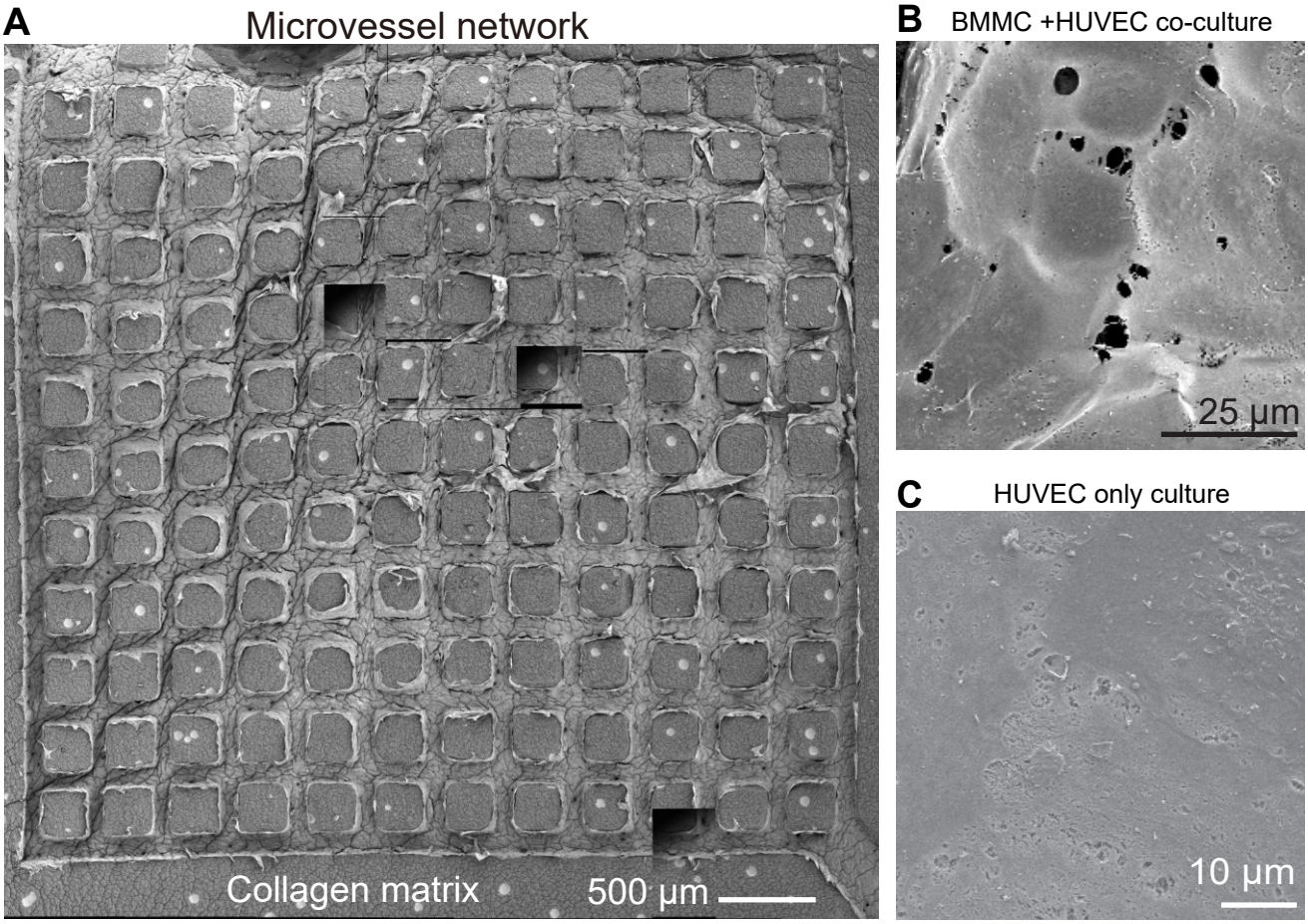

Supplementary Figure 2. HUVECs co-cultured with marrow mononuclear cells in microvessels. (A) Scanning electron microscopy shows an overview of the co-culture. (B-C) SEM images of the endothelium of the bone marrow cell co-cultured vessels showing holes from abluminal side (B). The luminal side of the endothelium with no co-cultured cells shows an intact, continuous endothelium.

Appendix B

Supplement to Chapter 3

List of Supplementary Figures

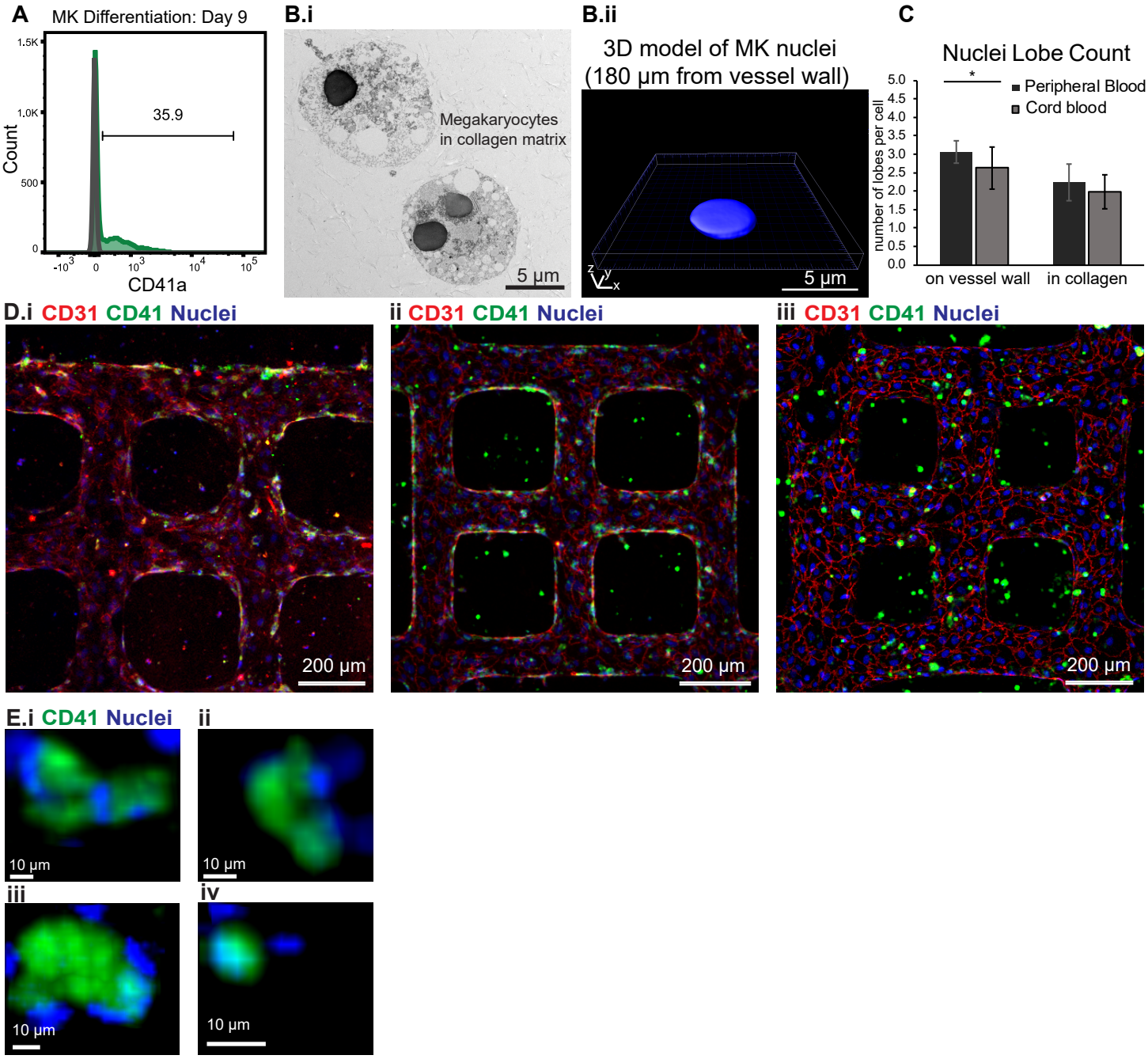

Supplementary Figure 1. Megakaryocytes differentiation and interaction with microvessels. A. An example flow analysis chart showing CD34+ cells after day 9 of differentiation in suspension had approximately 36% CD41+ megakaryocytes. Unstained population in gray, CD41+ stained cells in green. B. (i) TEM image of MKs far from the vessel wall within the collagen matrix shows low nucleus lobe number. (ii) 3D reconstruction of confocal image from a megakaryocyte nucleus 3 radius-lengths from the vessel wall also shows low nucleus lobe number. C. Quantification of nucleus lobe number for peripheral blood-derived and cord blood-derived MKs on the vessel wall and far from the vessel wall shows decreased lobe number in cord-blood derived MKs. D.i-iii. Human MKs line the vessel walls after 3 days of culture. E. (i) Zoomed view of MKs shown in cross section in Figure 2B confirm the CD41a+ cells contain nuclei. Cells shown are from (i) cross section 1 and (ii) 3 from the top panel, and cross section (iii) 2 and (iv) 3 from the bottom panel.

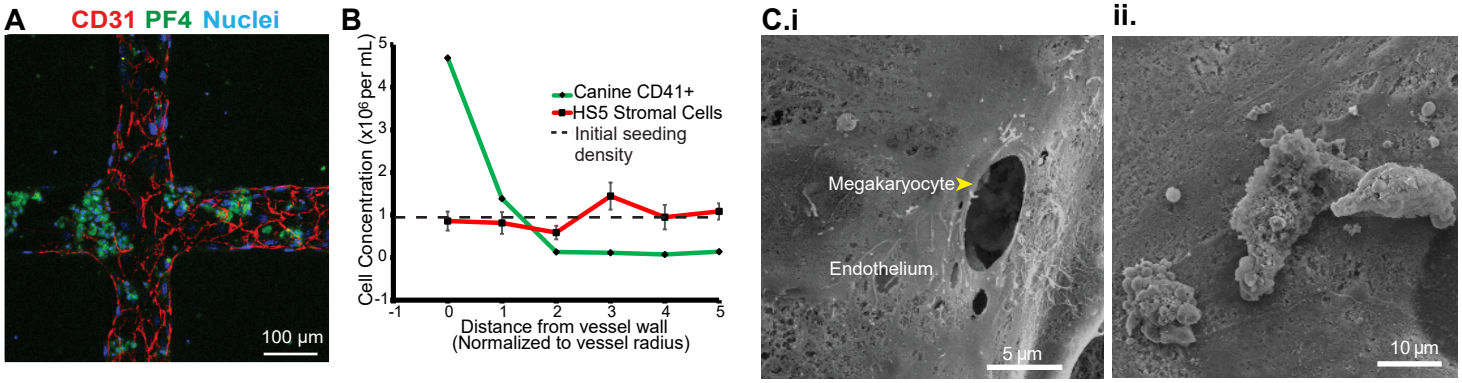

Supplementary Figure 2. Canine PF4-GFP megakaryocytes migrate to the vessel wall. A. MKs from canine marrow with PF4-driven GFP expression were isolated and seeded into the collagen matrix surrounding the microvessels. Canine MKs, similar to human MKs, migrated to the vessel wall after 3 days of culture. B. Quantification of canine MK distance from the vessel shows a nearly five-fold increase in MK concentration at the wall. Error bars indicate standard error. C. SEM images of the endothelium in co-culture with canine MKs shows a pore in the vessel wall with an MK behind it (i) and a pro-platelet cluster with MK fragments on the endothelium (ii).

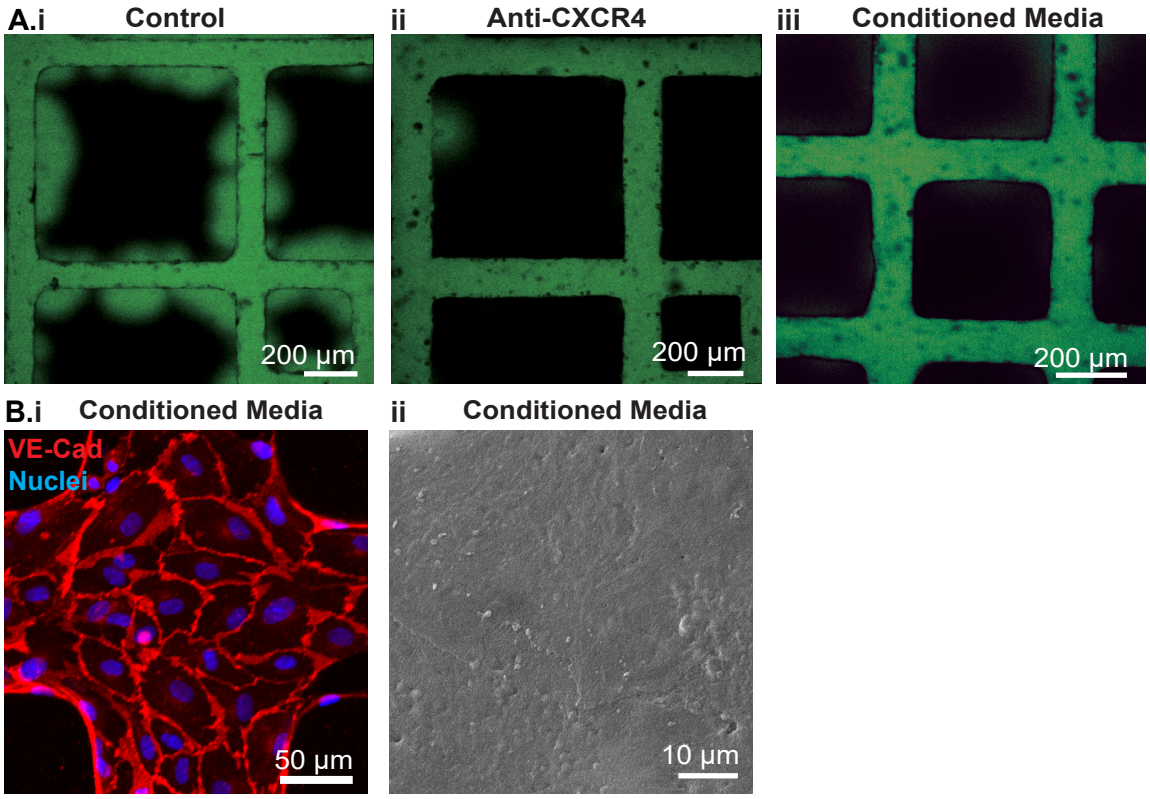

Supplementary Figure 3. Endothelial barrier function in co-cultured vessels. A. 40kD-FITC-Dextran was perfused through the MK co-cultured (control) vessels (i) and MK vessels treated with antiCXCR4 (ii) to visualize barrier function of the vessels. (iii) FITC-Dextran was als perfused through vessels fed with MK-conditioned media to test barrier function. B. Junctional staining (i) and scanning electron microscopy (ii) do not show holes in MK-conditioned media cultured vessels.

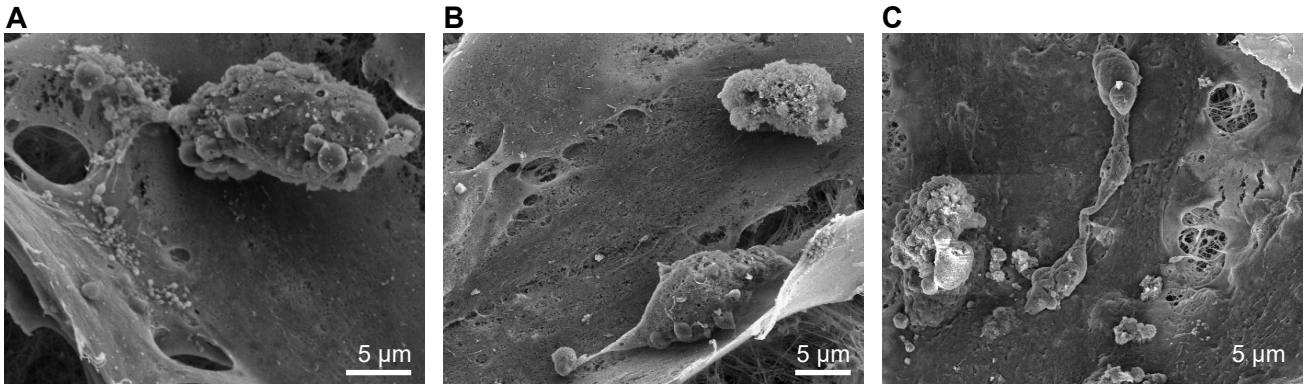

Supplementary Figure 4. Whole megakaryocytes penetrate into the vessel lumen. A-C. Scanning electron microscopy of a human thrombopoietic VME shows ultrastructure of whole megakaryocytes or large fragments within the vessel lumen.

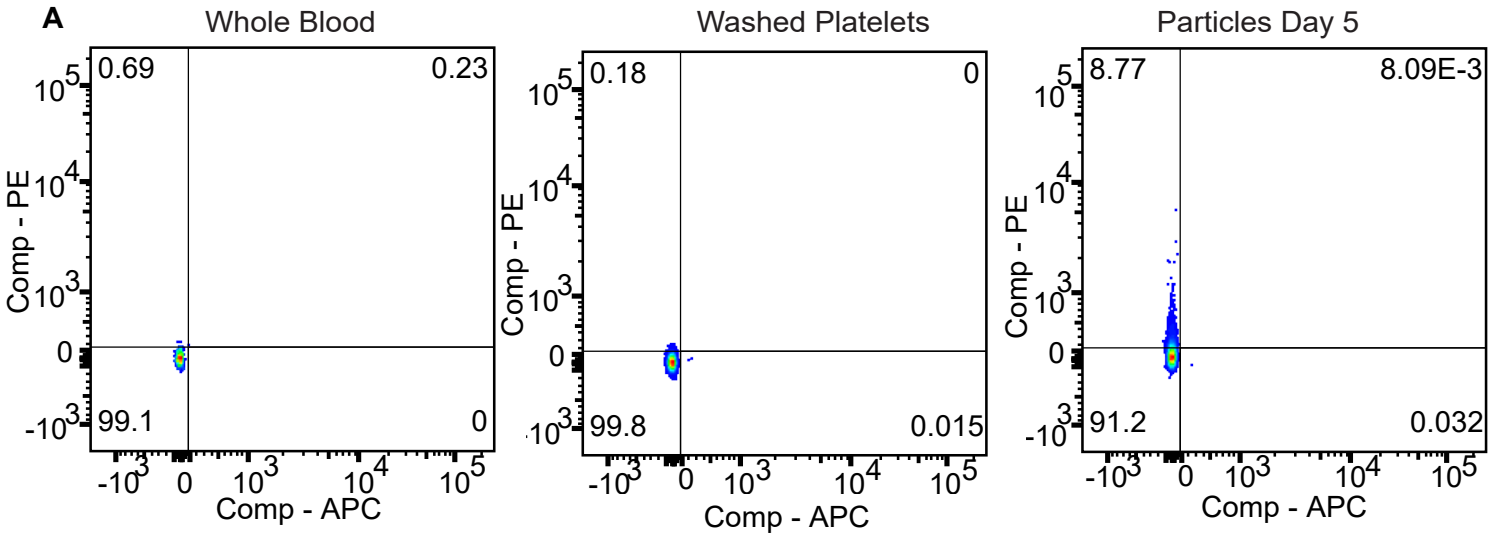

Supplementary Figure 5. Flow Cytometry Controls for generated particles. A. Corresponding plots to whole blood, washed platelet, and generated particle CD41a and CD42b staining show unstained populations, confirming lack of autofluorescence artifacts.

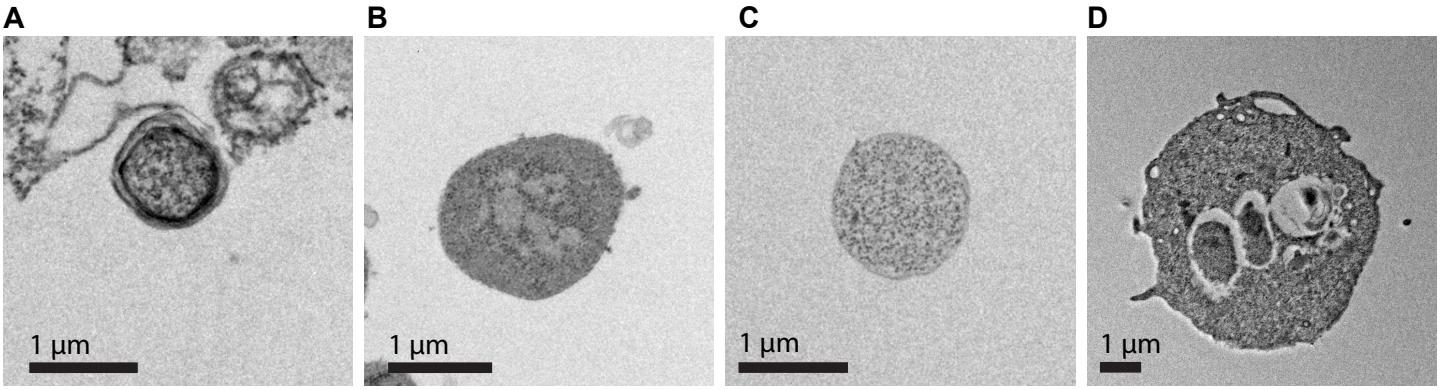

Supplementary Figure 6. Variation in morphology of generated particles. A-D. Transmission electron microscopy shows variation in particle morphology and contents.

Appendix C

Supplement to Chapter 4

List of Supplementary Figures

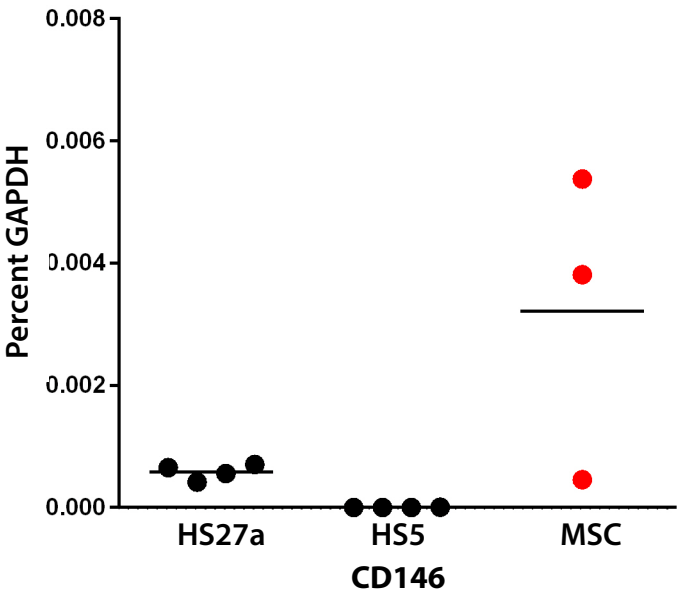

Supplementary Figure 1. Expression of CD146 by HS27a, HS5, and MSCs is shown via RT-PCR. MSC expression of CD146 is variable compared to the HS27a and HS5 cell lines.

Appendix C. Supplementary Figures to Chapter 4.
Supplementary Figure 2.

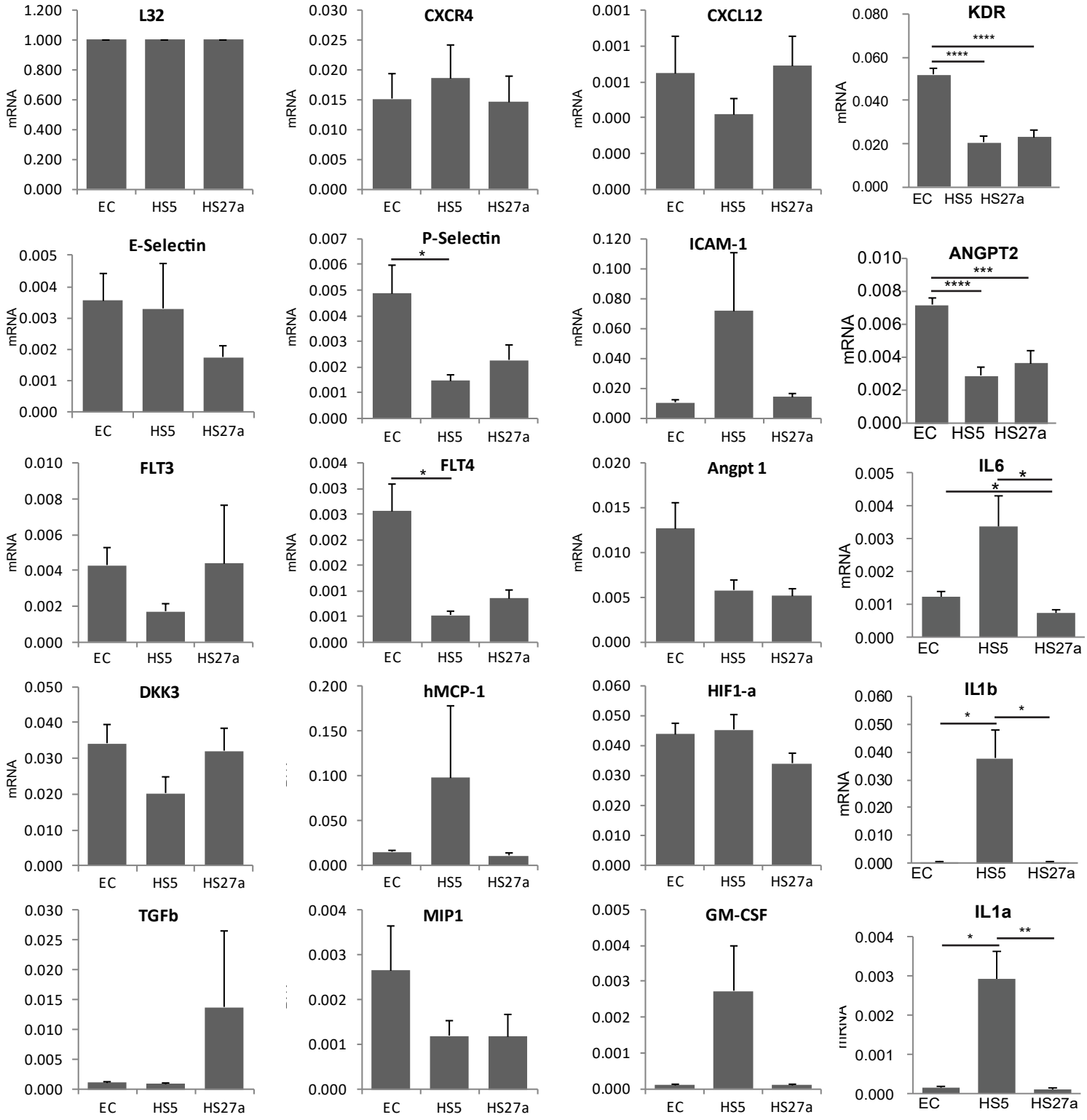

Supplementary Figure 2. RT-PCR of endothelial and stromal cells from microvessels. Similar expression of CXCR4, CXCL12, E-Selectin, ICAM-1, FLT-3, Angiopoietin-1, IL-6, DKK3, MCP-1, HIF-1a, IL-1b, TFGb, MIP1, and GM-CSF, IL-1a (normalized to L32 ribosomal protein) is shown in co-cultured vessels. KDR, P-Selectin, Angiopoeitin2, and FLT4 have increased expression in the endothelial-only vesels. IL6, IL1b, and IL1a have increased expression in the HS5 co-cultured vessels. *p < 0.05, **p < 0.01, *** p <0.001, ****p<0.0001.

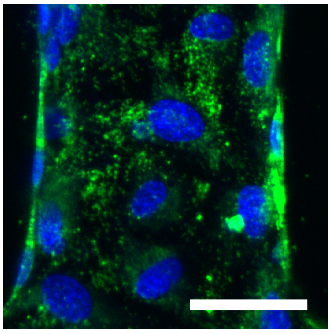

Supplementary Figure 3. Immunofluorescence staining of von WIllebrand Factor in an EC only vessel after 6 days of culture. Scale bar = 50 μm.

Supplementary Table 1. Primer information for RT-PCR analysis.

Primers used for RT-PCR	Sequence
L32 – for normalization	AGTTCCTGGTCCACAACGTC
	TTGGGGTTGGTGACTCTGAT
cMYC ex3 /hMYC Ex3	AAGGACTATCCTGCTGCCAA
	CGCCTCTTGACATTCTCCTC
ICAM1 ex7	GTACCTCTATAACCGCCAGC
	GCTTGTGTGTTCGGTTTCAT
VCAM1 ex9	ATGCCCATCTATGTCCCTTG
	GCAGTTACTGTTCTTCAGGC
MCP1 ex3	AAACCCAAACTCCGAAGACT
	ATAAAACAGGGTGTCTGGGG
TEK ex23	AGCCAGTCCCGTTTCATTTA
	TGTTAGCATCCTGGACTGAC
VWF ex52	ACCAATGGCTCTGTTGTGTA
	CTCACTTGCTGCACTTCCT
PECAM1 ex2	ACAACCCAGTAGAGATGCAG
	ATTTTCCACCATGACGCTTG
KDR ex 30-1	GCCCCATCCTCAAAGAAGTA
	CGAACACTTACATTGCCTGG
Angpt1 ex9	TCTGCCTGTAAGTGTCCAAG
	GGAGGCCCAGTAGCTTTATT
Angpt2 Ex9	TCTTATGAGCGAGAATGGGG
	AAGCTCCTCTCAGCAAAACT
cFOS ex4	TTCCTCTGACTCGCTCAGCTC
	AGTCCTTGAGGCCCACAGC
Egr1 ex2-2	ACTCCTCTGTTCCCCCTGCT
	GTCCTGGGAGAAAAGGTTGCT
CXCR4 ex2	GGCCAAGTTCTTAGTTGCTG
	GATTCACTACACGCTCTGGA
CXCL12 ex4	TCTGTGAGATCCGTCTTTGG
	AGACTTGTCTTTTGCGGGTA
FLT3 ex24	GGATTTGGGGCTACTCTCTC
	TAGGGATAGGTGGAGGGATG
FLT4 ex30	CGGTCTGGTTCTTCCCTTTA
	TCTCTCATGAGCTGGTTCAC
IL6 ex5	GGCACCTCAGATTGTTGTTG
	CATAAGTTCTGTGCCCAGTG
IL8 ex4	GTGTTGGTAGTGCTGTGTTG
	ATTGACTGTGGAGTTTTGGC
NFKB ex24	GCAAACTCAGCTTTACCGAG
	GTCCTTCCTGCCCATAATCA
RELA ex11	AGCCCACAAAGCCTTATCAA
	CTGGTATCTGGGGCGTTATT
DKK3 ex14	CCCTGTCCAGATTATTGGCT
	CATCTCCTCCCCTCAAACAA
SELE ex4	AGCAAAGGTGAAGAGACCAA
	TGTGCCAAGATTTTACAGCG

Supplementary Table 1 (Continued). Primer information for RT-PCR analysis.

Primers used for RT-PCR	Sequence
CSF2 Ex4	TTCCTGTGCAACCCAGATTA
	AAGGGGATGACAAGCAGAAA
HIF1a ex15	TTAGCATGTAGACTGCTGGG
	GCTGCCTTGTATAGGAGCAT
IL1a ex7	CCATCACAGGTAGTGAGACC
	AACAAGTTTGGATGGGCAAC
IL1b ex7	AGAGAGTCCTGTGCTGAATG
	AGACAACAGGAAAGTCCAGG
IL3 ex5	CGGAGGAAACTGACGTTCTA
	TGGACGTTGGACTCAAAAGA
IL1 ex4	GAAGGAAGCCAACCAGAGTA
	TCAGCTCGAACACTTTGAAT
TGFb ex7	ATGGGGGCTGTATTTAAGGA
	GCAGTCCTCTCTCCATCTTT
TGBS1 ex22	TCAAACCAGTGTAAGGCAGT
	TTCCTGCTACATCTGCACAA
TIMP1 ex6	CCCAGATAGCCTGAATCCTG
	AAAGATGGGAGTGGGAACAG
TIMP3 ex5	TGAGCCCAGACTTGATGTTT
	AGGGAACTTGTGTAGGTTGG
CHRDL1 ex12	TCAGCCAGATGTGTTCAAGT
	GCCCTTTTCAGATCTCTCCA
KITLG ex10	GCTTTGCACCTCTTTGGTAG
	TCACTCAGGAGGCAACATTT
MIP1a ex3	AAGCCACCAGACTGACAAAT
	TTATTATTTCCCCAGGCCGA
Notch1 ex34	TCCACCAGTTTGAATGGTCA
	AGAGGGTTGTATTGGTTCGG
OCLN ex9	ACAGCAATGGAAAACCACAC
	CCAAAGGAATGGGAAACGAC
PDGFb ex7	CGTTTTGAAGACGTGGACTC
	ACTCCATCTCTAACCCACCT
ROBO4 ex18	TGCCAAACAAAGGGTTCAAG
	TGACAACAGTACGAGGATGG
SELP ex17	CAGTGGTTGCTGTTGATGAG
	CTTGATTCTTGGCCTTCTGC
CDH5 ex5	GCCAATCCATGCTCTCTTTC
	TAAAGGCCACATCTTGGGTT
CSPG4 ex10	ACCAGGGTAACCTCCTACAT
	CCTTCTCCTTGCCCTCTTAG
FLT1 ex30	TAAGGTCAAGGGAAAACCCC
	AAACGTGACTGACTTCCTGT

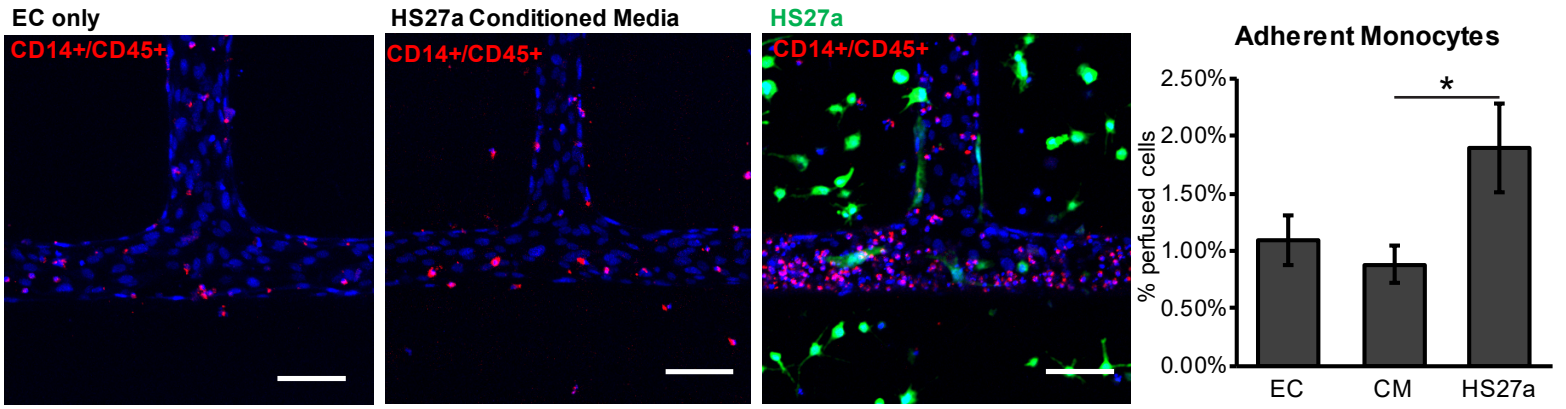

Supplementary Figure 4. Monocytes perfused through EC, EC with HS27a-conditioned media, or HS27a-co-cultured vessels. Quantification of monocyte adhesion shows no changes in adhesion between EC only and EC with HS27a-conditioned media but an increase within the HS27a-co-cultured vessels. Scale bars = 100 μm.

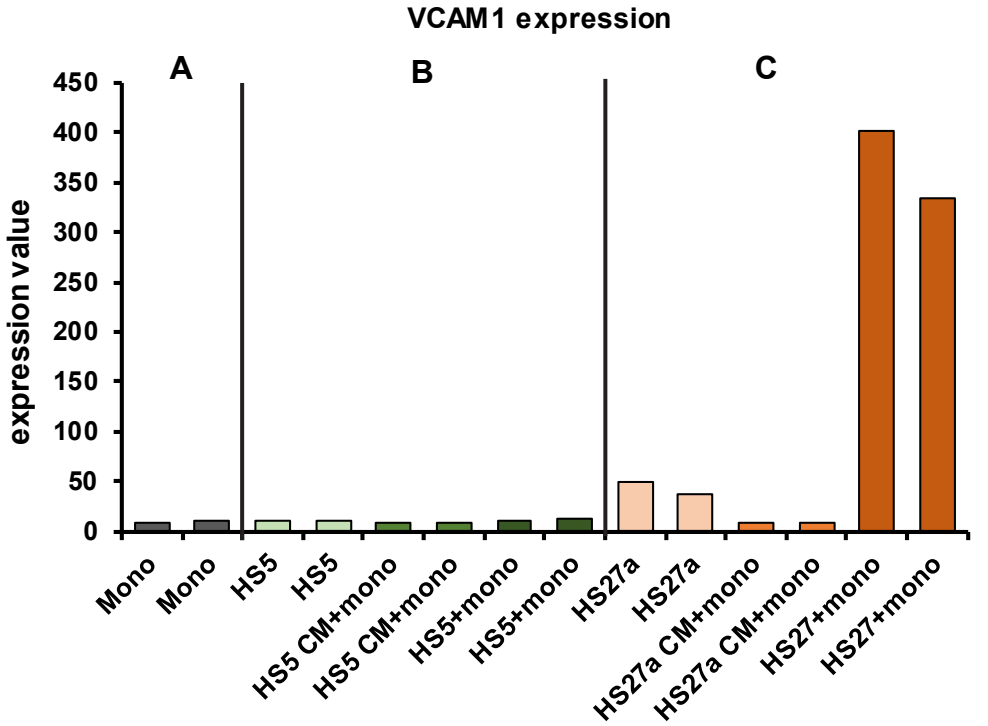

Supplementary Figure 5. Expression of VCAM1 in monocytes co-cultured with stromal fibroblasts and conditioned media. Microarray expression analysis of (A) monocytes from two different donors alone. (B) Expression of VCAM in HS5 cells, Monocytes cultured with HS5 conditioned media, and Monocytes co-cultured with HS5 cells. (C) Expression of VCAM in HS27a cells, Monocytes cultured with HS27a conditioned media, and Monocytes co-cultured with HS27a cells. Expression values extracted from microarray data from Iwata et al. (www.ncbi.nlm.nih.gov/geo/; accession numbers GSE9390 and GSE10595, gene ID: 203868_s_at)

Appendix D

Supplement to Chapter 5

List of Supplementary Figures

Appendix A, Supplementary Figures to Chapter 2.

Supplementary Figure 1

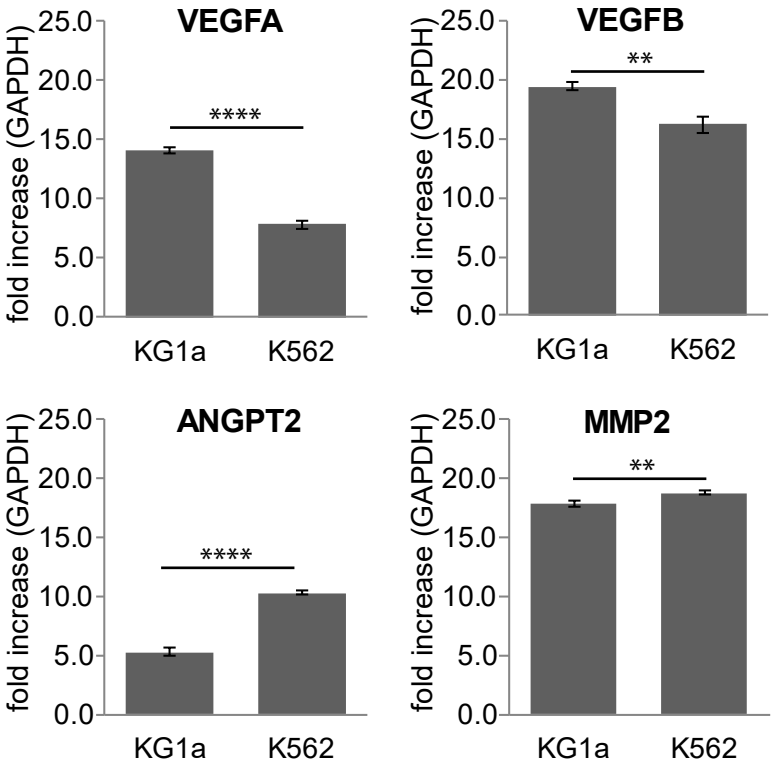

Supplementary Figure 1. RT-PCR of Leukemic cell lines KG1a and K562 cultured in collagen. RNA isolated from cell lines cultured in collagen shows significant differences in angiogenesis-associated genes. KG1a has increased expression of VEGFA and VEGFB, key ligands for the induction of angiogenic sprouting. K562 has increased expression of ANGPT2 and MMP2, genes involved in endothelial destabilization.